Luminescence dating of storm-surge sediment

Proefschrift

ter verkrijging van de graad van doctor
aan de Technische Universiteit Delft,
op gezag van de Rector Magnificus prof. ir. K.C.A.M. Luyben,
voorzitter van het College voor Promoties,
in het openbaar te verdedigen op dinsdag 30 augustus 2011 om 15.00 uur
door Alastair Charles CUNNINGHAM
Master of Science in Quaternary Science, University of London
geboren te London, Verenigd Koninkrijk

Dit proefschrift is goedgekeurd door de promotor:
Prof. dr. P. Dorenbos

Copromotor Dr. J. Wallinga

Samenstelling promotiecommissie:

Rector Magnificus,	voorzitter
Prof. dr. P. Dorenbos,	Technische Universiteit Delft, promotor
Dr. J. Wallinga,	Technische Universiteit Delft, copromotor
Prof. dr. ir. G. Jongbloed,	Technische Universiteit Delft
Prof. dr. ir. M.J.F. Stive,	Technische Universiteit Delft
Prof. A.S. Murray,	Aarhus University
Prof. dr. H. Middelkoop,	Universiteit Utrecht
Dr. S. van Heteren,	TNO, Utrecht

This research is supported by the Dutch Technology Foundation STW, which is part of the Netherlands Organisation for Scientific Research (NWO) and partly funded by the Ministry of Economic Affairs, Agriculture and Innovation (DSF.7553). The work was carried out at the Radiation Detection & Medical imaging (RD&M) section of the department of Radiation, Radionuclides & Reactors (R^3), Faculty of Applied Sciences, Delft University of Technology, The Netherlands.

Table of Contents

Chapter 1

Introduction

1.1 Motivation

The 20th century saw two devastating storm surges strike the Netherlands, in 1916 and 1953. These natural disasters illustrate the threat posed by storm surges, but it is likely that floods of far greater magnitude have occurred in the past, before reliable records were kept. Of course, such events will also happen in the future. By studying the events of the past, we can learn about the risk we face.

At the heart of a risk assessment lies probability – how likely is it that a major storm surge will occur in the future? To estimate probabilities, we need data on the timing and magnitude of storm surges. In the Netherlands, this data has been collected at various locations over a period of 50 – 100 years, but herein lies the problem. Extreme storm surges occur at a much lower frequency, so a measurement record stretching back 100 years is unlikely to contain data from the most high-magnitude events. It is clear that we must go beyond the measurement record to understand these events.

While measurement records are relatively short, there are other types of record which persist on a longer timescale. This thesis is concerned with the geological record of storm surges: sediments which are transported by storm-surges and deposited in new positions. By looking at geological records, we can potentially extract information on the sort of extreme storm surge which poses a real threat to the Netherlands.

There are two key pieces of information which need to be extracted from such deposits: what was the magnitude of the storm surge, and when did it occur? Thankfully, there are storm-surge deposits in the Netherlands which have the potential to give this information. They are located within the coastal dunes of North Holland, and lie several metres above sea level within the dune sands (Fig. 1). Because of the height of these sediments, the magnitude of the storm-surge responsible can be estimated. By dating such a deposit, we can add an extreme event to our observational record. The question then is, how can we date storm-surge sediments?

Fig. 1.1. Storm-surge sediment found within coastal sand dunes near Heemskerk, North Holland. *Left*: OSL sampling at a section containing the storm-surge unit, visible across the middle of the photo. *Upper right*: Sampling a frozen bluff-face section. The storm-surge unit truncates the whole section, just above head-height. *Lower right*: Detail of the shell-rich storm-surge deposit. Photographs by the author.

This thesis investigates a modern technique for dating sedimentary deposits. It is called Optically Stimulated Luminescence (OSL) dating (but also Optical dating, or Luminescence dating), and can estimate the age of a sample by measuring the amount of ionizing radiation absorbed by mineral grains over the burial period. There are several qualities of OSL dating that make it potentially useful for dating storm-surge deposits. In particular, OSL dating can directly date the sediment (grains of quartz or feldspar), rather than other material trapped within it; furthermore, it can be used to date sediments over a wide age range of between ~10 and over 100,000 years old. While OSL dating is an established and proven technique for some environments, applying OSL dating to storm-surge sediments requires certain methodological improvements.

1.2 OSL dating

The OSL mechanism in quartz is best described using an energy-band diagram (Fig. 1.2). There are two bands of electron energies that are relevant in this model, corresponding to the quantized energy states in which electrons are allowed to exist. The lower energy level is known as the valence band; electrons in this band have the highest energy permitted while linked to an individual atom (usually residing in the outer-most, 'valence' electron shell). The second band of interest is the conduction band, which represents the energy required for an electron to escape from the bond with an individual atom. Electrons in the conduction band are free to move around the crystal, becoming charge carriers. Between the valence band and conduction band lies the 'forbidden gap', which in a pure atomic lattice contains no permitted electron energy states.

The existence of the forbidden gap is the defining feature of a semiconductor (e.g. quartz, SiO_2); electric charge can only be carried through the material if electrons receive enough energy to escape the valence band. One way for this to occur is through the absorption of ionizing radiation. Within sediments, mineral grains are exposed to ionizing radiation from the decay of naturally occurring radioactive isotopes. This radiation may be absorbed by the quartz crystal, causing the excitation of a valence-band electron to the conduction band, and the creation of a 'hole' in the valence band. By the reshuffling of electrons in the (mostly filled) valence band, the hole is able to move and thereby carry charge. This process may be followed by relaxation, in which the excited electron recombines with a hole and returns to its equilibrium condition. Recombination involves a release of energy, usually as heat, but under some pathways the energy is released as a photon, providing a luminescence signal that can be measured.

Natural crystals contain localized energy levels within the band gap, caused by defects in the crystal lattice. These defects can be caused by missing atoms (e.g. an Si or O vacancy in the SiO_2 lattice), or by trace elements (e.g. Al, Ti, Fe) which replace the Si or occupy spaces in the crystal structure. These defects are responsible for the localized energy levels, which trap electrons from the conduction band or holes from the valence band. The more radiation absorbed by the crystal, the more electrons are trapped in the localized energy states. The charge contained within these traps may therefore indicate the amount of ionizing radiation received by the material, and this charge can be probed by luminescence measurements. The stability of the trapping centres is dependent on their depth below the conduction band (measured in eV). Electrons can be liberated from a trapping centre if provided with enough energy (e.g. heat or light), and can then recombine with a hole via the conduction band. For a trapping centre to be useful for OSL dating, two conditions must be met: it should have a sufficiently large thermal trap depth, such that the trapped charge will not escape at environmental temperatures; and the trap should be sensitive to light, so that a small amount of sunlight provides enough energy to empty the trap. In quartz, the trap which most satisfies these conditions is that associated with the 'fast' OSL component (OSL_F in Fig. 1.2).

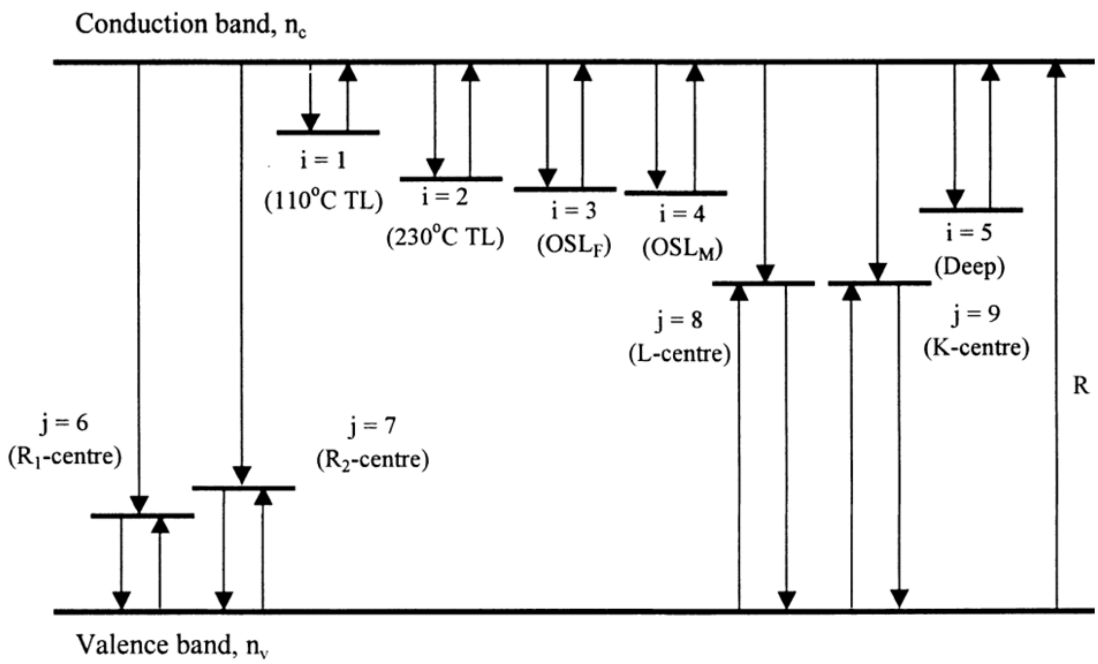

Fig. 1.2. An energy-band model for explaining luminescence in quartz. This model contains two optically sensitive electron traps (OSL_F and OSL_M), corresponding to the fast and medium OSL components, and three other electron traps not sensitive to optical stimulation (110ºC TL, 230ºC TL and Deep). There are four hole-trapping centres, of which only one produces a luminescence signal upon recombination (L-centre). From Bailey (2001) [Towards a general kinetic model for optically and thermally stimulated luminescence of quartz, Radiation Measurements 33, 17-45].

To obtain an OSL age, two key pieces of information are required – the total radiation dose which the grains have received, called the 'equivalent dose' and measured in grays (Gy); and the rate at which radiation is absorbed, measured in grays per thousand years (Gy ka^{-1}). The age equation is straightforward:

$$\text{Age (ka)} = \frac{\text{Equivalent dose, } D_e \text{ (Gy)}}{\text{Dose rate, } \dot{D} \text{ (Gy ka}^{-1}\text{)}}$$

To determine D_e, the quartz sample is illuminated using blue LEDs, providing enough energy to liberate electrons in the OSL_F and OSL_M traps. Some of the free electrons recombine at the L-centre, producing a luminescence signal (Fig. 1.3a). By measuring the OSL signal following a series of artificially given radiation doses, the 'natural' OSL signal can be used to estimate D_e (Fig. 1.3b).

The OSL measurement protocol includes a number of internal checks on the robustness of the D_e determination. These include a repeated OSL measurement of the signal induced by an artificially given ('regenerative') dose, also called 'recycling'; and an OSL measurement made without prior irradiation, the value of which is called the 'recuperation'.

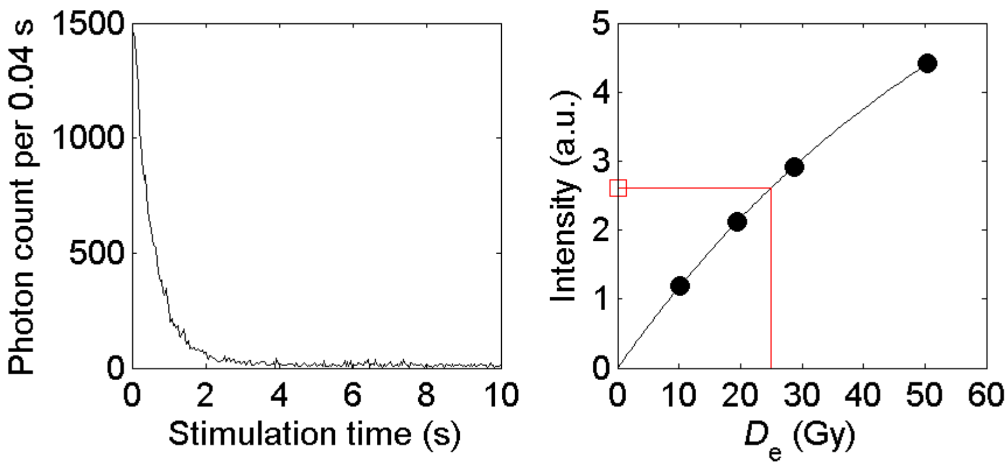

Fig. 1.3. (a) Example luminescence signal observed during 10 s of continuous optical stimulation. The curve consists of a number of overlapping, exponentially decaying functions, relating to a particular OSL component ('fast', 'medium', and several 'slow' components). The components are named according to their relative rates of decay under optical stimulation. (b) By comparing the intensity of the OSL signal (square) to that derived from a number of artificially given radiation doses, the equivalent dose (D_e) can be determined.

The dose rate to the quartz over the burial period must also be calculated. For the samples presented in this thesis, the dose rate is determined using high-resolution gamma spectrometry. Gamma spectrometry uses the energy spectrum of the gamma emission from a sample to identify the radioactive elements; the concentrations of these elements are used to calculate the dose rate applicable to the quartz grains.

1.3 Key problems to overcome

1.3.1 Partial bleaching

Strictly speaking, it is not the ‘age’ that is estimated in OSL dating, but the length of time since the mineral grains were last exposed to sunlight. It is sunlight that resets the OSL signal (during transport and deposition of the grains). When the grains are buried, they are not exposed to light, and the OSL signal can be built up through the absorption of naturally occurring background radiation. The amount of sunlight that the grains receive during transport and deposition is therefore crucial – too little and the OSL signal will not be fully reset, leading to an overestimate of the age. Full resetting of the signal takes some tens of seconds of bright sunlight, which is not a problem if the grains are transported by wind, or deposited on a beach. In fact, OSL dating has been shown to work very well for these depositional environments. On the other hand, if sunlight is less bright, for example if the grains are transported underwater, then the length of exposure required is necessarily much longer. It is common that under such conditions many grains do not receive enough light to reset the signal, and such samples are considered to be *partially bleached*.

It will be apparent that partial bleaching may occur in storm-surge deposits, for a couple of reasons. Firstly, storm-surge deposition is a rapid process, leaving little time for signal resetting. Secondly, deposition may occur at night, when there is insufficient ambient light. Partial bleaching is not just a problem for storm-surge sediment, but affects sediments in most fluvial or glaciofluvial environments. There is large amount of literature on the topic, and it provides a running theme throughout this thesis. Chapters 2, 3 and 6 are entirely devoted to dealing with partial bleaching; Chapters 4 and 5 also contain sections devoted to the topic.

1.3.2 Heterogeneity of the beta dose

During the burial period, quartz grains receive a radiation dose from their surroundings. This dose comes from radioactive nuclides in the sediments, principally from ^{40}K, and from the U and Th decay chains. While U and Th are present in low quantities, ^{40}K is abundant in sediment, and typically provides over half of the radiation dose. However, potassium is not distributed evenly in sandy sediment, but is concentrated in grains of potassium feldspar. This is significant, because the beta radiation emitted by ^{40}K has a very short range, on the order of 1 mm in sediment. It has been suggested that when the proportion of K-feldspar in the sediment is small, then the radioactive ^{40}K is unevenly dispersed, meaning that different quartz grains receive different radiation doses.

The effects of beta dose heterogeneity are difficult to quantify, but it is necessary to understand this process in order to interpret OSL measurements correctly. This thesis investigates beta-dose heterogeneity with two techniques. An experimental simulation is conducted in which artificially produced ^{24}Na is used to mimic the radioactive properties of ^{40}K. To complement the experiment, a set of numerical simulations of the same experiment are performed (Chapter 7). Monte Carlo simulations are also used in Chapter 5 to quantify the effect of shells on the beta dose; this simulation permits the direct dating of shell-rich deposits for the fist time.

1.3.3 Grain-to-grain variability in multi-grain aliquots

There are numerous reasons why the measured dose to quartz may vary between different grains of the same sample. Some of these have been mentioned above (partial bleaching and beta-dose heterogeneity). In this thesis and elsewhere, efforts to understand this natural variation are focused at the single-grain level. However, most OSL dating studies are carried out not on single grains, but on small aliquots (subsamples) containing tens to hundreds of grains. This leads to a relatively small but nonetheless important question: how should we convert information on single-grain variability for use in dating studies with multi-grain aliquots? This topic is addressed in Chapter 4.

1.4 Relevance

The majority of this thesis is devoted to the development of methods which will enable OSL to be used confidently to determine the age of storm-surge deposits. These methods have been applied to storm-surge sediment from the Netherlands, but the potential impact of these methods is much wider. Storm surges present a very real threat in many parts of the world, a threat that is likely to increase given a future rise in sea level; Tsunamis present similar questions to scientists and policy makers, and leave deposits which present the same issues for dating. It is hoped therefore, that the methods developed in this thesis will be used on a wide range of samples, thereby extending applicability of OSL dating.

1.5 Thesis outline

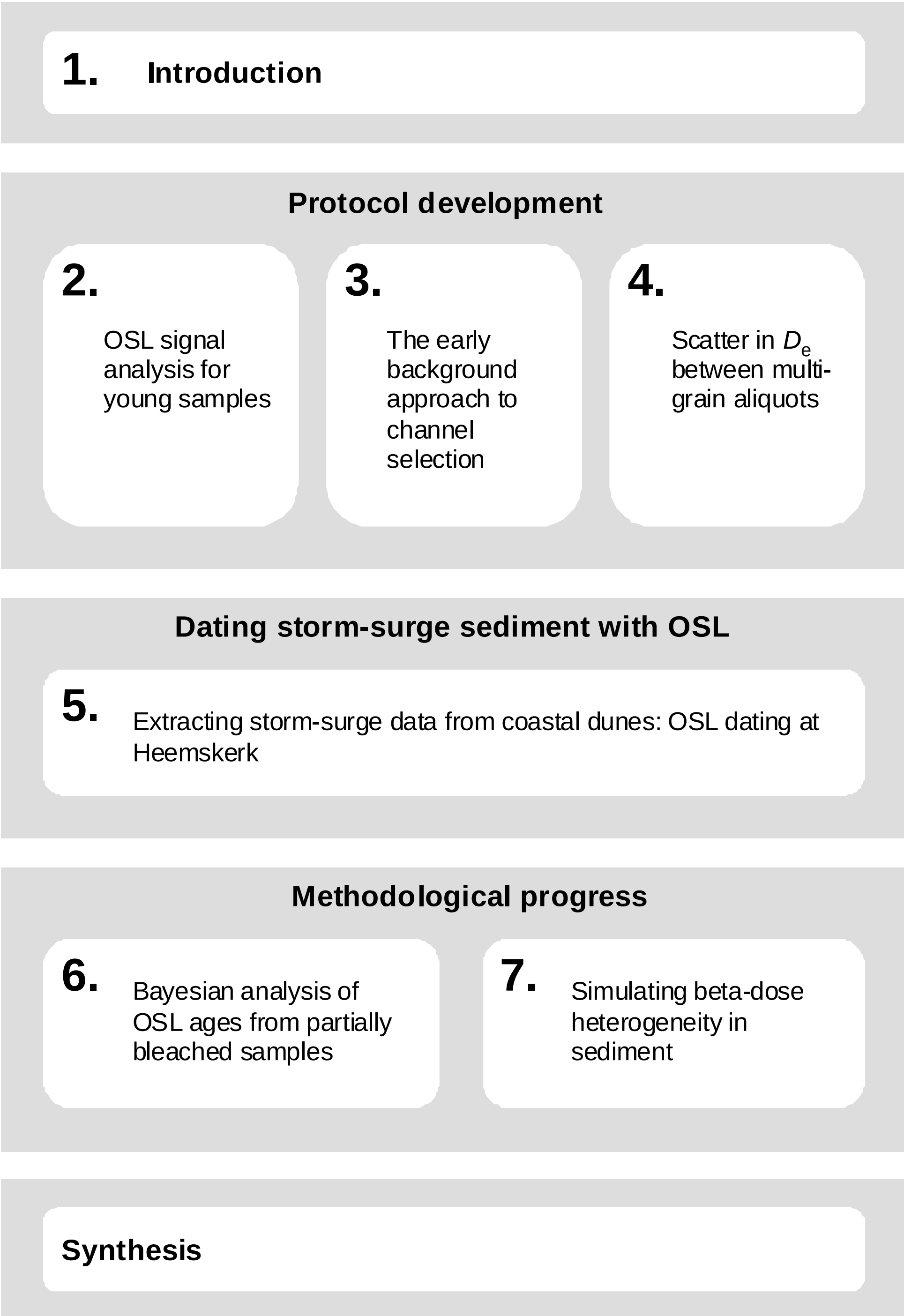

Chapter 2

Optically stimulated luminescence dating of young quartz using the fast component

Alastair C. Cunningham, Jakob Wallinga
Published in Radiation Measurements 44 (2009), 423-428.

Abstract

We have attempted to isolate the fast component of the quartz Optically Stimulated Luminescence (OSL) signal using a curve-fitting procedure. By pre-determining the decay constants, the procedure is simple enough to be scripted, allowing a large number of aliquots to be processed. A Monte Carlo error routine is used, in which simulated decay curves are fitted with several exponentials, which vary in their decay rates according to the measured distributions of fast and medium component decay rates. The derived error term is closely related to the intensity of the fast component signal, but is also influenced by the degree of similarity between the equivalent doses of the fast and medium OSL components. There are potential advantages in using this procedure to date both well-bleached and partially bleached quartz, of any depositional age.

2.1 Introduction

Since the introduction of the single aliquot regenerative dose (SAR) protocol in the late 1990's, the optically stimulated luminescence (OSL) signal of quartz has been widely used to date Late Quaternary sediments. OSL is particularly useful for dating young sediments (those less than 1000 years old), due to the lack of alternative dating methods: plateaux in the radiocarbon calibration curve make radiocarbon difficult to use on samples less than c.500 years old, even if suitable organic material can be found; ^{210}Pb and ^{137}Cs have upper age limits of 120 and 50 years respectively, and are restricted to fine-grained deposits. Given the near ubiquity of quartz (or feldspar) in sedimentary environments, OSL dating has the potential to bridge the gap between these methods and provide chronological continuity.

There are two oft-cited problems with dating of young quartz. The first is the relatively poor signal-to-noise ratio encountered. Despite this, OSL on young quartz has been shown to agree with independently evaluated ages provided by historical maps (Ballarini et al., 2003) and by radiometric methods (Madsen et al., 2005). A more likely source of error comes through partial bleaching, which is of particular concern for young samples where a weak signal can be swamped by any residual signal present at the time of deposition.

Efforts to overcome partial bleaching have two complimentary routes. Statistical methods have been designed to select the youngest parts of the equivalent dose (D_e) distribution (Galbraith et al., 1999). However, all statistical approaches are dependent on at least some of the dose distribution returning the true burial dose. Much effort has therefore been directed at isolating the most rapidly bleached 'fast' component of the OSL signal. The fast component is most likely to be well-bleached, is geologically stable over millions of years, and is less susceptible to thermal transfer of charge (Wintle and Murray, 2006). Singarayer and Bailey (2004) showed that experimental isolation of the fast component is possible through raised-temperature infrared (IR) stimulation. However, subsequent IR dating protocols which use either direct IR stimulated luminescence or IR depletion (e.g. Jain et al., 2005) are only applicable to older samples, since the low IR stimulation energy elicits a very slow OSL response with poor signal-to-noise ratios.

Other approaches to fast-component separation have focused on curve-fitting of the OSL data, in which the data is assumed to be the sum of multiple OSL components (such as the ultrafast, fast, medium and slow components). Such approaches assume the superposition of non-interactive first-order processes, such that their combined signal (i.e. the OSL data) can be separated mathematically.

Several authors (e.g. Rhodes et al., 2005; Li and Li, 2006; Choi et al., 2006) have applied the curve-fitting approach to Linearly Modulated (LM) OSL data, in which the intensity of stimulation light is ramped linearly throughout the measurement period. Under this stimulation mode, the OSL signal over the measurement time appears as a series of overlapping peaks corresponding to different OSL components. However, LM-OSL gives relatively poor signal-to-noise ratios, because the stimulation intensity is sub-maximum until the final time-interval, while at least part of the instrumental noise is independent of stimulation power. The signal-to-noise ratio is higher under (maximum intensity) Continuous Wave (CW) OSL, in which the stimulation light is held at a constant intensity for the duration of the measurement. Moreover, Wallinga et al. (2008) have shown that LM-OSL actually offers no improvement on CW-OSL in the degree of component separation, because the degree of component separation is independent of stimulation light intensity.

Some attempts at fast component isolation have previously been made through curve-fitting the CW-OSL signal (e.g. Watanuki et al., 2005), which is the method we use here. However, no fitting approach has gained widespread use for dating purposes, perhaps because of computational difficulties; the fitting of multiple exponential functions is an ill-posed problem, in the sense that there are many possible solutions (Istratov and Vyvenko, 1999). Nevertheless, here we make use of the CW-OSL signal so as to maximise the signal-to-noise ratio. Our curve-fitting procedure uses pre-defined decay constants, which reduces complexity and increases the speed of data analysis. A Monte Carlo protocol is employed to generate an appropriate error term for the fast component D_e.

2.2 Methods

2.2.1 Sample and measurement details

The curve fitting procedure is tested using two samples from the Netherlands: a well-bleached sample NCL-1108011 from a coastal dune in North Holland, and a poorly bleached sample NCL-3505030 from a fluvial channel bar deposit in the central Netherlands. Both samples are approximately 250 years old. Quartz grains 212-250 µm in diameter were extracted from the samples using standard laboratory procedures. A SAR protocol was used. For sample NCL-1108011, aliquots were preheated at 180ºC for 10 s, followed by OSL measurement at 125ºC. The cutheat following the test dose was 180ºC, and a 200ºC OSL bleach was used at the end of each SAR cycle (Murray and Wintle, 2003). For sample NCL-3505030 the OSL readout was at 125ºC, preheat and cutheat were at 200ºC, the OSL bleach was at 220ºC, and an additional 175ºC IR bleach prior to each OSL readout was used to minimise the feldspar contribution to the OSL signal (Wallinga et al., 2002).

Since the OSL signals were relatively weak, our SAR protocol contained two unusual features: we used a single regenerative dose of 2.24 Gy, and a relatively high test dose also of 2.24 Gy. These adaptations were designed to increase the number of aliquots processed, and to reduce the uncertainty of the sensitivity-corrected OSL signal. Assuming that the true dose response curve for our samples conforms to a saturating exponential function with a characteristic dose (D_0) of 80 Gy, then our use of a single regenerative dose implies a systematic overestimate of D_e of ~1 % (equation and definitions can be found in Duller (2007)). This value is insignificant compared with other sources of error, and can be corrected for if necessary.

Measurements were carried out on a Risø TL-DA-15 reader, using 470 nm blue diodes with a power at the sample position of ~35 mW cm^{-2}. Irradiation was with a $^{90}Sr/^{90}Y$ beta source providing a dose rate of 0.028 Gy s^{-1} to quartz grains at the sample position. The IR diodes emitted at a wavelength of 875 nm and power of ~116 mW cm^{-2}. A 7.5 mm Hoya U340 detection filter was used.

2.2.2 Component characterisation

The presence of multiple optically sensitive electron trap types in quartz has been well established (Bailey et al., 1997; Jain et al., 2003; Singarayer and Bailey, 2003). Assuming first-order kinetics (no re-trapping), then under continuous wave stimulation the OSL response $I_{cw}(t)$ can be described as the sum of N exponentials:

$$I_{CW}(t) = \sum_{i=1}^{N} n_{0,i}\, \alpha_i \exp(-\alpha_i t)$$

Each exponential corresponds to a component (fast, medium, slow etc.) with a decay rate under optical stimulation α_i (equal to photoionisation cross-section of component i multiplied by stimulation intensity), and initial trap concentration n_0 at t = 0 which can be used to define the D_e. Under CW-OSL, a constant background is also present. Deconvoluting multiple exponentials is computationally expensive due to the number of free parameters, and is highly sensitive to noise. However, if the number of components is known, and the decay rate parameters α_i are fixed, then the procedure becomes simple enough for routine analysis.

We have attempted to characterize the decay rates of the fast and medium components in each of our samples. For this, 32 aliquots of each sample were given a relatively large dose of 30 Gy, followed by the preheat and OSL steps described in section 2.2.1. Each decay curve was then fitted using Origin 7.5, which was able to describe most curves adequately using 3 components plus background. The average decay rate ratios for the 3 components are 1:0.2:0.01, similar to the relative cross-sections of the fast, medium and slow2 components of Jain et al. (2003), and they are henceforth referred to as the fast, medium and slow components. The distribution of decay rates for sample NCL-1108011 is shown in Fig. 2.1, which plots the fast component decay rate against that of the medium component.

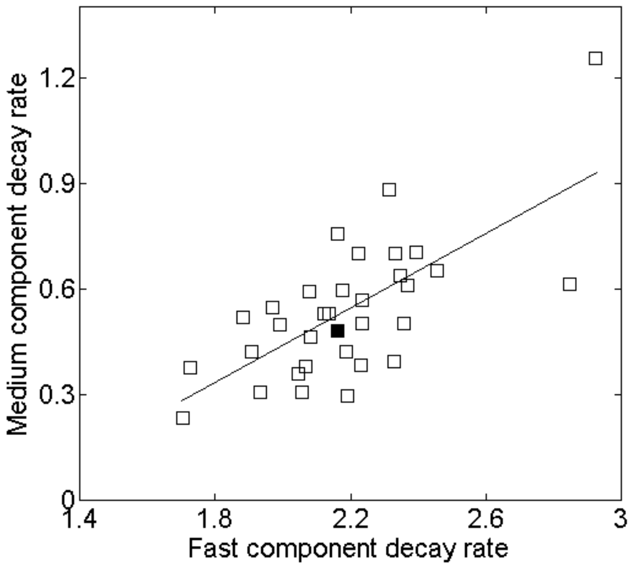

Fig. 2.1. Fast versus medium component decay rates for 32 aliquots of sample NCL-1108011 (open squares), based on curve-fitting the OSL signal after a 30 Gy dose. The weighted average (filled square) is used to calculate the D_e for all aliquots (section 2.3). The (un-weighted) linear fit (solid line) is used in generating the error term (section 2.4.2).

2.2.3 Calculation of D_e

Using the measured decay rates of Fig. 2.1, the average decay rates for the fast and medium components were then used to fit a multiple exponential function to each decay curve of the SAR cycle, using a simple least-squares routine (after subtraction of the separately measured background, see section 2.2.4). The slow component was treated differently, with the decay rate defined separately for each decay curve by fitting a single exponential plus background to the last 25 s of the 40 s OSL decay. This was required because the decay rate of the slow component varied over different OSL steps of the SAR cycle, most likely because it in fact contains several different slow components which bleach at different rates. D_e (and the repeat point) can be calculated after fitting each OSL decay curve. The OSL signal due to natural irradiation and the dose response curve for one aliquot are shown in Fig. 2.2 (a) and (b).

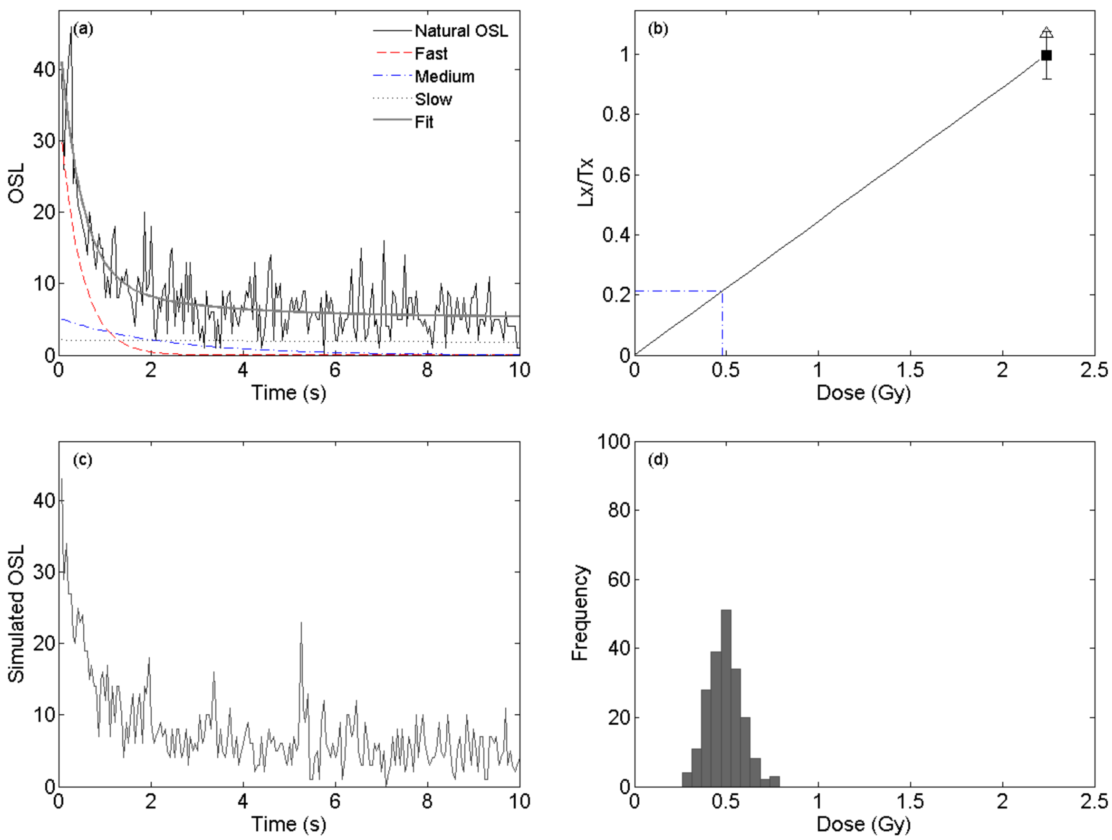

Fig. 2.2. D_e and error term calculation for one aliquot of partially bleached sample NCL-3505030: (a) The OSL signal following natural irradiation, fitted with 3 exponentials with pre-defined decay rates, plus a background (not shown). (b) The dose response curve, with dashed line indicating D_e, and with the recycle point also shown (open triangle). (c) An example simulation of the OSL signal due to natural irradiation. (d) Histogram of D_e values calculated using the Monte Carlo error routine.

2.2.4 Calculation of error

There are two principal sources of error in the fitting routine described above (assuming the model of quartz OSL stated in section 2.2.2 is adequate). The first comes from noise in the OSL data. The second comes from the assumptions introduced about the decay rates, i.e. the difference between the true fast and medium component decay rates for an OSL decay curve, and the average decay rate values which are used to fit the data. To take both these factors into account, we used a Monte Carlo error routine based on repeated curve fitting of simulated data.

Simulation of OSL decay curves

Simulation of decay curves was carried out using the original 3-component fit to the OSL data, which was added with simulated instrumental noise drawn randomly from a measured distribution. This distribution was obtained beforehand, by measuring the OSL of a number of blank discs at the same temperature as the SAR OSL. Each simulated curve was then randomized using the Poisson distribution. Figure 2.2(c) shows an example simulation of an OSL decay curve due to natural irradiation.

Curve fitting of simulated datasets

Each set of simulated decay curves for an aliquot was put through the fitting routine of section 2.2.3, but rather than using the average decay constants that were used for the central D_e values, new decay constants for the fast and medium components were drawn from a simulation of the measured distribution of Fig. 2.1. This distribution was modelled using the (as measured) normal distribution of fast component decay rates, and the relationship between fast and medium component decay rates ($r^2 = 0.5$). A residual was then added for the medium component based on the measured normal distribution of residuals.

Once new decay rates had been specified, the simulated decay curves could be fitted to obtain a new value of D_e. Repetition of this process (simulation of decay curves; selecting new decay rates; curve fitting) a large number of times (e.g. 200) leads to a distribution of Monte Carlo D_e values centred on the mean (Fig. 2.2(d)), from which the standard deviation provides the error term.

2.3 Results

The results of the CW-OSL fitting routine can be seen in Fig. 2.3, where it is compared with more standard methods of generating D_e for the two samples used. In Fig. 2.3(a), the curve-fitting approach to D_e is plotted against that derived from the Late Background (LBG) method for poorly bleached sample NCL-3505030. LBG has been the standard approach used in the literature, in which the first part of the OSL decay curve (e.g. 0.00-0.30 s) is used to define the dose, after subtracting a background taken from the last 4 seconds of stimulation. It can be seen that the curve-fitted fast component tends to give a lower D_e, especially for aliquots which yield imprecise estimates (Fig. 2.3(a)), and it always returns a larger error term (Fig. 2.3(b)). This relationship is to be expected, since the signal in the LBG method contains significant amounts of medium and slow components which are more likely to be partially bleached. Consequently, the LBG method returns a precise (but possibly inaccurate) D_e for each aliquot even when there is little or no fast component.

Figure 2.3(d) compares the curve fitting approach (for the same sample) to an improved method of OSL decay curve integrated time-interval (channel) selection suggested by Ballarini et al. (2007), in which the initial OSL signal is subtracted with a background taken from the channels immediately following. Here we have extended the initial signal length (0.00-0.80 s with background 0.80-1.60 s) to overcome weak signals. The early background (EBG) modification is designed to maximize the proportion of fast component contained in the net OSL signal, and indeed correlates well with the curve-fitted fast component estimate (Fig. 2.3(d)). The error term using EBG also correlates very well with the curve-fitting approach for aliquots returning a relatively precise D_e (Fig. 2.3(e)), although still gives smaller errors for aliquots returning a relatively imprecise D_e.

For the well-bleached sample NCL-1108011, estimated D_e is very similar whether obtained by curve-fitting or EBG (Fig. 2.3(g)) although there is perhaps a tendency for curve-fitting to increase D_e for aliquots which give less precise estimates. The error terms are also closely related, principally because this sample has a dominant (and well-bleached) fast component. Since this sample is well-bleached, there is little difference between the EBG and LBG methods, so no comparison between the curve-fitted fast component D_e and LBG D_e is shown.

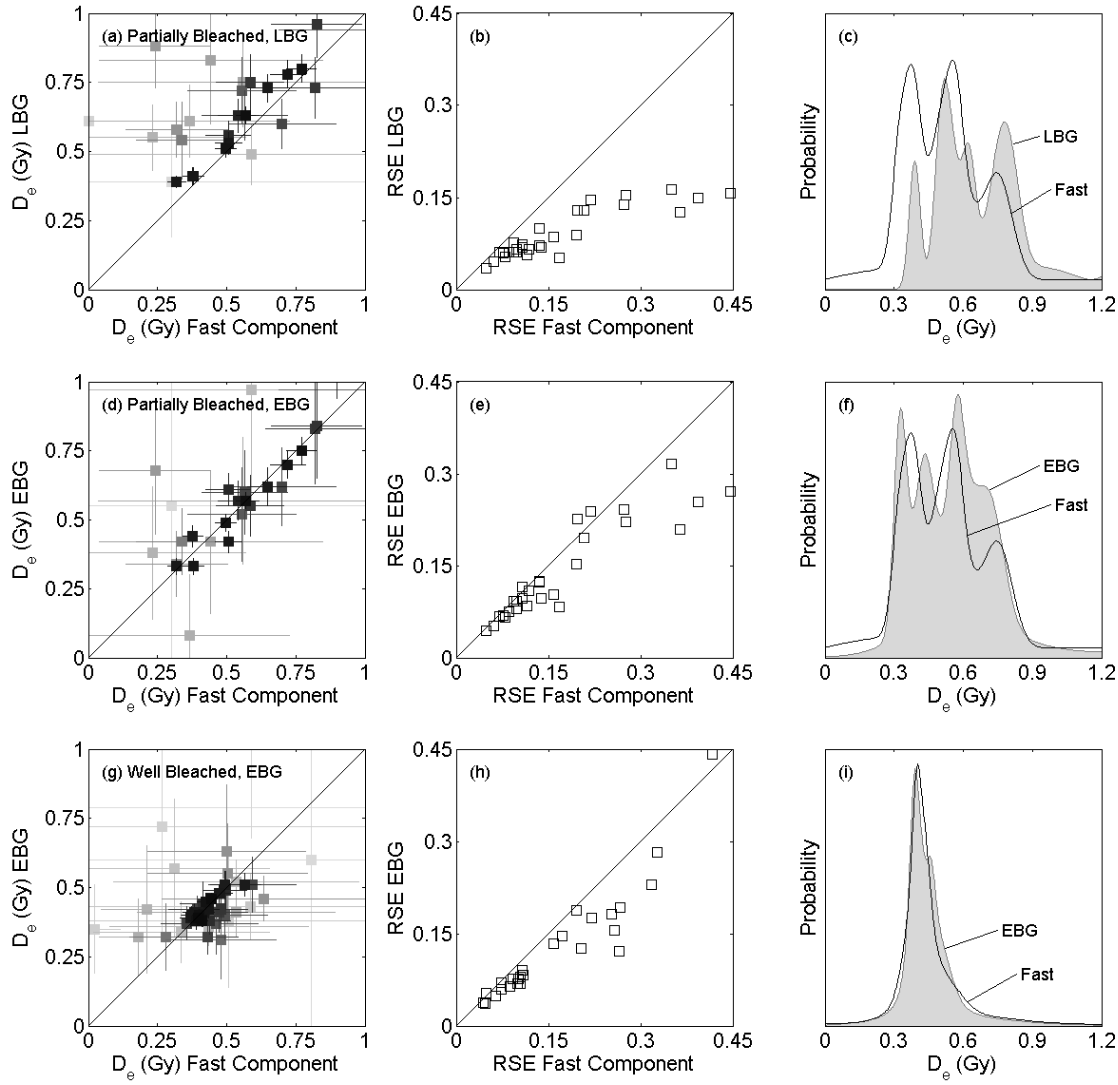

Fig. 2.3. Results of the curve-fitted fast component D_e compared to standard channel selection methods. The top row of graphs (a, b, and c) show the fast component versus the late background (LBG) method for partially bleached sample NCL-3505030; the middle row (graphs d, e and f) compare the fast component of the same sample with the early background (EBG) method; the bottom row (graphs g, h and i) show the fast component versus EBG for well-bleached sample NCL-1108011. Each row contains in the left hand column: a D_e comparison between the two methods indicated in the graph, with markers and 1σ error bars shaded in proportion to the relative error on their fast component D_e; in the middle column: a likewise comparison of the relative error; in the right hand column: probability density functions (PDFs), created using only those aliquots which passed acceptance criteria (recuperation of less than 0.05 Gy, recycling point within 10 % of unity). For channel selection methods (LBG and EBG), D_e was calculated as outlined by Duller (2007) with Monte Carlo error terms, after measurement errors were estimated using the method of Li (2007).

2.4 Discussion

The curve-fitting procedure outlined above appears to give the results which could be expected if:

a) The assumed model of the OSL process provides an adequate reflection of reality.
b) The curve-fitting procedure is performing as intended.

After testing the curve-fitting procedure on a well-bleached sample and a partially bleached sample, there seem to be potential benefits of using it to date young quartz. Firstly, the D_e obtained using this method is approximately that of the fast component, so is more likely to indicate the true burial dose than usual background subtraction methods, which may yield D_e values from mixes of the fast and the slower components. Secondly, the error term is directly related to the signal intensity of the fast component, and has little relation to the signal intensities of other components. This contrasts with background subtraction methods, in which a strong medium or slow component signal can lead to a precise but inaccurate D_e estimate, even when there is no fast component present (although this is less of a problem with EBG).

Besides assessing the influence of background noise on D_e, the Monte Carlo error term also includes uncertainty derived from changing the decay constants. This has an agreeable implication for dating of partially bleached samples. For aliquots where all components indicate the same burial dose, artificially altering the decay rate parameters has little or no effect on D_e. By contrast, with aliquots for which the fast and medium component have different true palaeodoses (e.g. partially bleached aliquots), the D_e will be sensitive to a change in the decay rates. In other words, partially bleached aliquots will tend to generate a larger error term than well-bleached aliquots. While the occurrence of identical D_e values, calculated using the fast or the medium components, is not necessarily the harbinger of a well-bleached aliquot, it may nonetheless offer an indication that sufficient bleaching occurred (e.g. Bailey and Arnold, 2006). Because the error term is affected by the difference between the fast component D_e and the medium component D_e, the resulting curve-fitted D_e distribution should have an inbuilt bias towards well-bleached aliquots. Nonetheless, the effect is small in comparison to the error derived from the signal-to-noise ratio, at least for young samples such as those examined here.

Overall, the error term derived from the curve-fitting procedure is larger than standard methods for almost all aliquots measured. However, this need not imply a less precise palaeodose estimate, since in contrast to channel-selection methods, the curve-fitted fast component D_e distribution is dominated by the most suitable aliquots for dating. This may be true even for well-bleached samples; for sample NCL-

1108011 used here (Fig. 2.3(g-i)), overdispersion of D_e was reduced from 7.0 ± 2.4 % using EBG to 2.2 ± 4.0 % using the curve-fitted fast component. A reduction in overdispersion may reduce the number of apparent dose populations in a D_e distribution, making it simpler to apply and interpret the results of a statistical age model. Furthermore, since the Monte Carlo error routine provides a histogram of the spread in D_e for each aliquot, there is no need to assume that the spread is normally distributed. The histograms of each aliquot could potentially be added together to form a PDF, which could then be used as the input for an age model.

While scripting large parts of the procedure reduces much of the usual tedium of curve fitting, there are some additional steps required prior to analysis. The first is to identify the distribution of decay rates for the fast and medium components by deconvoluting the OSL decay after a high dose. Optical decay rates may vary due to a number of factors, such as grain size and grain opacity, even if we assume the fast and medium components are common in all samples. Furthermore, if the stimulation light intensity is non-uniform across the disc, then the number of bright grains on an aliquot, and their position, may also contribute to variability. It is therefore difficult to define the number of aliquots necessary to get a representative distribution of decay rates. We found at least 30 were required. This is a slightly tedious number of deconvolutions, but the resulting distribution can be applied to many samples with the same source material and grain size (i.e. calculated on a site-by-site basis).

The distribution of instrumental background was also pre-determined. Like the component characterization, it is machine-specific, but can also change over time due to disturbance and settling of the photomultiplier tube. It is also possible that instrumental background is different with grains on the disc, although Li (2007) found otherwise. Even so, it would require a large difference to significantly affect D_e.

There is room to improve some aspects of the program. For example, fitting could be streamlined by using only the first 10 seconds of the decay curve; curve simulation might be better achieved using a smoothing algorithm rather than fitting. For a rigorous assessment of the method, testing will be required on full sedimentary sequences with tight age-control. Nevertheless, the program in its current form has given results which would be expected from a true fast-component protocol, while simultaneously permitting the swift analyses of a large number of aliquots. The combination of these aspects is likely to be of great benefit for quartz OSL dating.

Although the procedure outlined here was specifically designed for young samples, it may be advantageous to use a similar method to date older samples too. For example, there are doubts over the stability of a medium and/or slow component, giving a further reason (besides partial bleaching) for obtaining a fast component signal. In fact, for older samples the procedure could be simplified, since the initial high dose step of section 2.2.2 would already have been carried out during construction of the dose response curve. It would then be simple enough to tailor the decay constants to each aliquot. Applying this method to single grains would be equally possible, with the added advantage that numerous decay curves could be obtained by giving a high dose to just a few aliquots.

2.5 Conclusion

We have presented a curve fitting procedure for CW-OSL data for dating young quartz. By pre-defining key fitting parameters, the algorithm constructed is simple enough for processing the large number of aliquots necessary for dating young samples. There are three key improvements over standard channel selection methods:

1. The calculated D_e is approximately that of the fast component.
2. The error term is closely related to the intensity of the fast component signal.
3. The error term contains a bias towards well-bleached aliquots. Partially bleached aliquots return a larger error term if the equivalent doses of the fast and medium component differ.

The method is potentially beneficial for dating both well-bleached and partially bleached samples. While it has been designed with young quartz in mind, it could also be used with little modification to improve the accuracy of dating older samples.

Acknowledgments

We would like to thank an anonymous reviewer for helpful comments on the manuscript. The authors are supported by an NWO innovative research grant (DSF7552).

References

Bailey, R.M., Arnold, L.J. 2006. Statistical modelling of single grain quartz D-e distributions and an assessment of procedures for estimating burial dose. Quaternary Science Reviews 25, 2475-2502.

Bailey, R.M., Smith, B.W., Rhodes, E.J. 1997. Partial bleaching and the decay form characteristics of quartz OSL. Radiation Measurements 27, 123-136.

Ballarini, M., Wallinga, J., Wintle, A.G., Bos, A.J.J. 2007. A modified SAR protocol for optical dating of individual grains from young quartz samples. Radiation Measurements 42, 360-369.

Ballarini, M., Wallinga, J., Murray, A.S., van Heteren, S., Oost, A.P., Bos, A.J.J., van Eijk, C.W.E. 2003. Optical dating of young coastal dunes on a decadal time scale. Quaternary Science Reviews 22, 1011-1017.

Choi, J.H., Duller, G.A.T., Wintle, A.G., Cheong, C.S. 2006. Luminescence characteristics of quartz from the Southern Kenyan Rift Valley: Dose estimation using LM-OSL SAR. Radiation Measurements 41, 847-854.

Duller, G. 2007. Assessing the error on equivalent dose estimates derived from single aliquot regenerative dose measurements. Ancient TL 25, 15-24.

Galbraith, R.F., Roberts, R.G., Laslett, G.M., Yoshida, H., Olley, J.M. 1999. Optical dating of single and multiple grains of quartz from jinmium rock shelter, northern Australia, part 1, Experimental design and statistical models. Archaeometry 41, 339-364.

Istratov, A.A., Vyvenko, O.F. 1999. Exponential analysis in physical phenomena. Review of Scientific Instruments 70, 1233-1257.

Jain, C., Murray, A.S., Botter-Jensen, L., Wintle, A.G. 2005. A single-aliquot regenerative-dose method based on IR (1.49 eV) bleaching of the fast OSL component in quartz. Radiation Measurments 39, 309-318.

Jain, M., Murray, A.S., Botter-Jensen, L. 2003. Characterisation of blue-light stimulated luminescence components in different quartz samples: implications for dose measurement. Radiation Measurements 37, 441-449.

Li, B. 2007. A note on estimating the error when subtracting background counts from weak OSL signals. Ancient TL 25, 9-14.

Li, S.H., Li, B. 2006. Dose measurement using the fast component of LM-OSL signals from quartz. Radiation Measurements 41, 534-541.

Madsen, A.T., Murray, A.S., Andersen, T.J., Pejrup, M., Breuning-Madsen, H. 2005. Optically stimulated luminescence dating of young estuarine sediments: a comparison with Pb-210 and Cs-137 dating. Marine Geology 214, 251-268.

Murray, A.S., Wintle, A.G. 2003. The single aliquot regenerative dose protocol: potential for improvements in reliability. Radiation Measurements 37, 377-381.

Rhodes, E.J., Singarayer, J.S., Raynal, J.P., Westaway, K.E., Sbihi-Alaoui, F.Z. 2006. New age estimates for the Palaeolithic assemblages and Pleistocene succession of Casablanca, Morocco. Quaternary Science Reviews 25, 2569-2585.

Singarayer, J.S., Bailey, R.M. 2003. Further investigations of the quartz optically stimulated luminescence components using linear modulation. Radiation Measurements 37, 451-458.

Singarayer, J.S., Bailey, R.M. 2004. Component-resolved bleaching spectra of quartz optically stimulated luminescence: preliminary results and implications for dating. Radiation Measurements 38, 111-118.

Wallinga, J., Murray, A.S., Botter-Jensen, L. 2002. Measurement of the dose in quartz in the presence of feldspar contamination. Radiation. Protection Dosimetry 101, 367-370.

Wallinga, J., Bos, A.J.J., Duller, G. 2008. On the Separation of quartz OSL signal components using different stimulation modes. Radiation Measurements 43, 742-747.

Watanuki, T., Murray, A.S., Tsukamoto, S. 2005. Quartz and polymineral luminescence dating of Japanese loess over the last 0.6 Ma: Comparison with an independent chronology. Earth and Planetary Science Letters 240, 774-789.

Wintle, A.G., Murray, A.S. 2006. A review of quartz optically stimulated luminescence characteristics and their relevance in single-aliquot regeneration dating protocols. Radiation Measurements 41, 369-391.

Chapter 3

Selection of integration time-intervals for quartz OSL decay curves

Alastair C. Cunningham, Jakob Wallinga
Published in Quaternary Geochronology 5 (2010), 657-666.

Abstract

In quartz optically stimulated luminescence (OSL) dating protocols, an initial integral of the OSL decay curve is used in the calculation of equivalent dose, once a background integral has been subtracted. Because the OSL signal commonly contains a number of exponentially decaying components, the exact choice of time intervals used for the initial-signal and background integrals determines the composition of the net signal. Here we investigate which combination of time-intervals will produce the net signal most dominated by the fast OSL component, while keeping an acceptable level of precision. Using a three-component model of OSL decay, we show that for a specified level of precision, the net signal most dominated by the fast component can be obtained when the background integral immediately follows the initial signal and is approximately 2.5 times its length. With this 'early background' approach, the contribution of slow components to the net signal is virtually zero. We apply our methods to four samples from relatively young deposits. Compared to the widely used 'late background' approach, in which the background integral is taken from the last few seconds of OSL, we find less thermal transfer, less recuperation and a higher proportion of aliquots yielding an equivalent dose in agreement with expectations. We find the use of an early background to be a simple and effective way of improving the accuracy of OSL dating, and suggest is should be used in standard protocols.

3.1 Introduction

In the dating of quartz grains using Optically Stimulated Luminescence (OSL), the OSL signal is commonly measured by stimulating the sample with blue light at a constant intensity for several tens of seconds, while holding the sample at approximately 125ºC. Under such Continuous Wave (CW) stimulation, the OSL signal measured in the UV region decays over a number of seconds. Some portion of the decay curve is used for the calculation of equivalent dose (D_e), once corrected for sensitivity change, and calibrated against the OSL response to one or more known doses (e.g. the Single Aliquot Regenerative dose (SAR) protocol of Murray and Wintle, 2000). However, the quartz OSL decay curve consists of a number of first-order exponential components, corresponding to different trap types in the quartz crystal (Smith and Rhodes, 1994; Bailey et al., 1997; Jain et al., 2003). The 'fast' component has been identified as the most suitable for dating, as it is stable on geological timescales, rapidly bleached by sunlight, and less susceptible to thermal transfer of charge (Wintle and Murray, 2006). Moreover, the SAR protocol has been designed and tested for samples dominated by the fast component. It is therefore desirable to use measurement procedures that maximise the influence of the fast component on D_e.

In typical OSL dating protocols, the integrated photon count from the initial part of the decay curve is used for D_e determination, after subtracting the integrated photon count from the last few seconds of decay. In a multi-component system however, the choice of time-intervals used for the 'initial signal' and 'background' inevitably influence the proportion of the net signal that comes from each component. While it is not possible to isolate the fast component through background subtraction, it is possible to maximise its contribution. The optimum choice of time-intervals depends on the relative magnitude of each component and their photo-ionisation cross-sections, the intensity and wavelength of stimulation light, the signal-to-noise ratio, and the desired measurement precision. The optimum time-intervals therefore vary between instruments, samples and even aliquots.

The aim of this paper is to identify the most appropriate time-intervals for practical use in quartz CW-OSL dating, assuming that the fast component is both present and desired, and 470 nm stimulation light is used. We focus primarily on the dating of young samples, for two reasons: 1) young samples are more susceptible to effects of thermal transfer and partial bleaching, resulting in different D_e for different components; and 2) for young samples, the application of methods to isolate the fast component is challenging because of poor signal-to-noise ratios.

3.2 Samples and equipment

In this study we make use of four samples from the Netherlands. The samples are all relatively young, and were deposited under less than ideal bleaching conditions. Since different components bleach at different rates, we expect the calculated ages to depend on the choice of time-intervals used. Two of the samples also benefit from good age control.

- Sample NCL-3505030 is from a recent floodplain deposit of the River Waal. Historical maps of the area indicate that the section of floodplain from which the sample was taken was formed between 1723 and 1810 AD (Middelkoop, 1997; Bakker et al., 2007).
- Sample NCL-1109004 is from a storm-surge sediment (consisting mostly of sand) collected from the coastal dunes of North Holland. A large series of OSL dates from the site indicate that the sample was deposited in the late 18th century, and a comparison with documentary sources suggests a likely date of deposition of AD 1775 or 1776 (Cunningham et al., 2009).
- Sample NCL-1107136 is from a very young embanked floodplain of the River Waal (Hobo et. al, 2010). Stratigraphically consistent OSL ages for the site have been provided by Wallinga et al. (2010), from which we can be confident that the deposition age is < 55 a.
- Sample NCL-9908154 comes from sandy sediments sampled just below a Medieval rampart structure near Nijkerk (Doesburg et al., 2010). Depositional environment, bleaching conditions and age of the sample are not known.

Prior to measurement, samples were sieved and treated with HCl, H_2O_2 and HF to isolate the quartz fraction. OSL measurements were carried out on Risø TL-DA-15 readers (Bøtter-Jensen et al., 2000). Stimulation was with 470 nm blue diodes with a power at the sample position of ~35 mW cm^{-2}. One reader had a higher stimulation power, for which corrections were made in analysis. Irradiation was with ^{90}Sr/^{90}Y beta sources providing dose rates between 0.028 and 0.14 Gy s^{-1} to quartz grains at the sample position. The IR diodes emitted at a wavelength of 875 nm and power of ~116 mW cm^{-2}. A 7.5 mm Hoya U340 detection filter was used.

OSL measurements are based on the SAR protocol of Murray and Wintle (2000; 2003), details of which are given in Table 3.1. OSL was measured using a channel step-size of 0.05 s unless stated (this step-size is also used in the calculations of section 3.3). Preheat conditions were selected on the basis of a thermal transfer test (section 3.4.3). The grainsize used was 180 to 212 µm (NCL-1109004 and NCL-9908154), 212 to 250 µm (NCL-3505030), and 180 to 250 µm (NCL-1107136), with each aliquot containing about 200 to 300 grains. Three samples were expected to indicate a dose of less than 0.5 Gy, for which it is not necessary to ascertain the saturation point of the dose-response curve. For this reason, and to reduce measurement time, the regenerative-dose curve for these three samples was constructed with a single (small) given-dose and forced through the origin (see chapter 6 of Ballarini (2006)) for a discussion on this point). For sample NCL-3505030 we included a 175ºC IR bleach for 40 s prior to each OSL step, to reduce the effect of any remaining feldspar grains or inclusions (Wallinga et al., 2002). This IR beaching step is likely to deplete the fast OSL component by a very small amount (~0.5 %) in both the natural and regenerative signal (derived from Jain et al. (2005)). The OSL following zero dose was measured, followed by a repeat of the first given dose. For D_e calculations, aliquots were accepted only if the recuperated dose was less than 0.05 Gy, and the recycling ratio was within 10% of unity. For very young sample NCL-1107136, permissible recuperation values included those consistent with zero within one standard error. To estimate the environmental dose rate to our samples we used a high-resolution gamma ray spectrometer, after preparing our samples using the procedure described in Wallinga et al. (2010).

Step	Treatment	NCL-3505030	NCL-1109004	NCL-1107136	NCL-9908154
1	Dose	N, 2.2, 0, 2.2 Gy	N, 3.2, 0, 3.2 Gy	N, 5, 0, 5 Gy	N, 5, 10, 15, 0, 5 Gy
2	Preheat	200°C for 10s	180°C for 10s	200°C for 30s	240°C for 10s
3	IR Bleach (875 nm)	175°C for 40s	-	a	-
4	OSL (470 nm)	125°C for 40s	125°C for 40s	125°C for 40s	125°C for 20s
5	Test dose	2.2 Gy	3.2 Gy	5 Gy	5 Gy
6	Cutheat	200°C	170°C	200°C	220°C
7	IR Bleach (875 nm)	175°C for 40s	-	a	-
8	OSL (470 nm)	125°C for 40s	125°C for 40s	125°C for 40s	125°C for 20s
9	OSL Bleach (470 nm)	220°C for 40s	180°C for 40s	220°C for 40s	250°C for 40s

[a]This protocol used a 20s IR bleach during the preheat and cutheat steps (see Wallinga et al., 2010)

Table 3.1. Details of the SAR protocol used for each sample.

3.3 Methods

3.3.1 Early background subtraction

Standard practice for selection of integration time-intervals follows Banerjee et al. (2000), with an initial integral of the decay curve (e.g. 0 - 0.30 s) usually taken as indicative of the fast component signal, once a late background (e.g. 36 - 40 s) has been subtracted (and corrected to the length of the initial signal). Using the last few seconds of the decay as background adequately removes photomultiplier dark noise and stimulation-light leakage from the signal, and also subtracts the majority of the slow component. The length of the initial signal is usually kept short, since the shorter it is, the larger the proportion of fast component in the net signal.

However, since the fast component is usually the most rapidly decaying, it follows that to maximize the proportion of fast component in the net signal, the time-interval used for the background subtraction should immediately follow that of the initial signal. Such a procedure has been hinted at before (Aitken and Xie, 1992; Singhvi and Lang, 1998; Ballarini et al., 2007), but has not yet become standard practice, perhaps because of the detrimental effect on measurement precision. No comprehensive analysis of time-interval choice has yet been published, so we explore this topic in the following sections.

3.3.2 Selection of time-intervals

The choice of channels used for defining the 'initial signal' and 'background' integrals determine the proportion of each component in the net signal, and the relative error due to counting statistics. Moreover, for any choice of time-intervals the proportion of each component in the net signal will vary between aliquots due to variations in the intensity and decay rate of each OSL component between grains. To understand how the composition of the net OSL signal is influenced by the choice of integration time intervals, we discuss first a simulated decay curve. The simulated curve used here consists of three exponentially decaying components of the form $n_{0i}\alpha_i exp(-\alpha_i t)$, where t is time (s), n_{0i} is the initial population of component i, and α_i is the decay rate of component i. The decay rate of each component is governed by its photoionisation cross-section at the stimulation wavelength, and the intensity of stimulation light. The decay rates used here (α_1 = 2.2 s^{-1}, α_2 = 0.44 s^{-1}, α_3 = 0.02 s^{-1}) were determined during a previous curve-fitting exercise (Cunningham and Wallinga, 2009), and are broadly representative of the fast, medium and slow2 components of Jain et al. (2003) under (470 nm wavelength) stimulation light intensity of ~35 mW cm^{-2}. The populations n_{0i} in this example are 100, 100 and 1000; i.e. the same trap populations for the fast and medium components, with a much larger slow component. The simulated decay curve was produced with 0.05 s time-steps, and for clarity no noise was included. Using this simulated decay curve, the contribution of each component to the net OSL signal can be calculated for every time-interval combination used for signal and background collection. The error due to counting statistics can also be determined, and is given henceforth as the Relative Standard Error (RSE) term of Li (2007).

The results of this exercise can be seen in Fig. 3.1. In Fig. (3.1(a)), the proportion of fast component in the simulated net OSL signal is shown as a function of the time-interval used for the initial signal and the time-interval used for the background subtraction (which is taken immediately following the initial signal). The horizontal plane indicates the equivalent value calculated using the 'Late background' time-intervals (0 – 0.30 s for the initial signal, 36 - 40 s for the background). Figs (3.1(b-c)) show the same for the medium and slow components. It is clear that the slow component is almost wholly removed with any combination of early background time-intervals. It is also evident from these plots that the maximisation of the fast component and minimisation of the medium component is best achieved by using a short time interval for the initial signal, and a short time interval for the background. However, the use of short time intervals, especially for the background, leads to a reduction in the precision with which the net signal is known (Fig. 3.1(d)). It is therefore necessary to introduce some criteria for an acceptable level of precision. The best combination of time-intervals is the one which gives the net signal with the largest percentage of fast component, while keeping the RSE below this threshold. Some criteria are therefore needed to select the best channel combination. As an example, we have plotted an RSE threshold of 5 % as a horizontal plane on Fig. 3.1(d). The combination of time-intervals which gives the largest proportion of the net signal from the fast component while satisfying the RSE criteria is indicated by the black square on Fig. 3.1(a).

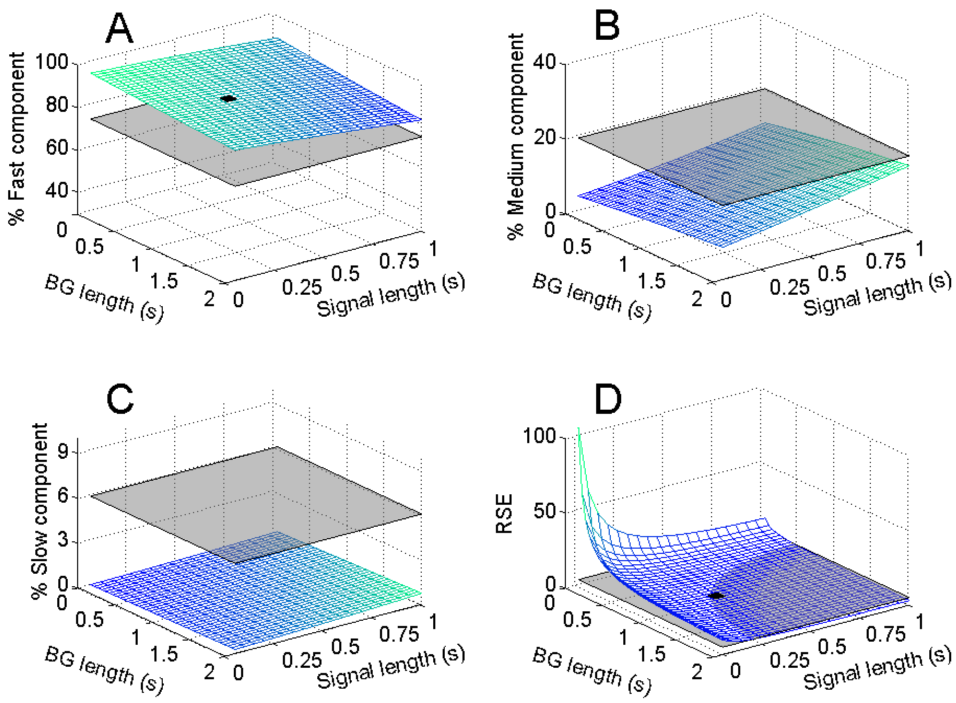

Fig. 3.1. The influence of OSL integration time-intervals on the composition of the net signal for a simulated decay curve. Gridded surfaces show the percentage of (a) fast component, (b) medium component and (c) slow component, and also (d) the relative error (RSE) on the net count. In all cases the background interval immediately follows the initial signal interval. The grey shaded horizontal planes in (a), (b) and (c) indicate the values derived from using the late background combination of time-intervals (0 - 0.30s for initial signal; 36 - 40s for background). In (d) the shaded plane indicates an RSE of 5 %. The black square indicates the combination of time intervals that (in this example) maximise the fast-component proportion of the net signal while keeping the RSE below 5 %. Please note the different scales used for the ‘signal length’ axis and the ‘BG length’ axis.

3.4 Results

3.4.1 Validation of the 3-component model

Example (regenerative) decay curves have been fitted with three (unconstrained) components, and are plotted in Fig. 3.2. The parameters vary slightly between each plot, as expected. All samples have a fast and slow component. While sample NCL-9908154 has little or no medium component, a three component model can still be applied (which mean the n_{02} parameter will equal zero, or be very small).

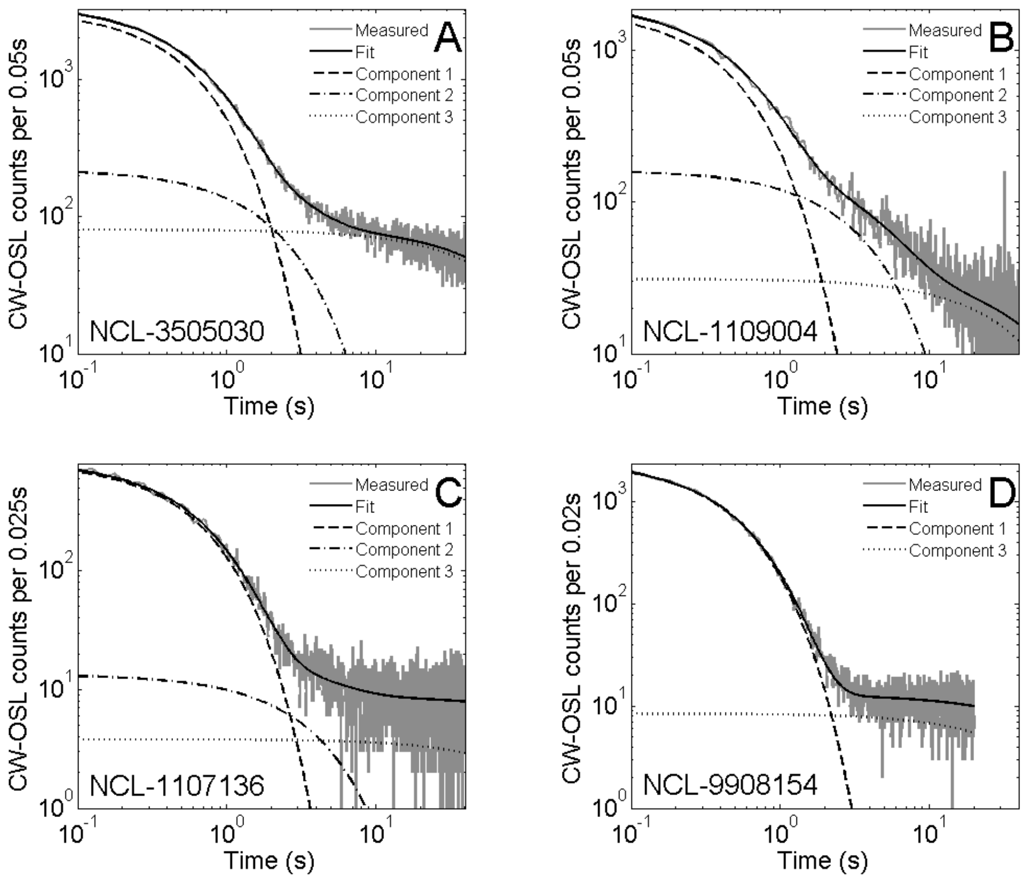

Fig. 3.2. A check on the suitability of a three-component model of OSL decay for the samples studied here. The (CW)-OSL was measured following a regenerative dose, and is plotted on a log-log scale to improve clarity.

3.4.2 Calculations for real data

In order to perform time-interval calculations for real OSL decay curves, it is necessary to first estimate the magnitude of the various components. Here we have applied a simple curve-fitting routine to decay curves following a regenerative dose given to 24 aliquots of each sample. By assuming a maximum of three components are present, and their photo-ionisation cross-sections are predetermined, it is computationally simple to gain an approximation of the magnitude of each component using a non-negative least squares method. As no variation in decay rate α is permitted, the outcome does not give a rigorous fit, but provides a good approximation of the magnitude of each component. With an estimate of the decay-curve composition, the calculation of the optimal integration time-intervals can be done according to the method outlined in section 3.2, which now depends solely on the desired level of precision. The influence of desired precision on time-interval selection is shown in Fig. 3.3, for two aliquots of sample NCL-3505030. For aliquot (a), a reduction in the precision threshold (an increase in RSE) allows the proportion of fast component in the net signal to be increased, which is achieved by decreasing the length of the integration time-intervals for both the initial-signal and (subsequent) background intervals. However, it is apparent that the improvement in the percentage of fast component gained through a reduction in precision suffers from diminishing returns, with little benefit obtained by increasing the RSE beyond 2.5 %. Fig. 3.3(b) shows the same information for an aliquot with a less dominant fast component. In this case, a significant improvement in the proportion of fast component can be achieved by accepting less precision.

It is important to note that for both aliquots shown in Fig. 3.3 the implied range of suitable integration lengths is similar. Furthermore, as the RSE threshold is changed, the relationship between signal length and background length is similar for all four samples. This can be seen more clearly in Fig. 3.4, which plots the optimum background-length to signal-length ratio for 24 aliquots of each sample, as a function of RSE threshold. Each strand represents one aliquot, which has had its component magnitudes n_{0i} estimated using the constrained fitting described above. For each RSE threshold on the regenerative signal, the channel combination resulting in the net signal most dominated by the fast component was identified, and the ratio plotted. Sample NCL-3505030 (Fig. 3.4(a)) has relatively weak signals, with a dominant slow component (Fig. 3.2(a)). For less stringent (for this sample) RSE thresholds of 10-15 % (which leads to shorter integration lengths), the ratio for all aliquots lies between two and four. As the RSE threshold is made more stringent (leading to longer integration lengths), aliquots with a more dominant fast component tend to keep this ratio. For aliquots with less fast component, the RSE threshold can only be achieved by using a very long background interval, leading to a high ratio. For many aliquots in this example, it is not possible to obtain a stringent RSE. For sample NCL-1109004 we can see a similar pattern, with the ratio staying mostly between 2 and 3. Samples NCL-1107136 and NCL-9908154 are characterised by a much more dominant fast component (Fig. 3.2(c) and 3.2(d)), and for more stringent RSEs have a ratio close to 2.5. Because the regenerative signals from these samples are strong, relaxation of the RSE threshold leads to very short integration lengths, causing sharp jumps in the ratio.

While the level of precision ultimately chosen may be arbitrary, it is important to note that the ratio of background length to signal length required to maximise the fast component remains between 2 and 3, and this ratio holds across a greater range of RSE thresholds for aliquots with a more dominant fast component. In practice, the length of the time-intervals may be governed by the signal-to-noise ratio, but the ratio of background length to signal length should remain between 2 and 3. For the samples shown here, we kept this ratio at 2.5, but changed the integration lengths according to signal strength. For samples NCL-3505030 and NCL-1109004 (estimated age between 200 and 300 a) we used signal and background intervals of [0 – 0.40; 0.40 –

1.40 s] (Fig. 3.5(a) and (b)). Sample NCL-1107136 has a very weak natural signal, so to ensure enough signal was collected for acceptable precision, the integration intervals were lengthened to [0 – 0.60; 0.60 – 2.10 s]. Sample NCL-9908154 is far more sensitive to OSL, and we were able to reduce the length of the integration intervals to [0 – 0.20; 0.20 – 0.70 s] while maintaining reasonable precision.

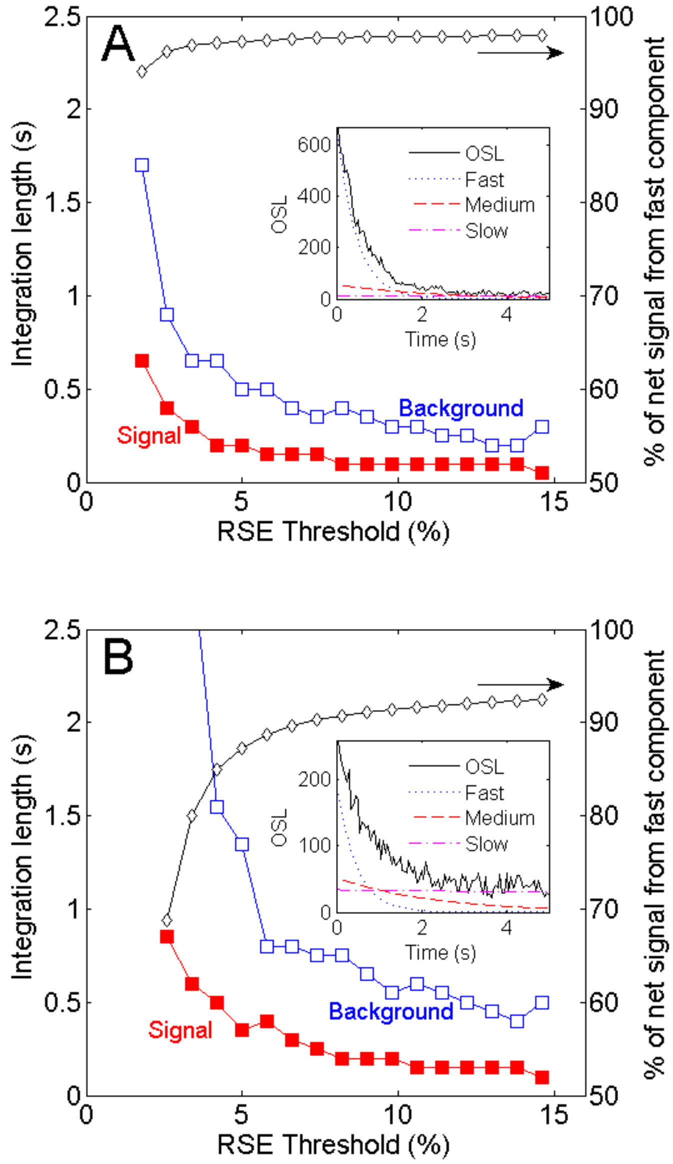

Fig. 3.3. The integration time-intervals which result in the net signal with the largest proportion of fast component, for a given RSE threshold. (a) and (b) show calculations for different aliquots of sample NCL-3505030. The proportion of the net signal composed of fast component, resulting from the specified combination of time-intervals, is shown on the right-hand axis. Insets show the OSL decay curves for these aliquots, which were fitted with three exponential functions so that the effects of time-interval selection could be ascertained.

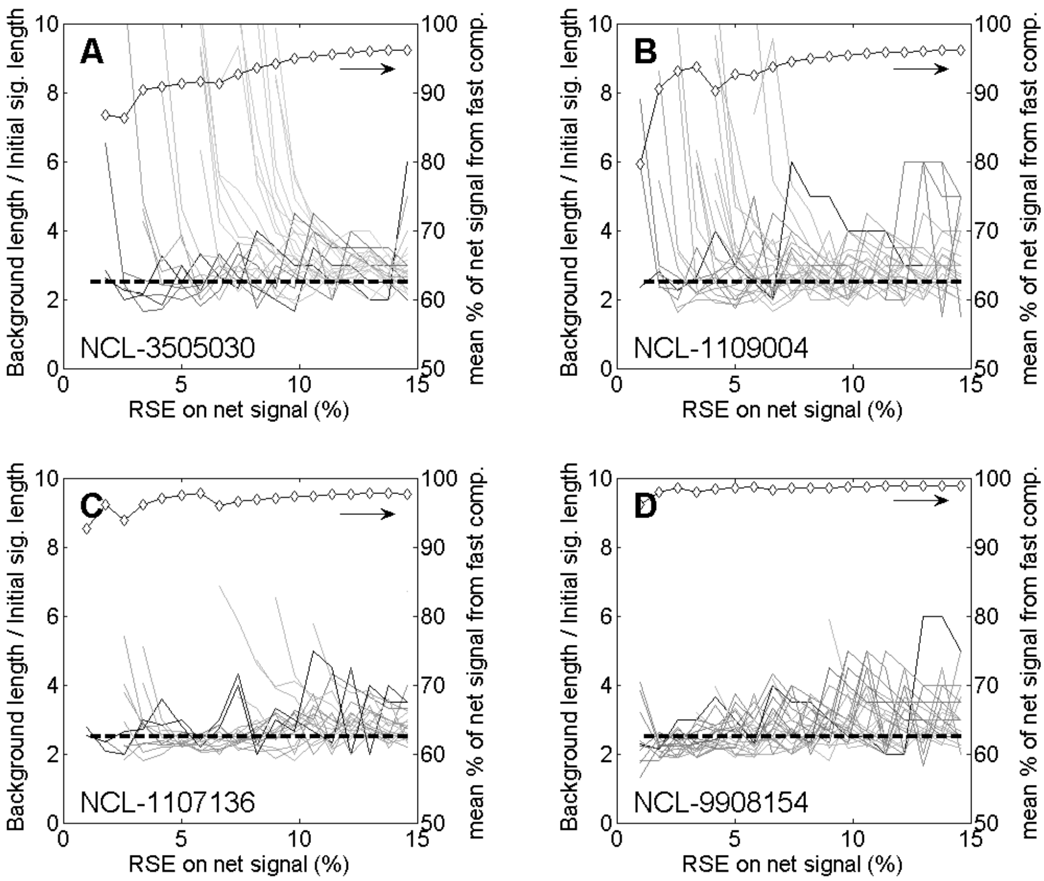

Fig. 3.4. The calculated ratio of background length to initial-signal length which gives the net signal with the maximum possible proportion of fast component, for RSE thresholds between 1 and 15 % on the (first) regenerative OSL signal. Each line represents one aliquot, the decay curve of which has been fitted with three exponential functions to represent the fast, medium and slow components so that the effects of using different integration intervals can be calculated. Within each sub-plot, the lines are shaded according to the estimated strength of the fast component (n_{01}) for that aliquot, with darker shading for larger fast components. The shading scale differs between samples. The dashed line indicates a ratio of 2.5. Also shown is the average percentage of fast component in the net signal (open symbols, plotted on the second y-axis), when calculated using the optimum integration lengths (this means that the integration lengths vary between aliquots at any one threshold). OSL measurements used in plot (d) were carried out on a reader with a higher stimulation power.

3.4.3 Thermal transfer

Our OSL measurements are preceded by a preheat, the purpose of which is to empty thermally unstable OSL traps which would otherwise contribute to the signal. However, preheating can lead to thermal transfer of charge from light-insensitive traps (which may contain large accumulated doses), to the traps responsible for OSL (Wintle and Murray, 2006). This is a particular problem for young samples given their comparatively small D_e. When this occurs following the regenerative doses, it is detectable in the OSL following a zero dose (recuperation). Based on curve fitting the OSL signals, Jain et al. (2003) and Tsukamoto et al. (2003) found the fast component to show far less recuperation than the medium or slow components.

If the D_e calculated using the early background is indeed a better reflection of the fast component D_e, we would expect to see less thermal transfer and recuperation than with the late background. To test for thermal transfer, we first bleached eight aliquots of each sample with 470 nm LEDs at room temperature for 40 s, which was repeated after a 1000 s pause. This treatment aims to empty trapped charge giving rise to the fast (and medium) component, whilst leaving a large part of the less light-sensitive trapped charge in place. A low (140ºC) preheat was then given, followed by OSL at 125ºC. Successive preheats to higher temperatures (160ºC, 180ºC … 220ºC) were then applied, each followed by an OSL measurement. Finally the OSL signal was reset by a high temperature bleach, after which the OSL response to a single dose point was measured to allow translation of the thermal transfer OSL signals to an approximate D_e. The cumulative D_e indicates the amount of thermal transfer at each preheat temperature, albeit with a slight temperature shift caused by the earlier preheats. This procedure is explained fully in Wallinga et al. (2009), and differs slightly from the approach of Jain et al. (2004) and Truelsen and Wallinga (2003) in that no test dose is given. The results clearly show that less thermal transfer is measured if the early background is used (Fig. 3.5(c) and (d)). Measurements of recuperation also yield lower values for the early background than for the late background (Table 3.2).

Sample	Time-intervals	Recycling ratio	Recup. dose (Gy)	No. Accepted / Total aliquots	No. giving expected D_e [a]	Dose rate (Gy ka^{-1})
NCL-3505030	Late BG	0.996 ± 0.016	0.033 ± 0.006	14 / 48	2	1.31 ± 0.05
	Early BG	0.980 ± 0.020	0.011 ± 0.005	21 / 48	7	
NCL-1109004	Late BG	0.997 ± 0.010	0.007 ± 0.003	30 / 48	12	1.37 ± 0.05
	Early BG	0.988 ± 0.015	-0.008 0.006	15 / 48	11	
NCL-1107136	Late BG	0.972 ± 0.009	0.034 ± 0.006	23 / 84	-	2.06 ± 0.06
	Early BG	0.970 ± 0.009	0.026 ± 0.004	25 / 84	-	
NCL-9908154	Late BG	1.022 ± 0.009	0.011 ± 0.002	30 / 38	-	1.01 ± 0.03
	Early BG	1.020 ± 0.014	0.007 ± 0.003	26 / 38	-	

[a] Agreement within 2σ. Uncertainty in the dose rate has been included, hence the small difference with Fig. 3.6.

Table 3.2. Standard tests for each sample, calculated with both early and late backgrounds. Age control for the latter two samples is speculative or absent, so direct comparisons have not been made.

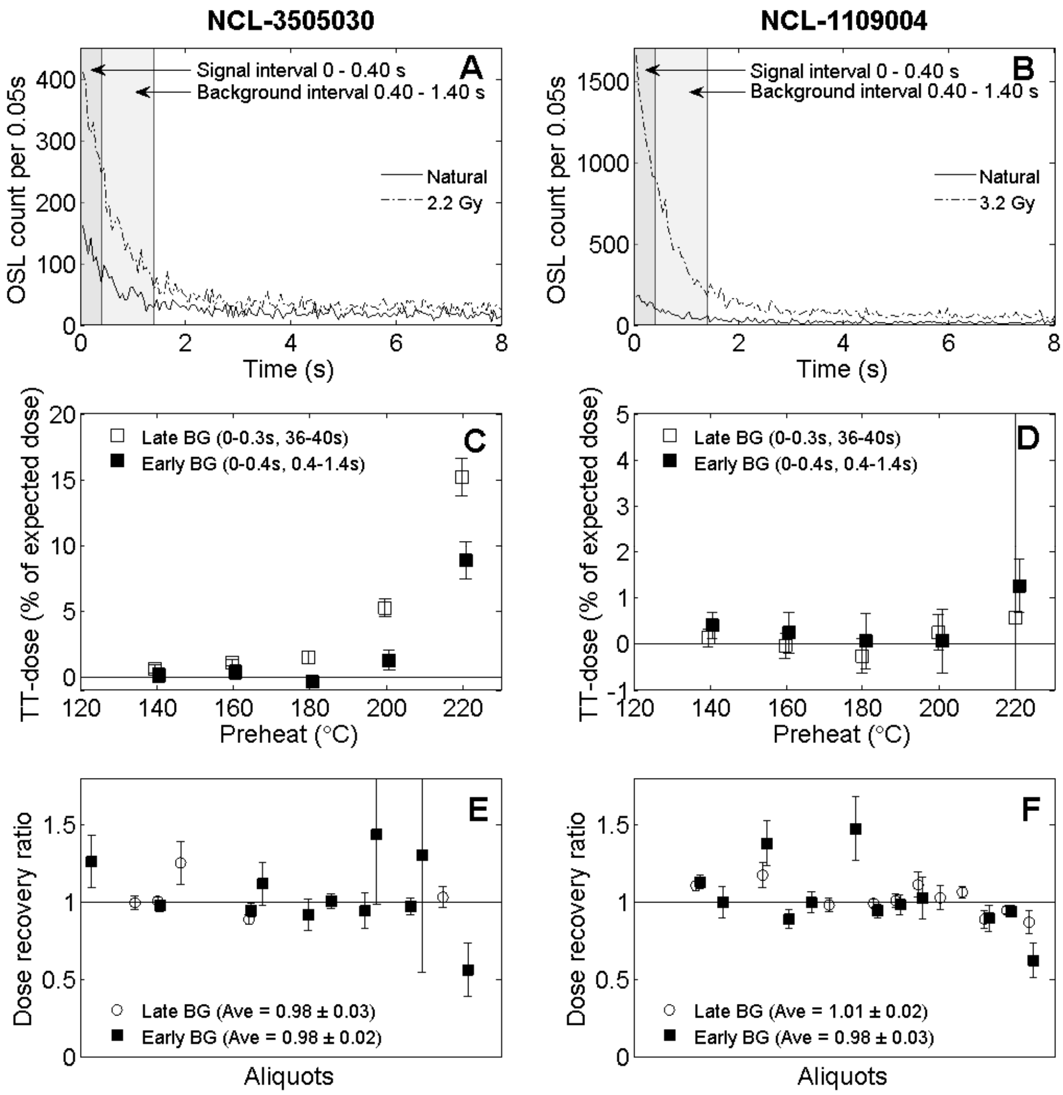

Fig. 3.5. (a-b) Example OSL decay curves for two samples, showing the natural and regenerative signals. Also shown are the integration intervals suggested in this paper to be suitable for these samples. (c-d) The thermally transferred dose (given as a percentage of the expected dose) as a function of preheat temperature, details in section 3.4.3. (e-f) Results of dose recovery tests following a given dose of ~3.2 Gy, under the same conditions used for measurement of D_e.

3.4.4 Equivalent dose

The use of the early background has a significant effect on the D_e distribution for three of the samples shown here. For fluvial sample NCL-3505030 (Fig. 3.6(a-c)), the reduction in the measured recuperation values when the early background is used lead to more aliquots passing the acceptance criteria. There is a reduction in D_e compared with the late background for most aliquots, which could be due to the reduction in thermal transfer and/or smaller contributions from less light-sensitive components. More aliquots, and a higher proportion of aliquots, give results in agreement with the expected D_e. For storm-surge deposited sample NCL-1109004, the impact of partial bleaching and thermal transfer are less obvious, but the early background still has a beneficial effect on D_e. While less aliquots pass acceptance criteria than with the late background, those which remain show a tighter distribution, and are largely in agreement with the expected D_e (Fig. 3.6(d-f)).

Probability density functions (PDFs) of D_e for samples NCL-1107136 and NCL-9908154 can be seen in Fig. 3.7, along with example decay curves. The PDF plots appear to show early background datasets which are more in line with the expected results than the late-background counterparts. For sample NCL-9908154 this is a little surprising – decay curves from this sample show virtually no medium or slow components (e.g. Fig. 3.2(d)), so we would not expect the choice of integration intervals to affect D_e. The difference may be due to random effects, e.g. which aliquots happen to pass acceptance criteria; it may be due to the larger errors in the EBG dataset for this sample; or perhaps because the error term of Li (2007) employed here is more appropriate for use with the early background (as it assumes there is no slow component in the net signal).

Fig. 3.6. (a) Probability density functions (PDFs) of D_e calculated using both early background (0-0.40 s; 0.40-1.40 s) and late background (0-0.30 s; 36-40 s) intervals, for sample NCL-3505030. (b) and (c) show the same data in radial plot form. The shaded regions indicate values within 2 s.e. of the mean expected age. Similarly, (d) shows the PDFs for sample NCL-1109004, with the radial plots in (e) and (f).

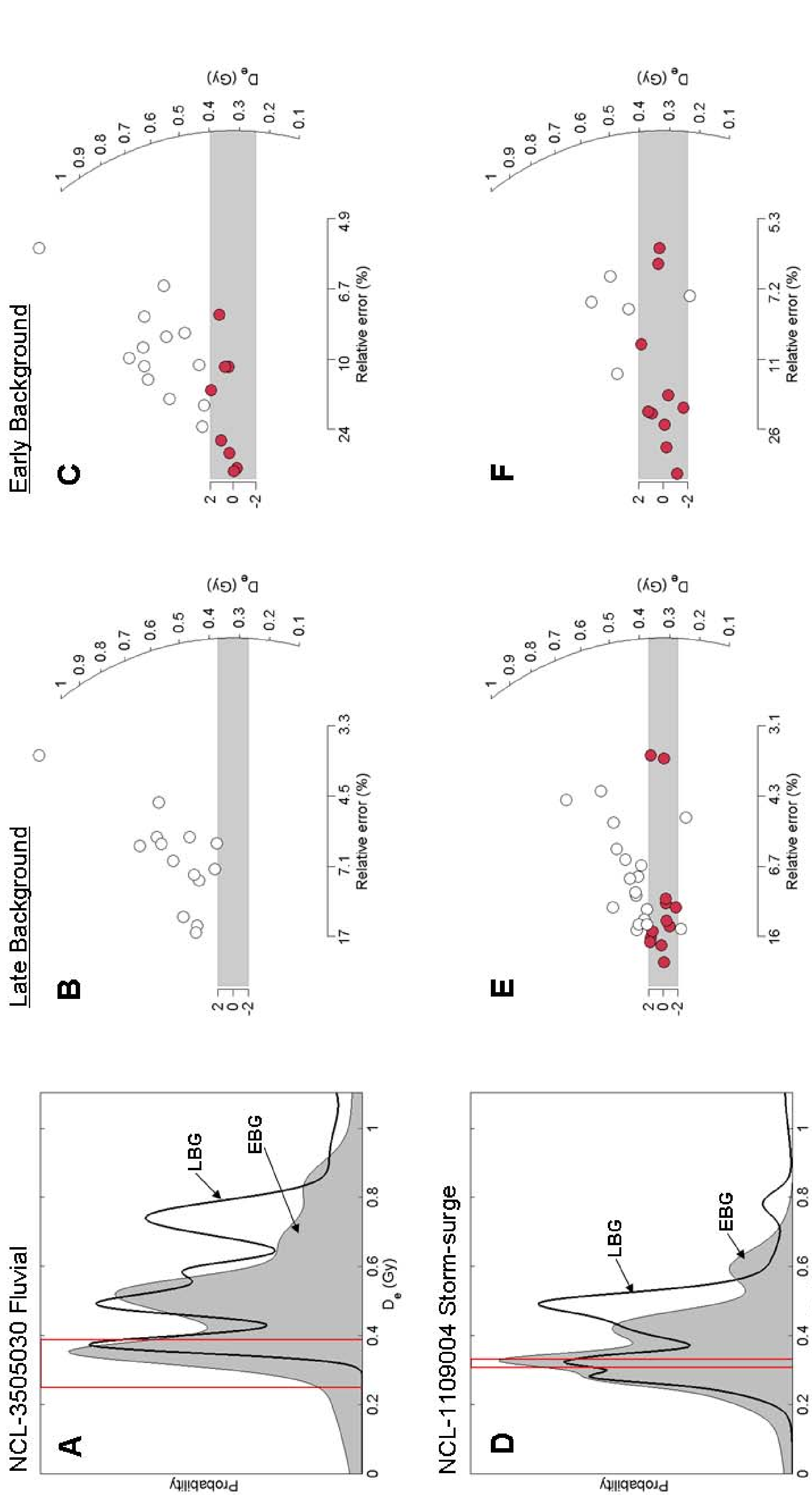
NCL-3505030 Fluvial
A
B
C
Late Background
Early Background
NCL-1109004 Storm-surge
D
E
F
LBG
EBG
Probability
De (Gy)
Relative error (%)

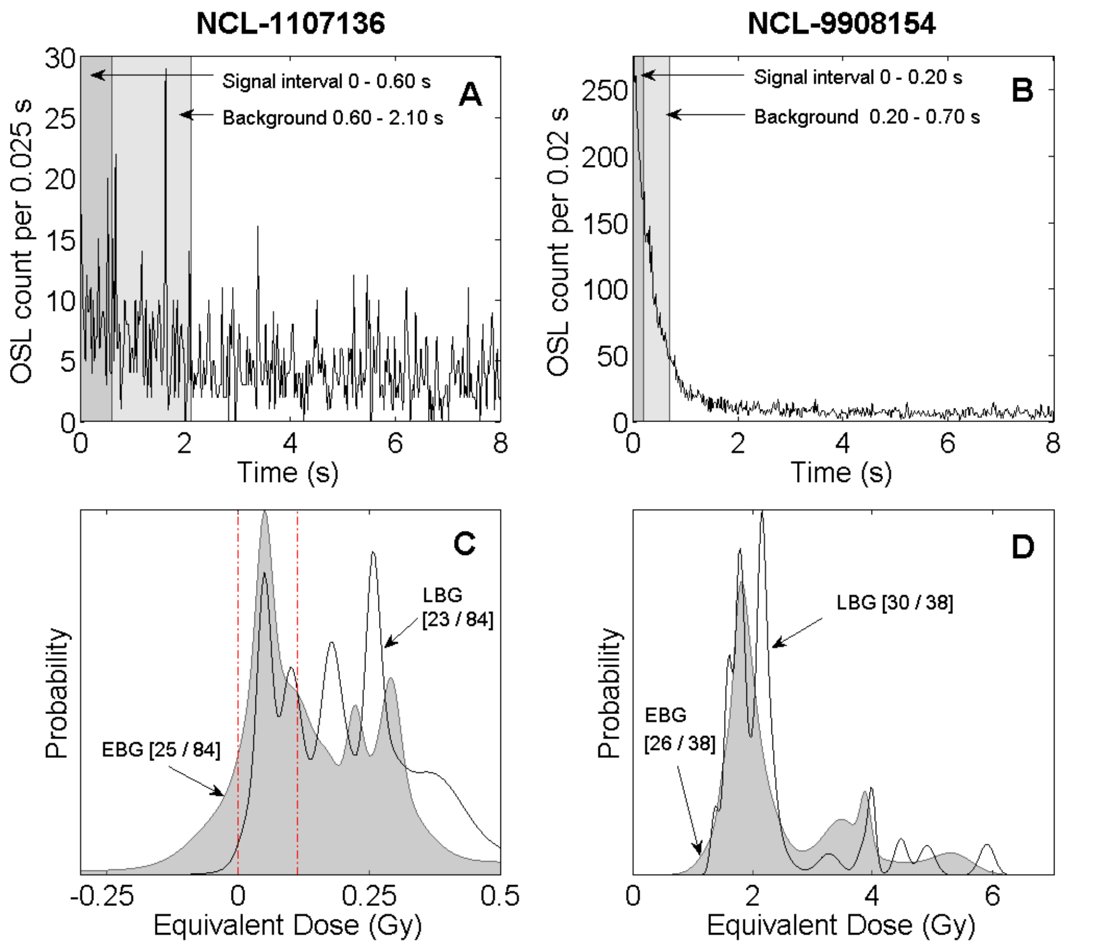

Fig. 3.7. Examples in the use of an early background, using samples of different OSL sensitivity. On the left, sample NCL-1107136 (very young fluvial sample); on the right, sample NCL-9908154. (a) and (b) show typical OSL decay curves, with the early background intervals indicated (see section 4.2). Please note that the channel step-size differs between these samples (0.02 s and 0.025 s, both shorter than in the previous examples (Fig. 3.5)). In addition, OSL measurements for plot (b) were carried out under higher stimulation power, leading to faster OSL decay. (c) and (d) show probability density functions of the D_e distributions calculated using the indicated early background intervals (shaded area) and the standard late-background intervals (solid line).The PDFs have been normalised by area. Numbers in brackets indicate [Number of accepted aliquots / Total Number of aliquots measured].

3.5 Discussion

3.5.1 Implications of early background subtraction for young samples

For the young samples studied here, it is clear that the use of the early background time-intervals has a beneficial effect on the D_e distribution, by increasing the number and proportion of accepted aliquots which have D_e consistent with a single population, and also with the expected D_e. This is achieved through two effects:

1. *The almost complete removal of the slow component from the net signal.* The proportion of the net signal belonging to the slow component is an order of magnitude less with the early background compared to the late background (Fig. 3.1(c)). This results in a significant and consistent reduction in the measured amounts of thermal transfer and recuperation, and is likely to lessen the severity of partial bleaching in the D_e distribution. Differences in the precise choice of early background intervals have a minor effect on the D_e distribution, which implies that the removal of the slow component is the most important effect (since the slow component is removed by any combination of early background time-intervals). Ballarini et al. (2007) also came to this conclusion when testing integration intervals for single-grain measurements, although the 525 nm stimulation wavelength they used would have lead to a larger difference in the photoionisation cross-sections of the fast and medium components (Singarayer and Bailey, 2004).
2. *Improved auto-weighting of aliquots according to the dominance of the fast component.* When the early background is used, aliquots with little or no fast component will tend to give imprecise D_e. The resulting D_e distribution is then naturally weighted towards aliquots with a strong fast component, as they retain a relatively precise D_e. Any age model then applied to the D_e dataset, provided it takes account of the errors on each aliquot (e.g. central and minimum age models of Galbraith et al. (1999)), will be preferentially influenced by the desirable, fast-component dominated aliquots. This may result, for instance, in a reduction in the number of apparent age populations and an increase in precision on the age-model derived D_e.

Use of an early background may also reduce the feldspar component of the ‘quartz’ signal. Although standard laboratory preparation for quartz includes chemical treatment to remove feldspars, there can often be a remnant signal from, for instance, feldspar inclusions within quartz grains (Huntley et al., 1993). Since feldspar OSL decay is slower than quartz under 470 nm stimulation (e.g. Wallinga et al., 2002), the use of an early background will remove more of the feldspar signal than with a late background.

3.5.2 Sensitivity in the choice of early background time-intervals

Complete isolation of the fast component is not possible with any combination of integration time-intervals, if there are other components present in the signal. The percentage of each component in the net signal also varies dramatically between aliquots, due to inter-grain differences in the strength of each component and the absorbed dose. External factors such as stimulation light intensity (and wavelength) and the level of dark noise also have a significant effect. However, for the practical purpose of maximising the fast component under 470 nm stimulation, the actual range of suitable time-intervals remains small. This is because the relative cross-sections of each component remain similar across different aliquots/grains (Jain et al., 2003), and because of the consistent removal of the slow component regardless of the exact integrals used.

The level of precision on the net OSL count also depends on time-interval choice and OSL intensity. For the samples studied here, we have found that for practical levels of precision, the percentage of the net signal coming from the fast component is maximised by keeping the background time-interval approximately 2.5 times the length of the initial interval (and immediately following it). This ratio is weakly sensitive to the intensity and dominance of the fast component; small differences in the ratio make little difference to D_e.

3.5.3 Implications for older samples

The removal of the slow components by using an early background is highly beneficial for young samples, because either through partial bleaching or thermal transfer the slow components are likely to cause most scatter in D_e. Furthermore, weak signal-to-noise ratios with young samples make the extraction of the fast component through curve fitting challenging (Cunningham and Wallinga, 2009). The early background method therefore represents an extremely simple and efficient way of obtaining a predominantly fast-component derived signal.

When it comes to older samples, other sources of scatter, rather than partial bleaching, are likely to be more important. Several authors have noted a significant underestimation of age, which becomes more apparent for older samples (Murray et al., 2008; Stokes et al., 2003). Singarayer and Bailey (2003) identified a slow component ‘S2’ which appeared to be thermally unstable, and Rhodes et al. (2006)

considered this component to be causing D_e underestimates in their bulk OSL signal. Where D_e underestimation is caused by an unstable slow component, the use of an early background is likely to be beneficial, and lead to an increase in D_e compared to the late-background approach. Recently however, Bailey (2010) suggested that an unstable medium component is present in some samples, some of which will still be included in the net signal when the early background is used. While the early-background approach is an improvement on the late-background approach for such samples, the brightness of the OSL signals for most older samples would facilitate more sophisticated methods of fast-component isolation to be used instead. This could be approached by curve-fitting of the OSL signal (although this is by no means simple, see Wallinga et al. 2008); or through IR stimulation (Bailey, 2010) or IR depletion (Jain et al., 2005).

3.5.4 The ultrafast component

Jain et al. (2003, 2008) have detected an ultrafast OSL component in several quartz samples. The low thermal stability of the ultrafast component makes it unsuitable for dating, and its presence in regenerative signals can lead to dose underestimation. Even a small ultrafast component will have a significant effect on D_e. As the signal from the ultrafast component is completely removed after 0.15 s, it is always contained within the initial signal interval. As such, the proportion of the net signal constructed from the ultrafast component is largely unaffected by the choice of intergration time-intervals, but is negatively correlated with net signal intensity. The use of an early background therefore has no adverse effects with respect to the ultrafast component compared to a late background. To avoid influence of the ultrafast component on the D_e estimate, IR bleaching may be beneficial (Wallinga et al., 2010).

3.6 Conclusion

When using integration intervals of CW-OSL data for the purpose of dating, the choice of time-intervals influences the proportion of each OSL component in the net OSL count, and the error due to counting statistics. We have tried to identify which combination of time-intervals should be used for dating, when the stimulation wavelength is 470 nm, and conclude that:

1. By using a background interval which immediately follows the interval for the initial signal (rather than at the end of the stimulation period), the proportion of fast component in the net OSL count is much improved, while the

proportion of slow components is diminished by approximately one order of magnitude.

2. For a specified (and practical) level of precision, the proportion of the net OSL count coming from the fast component can be maximised by using a background interval approximately 2.5 times longer than the initial signal (and immediately following it)

For two young samples of known age, we found that (with the stimulation power at 35 mW cm^{-2}) an initial signal of 0 - 0.40 s with background interval from 0.40 - 1.40 s produced results showing less thermal transfer, less recuperation, tighter D_e distributions and more aliquots with D_e in line with the expected D_e than using the alternative, late background time intervals. We consider this improvement to be largely due to the almost complete removal of the slow components from the net signal. Given that the use of an early background is extremely easy to implement and does not seem to have any detrimental effects, we suggest it should be used routinely to improve the accuracy of quartz OSL dating.

Acknowledgements

The authors are sponsored by NWO/STW grant DSF.7553. We thank Denise Maljers for sample NCL-3505030, and Jan Willem de Kort and Jan van Doesburg for sample NCL-9908154. Marcel Bakker, Tammy Rittenour, Jon Olley and Bert Roberts are thanked for their comments on an earlier version of our manuscript. We also owe thanks to Andrew Murray for encouraging us to pursue this topic.

References

Aitken, M.J., Xie, J. 1992. Optical dating using infrared diodes: young samples. Quaternary Science Reviews 11,147-152.

Bailey, R.M. 2010. Direct measurement of the fast component of quartz optically-stimulated luminescence and implications for the accuracy of optical dating. Quaternary Geochronology 5, 559-568.

Bailey, R.M., Smith, B.W., Rhodes, E.J. 1997. Partial bleaching and the decay form characteristics of quartz OSL. Radiation Measurements 27, 123-136.

Bakker, M.A.J., Maljers, D., Weerts, H.J.T. 2007. Ground-penetrating radar profiling on embanked floodplains. Netherlands Journal of Geosciences - Geologie en Mijnbouw 86, 55-61.

Ballarini, M. 2006. Optical dating of quartz from young deposits. PhD Thesis, Delft University of Technology.

Ballarini, M., Wallinga, J., Wintle, A.G., Bos, A.J.J. 2007. A modified SAR protocol for optical dating of individual grains from young quartz samples. Radiation Measurements 42, 360-369.

Banerjee, D., Bøtter-Jensen, L., Murray, A.S. 2000. Retrospective dosimetry: estimation of the dose to quartz using the single-aliquot regenerative-dose protocol. Applied Radiation and Isotopes 52, 831-844.

Bøtter-Jensen, L., Bulur, E., Duller, G.A.T., Murray, A.S. 2000. Advances in luminescence instrument systems. Radiation Measurements 32, 57-73.

Cunningham, A.C., Wallinga, J. 2009. Optically Stimulated Luminescence dating of young quartz using the fast component. Radiation Measurements 44, 423-428.

Cunningham, A.C., Wallinga, J., van Heteren, S., Bakker, M.A.J., van der Valk, L., Oost, A.P., van der Spek, A. 2009. Optically stimulated luminescence dating of storm surge sediments: a test case from the Netherlands. In Wallinga, J. and Storms, J. (eds) NCL Symposium series, Volume 6.

Doesburg, J. van, Kort, J.W. de, Schut, P.A.M. 2010. IJzer en aarde. Waarderend onderzoek naar een ringvormig aardwerk in Appel (gemeente Nijkerk) in 2008, Rapport Archaeologische Monumentenzorg, Rijksdienst voor het Cultureel Erfgoed, Amersfoort

Galbraith, R.F., Roberts, R.G., Laslett, G.M., Yoshida, H., Olley, J.M. 1999. Optical dating of single and multiple grains of quartz from jinmium rock shelter, northern Australia, part 1, Experimental design and statistical models. Archaeometry 41, 339-364.

Hobo, N., Makaske, B., Middelkoop, H., Wallinga, J. 2010. Reconstruction of floodplain sedimentation rates: a combination of methods to optimize estimates. Earth Surface Processes and Landforms 35, 1499-1515.

Huntley, D.J., Hutton, J.T., Prescott, J.R. 1993. Optical dating using inclusions within quartz grains. Geology 21, 1087-1090.

Jain, M., Murray, A.S., Bøtter-Jensen, L. 2003. Characterisation of blue-light stimulated luminescence components in different quartz samples: implications for dose measurement. Radiation Measurements 37, 441-449.

Jain, M., Thomsen, K.J., Bøtter-Jensen, L., Murray, A.S. 2004. Thermal transfer and apparent-dose distributions in poorly bleached mortar samples: results from single grains and small aliquots of quartz. Radiation Measurements 38, 101-109.

Jain, C., Murray, A.S., Bøtter-Jensen, L., Wintle, A.G., 2005. A single-aliquot regenerative-dose method based on IR (1.49 eV) bleaching of the fast OSL component in quartz. Radiation Measurements 39, 309-318.

Jain, M., Choi, J.H., Thomas, P.J. 2008. The ultrafast OSL component in quartz: Origins and implications. Radiation Measurements 43, 709-714.

Li, B. 2007. A note on estimating the error when subtracting background counts from weak OSL signals. Ancient TL 25, 9-14.

Middelkoop, H. 1997. Embanked floodplains in the Netherlands. Geomorphological evolution over various timescales. PhD-thesis Utrecht University, the Netherlands.

Murray, A.S., Wintle, A.G. 2000. Luminescence dating of quartz using an improved single-aliquot regenerative-dose protocol. Radiation Measurements 32, 57-73.

Murray, A.S., Wintle, A.G. 2003. The single aliquot regenerative dose protocol: potential for improvements in reliability. Radiation Measurements 37, 377-381.

Murray, A., Buylaert, J.P., Henriksen, M., Svendsen, J.I., Mangerud, J. 2008. Testing the reliability of Quartz OSL ages beyond the Eemian. Radiation Measurements 43, 776-780.

Rhodes, E.J., Singarayer, J.S., Raynal, J.P., Westaway, K.E., Sbihi-Alaoui, F.Z. 2006. New age estimates for the Palaeolithic assemblages and Pleistocene succession of Casablanca, Morocco. Quaternary Science Reviews 25, 2569-2585.

Singarayer, J.S., Bailey, R.M. 2003. Further investigations of the quartz optically stimulated luminescence components using linear modulation. Radiation Measurements 37, 451-458.

Singarayer, J.S., Bailey. R.M. 2004. Component-resolved bleaching spectra of quartz optically stimulated luminescence: preliminary results and implications for dating. Radiation Measurements 38, 111-118.

Smith, B.W., Rhodes, E.J. 1994. Charge movements in quartz and their relevance to optical dating. Radiation Measurements 23, 329-333.

Singhvi, A.K., Lang, A. 1998. Improvements in infra-red dating of partially bleached sediments – the 'Differential' Partial Bleach Technique. Ancient TL 16, 63-71.

Stokes, S., Ingram, S., Aitken, M.J., Sirocko, F., Anderson, R., Leuschner, D. 2003. Alternative chronologies for Late Quaternary (Last Interglacial-Holocene) deep sea sediments via optical dating of silt-sized quartz. Quaternary Science Reviews 22, 925-941.

Truelsen, J.L., Wallinga, J. 2003. Zeroing of the OSL signal as a function of grain size: investigating bleaching and thermal transfer for a young fluvial sample. Geochronometria 22, 1-8.

Tsukamoto, S., Rink, W.J., Watanuki, T., 2003. OSL of tephric loess and volcanic quartz in Japan and an alternative procedure for estimating D_e from a fast OSL component. Radiation Measurements 37, 459-465.

Wallinga, J., Murray, A.S., Bøtter-Jensen, L. 2002. Measurement of the dose in quartz in the presence of feldspar contamination. Radiation Protection Dosimetry 101, 367-370.

Wallinga, J., Bos, A.J.J., Duller, G.A.T. 2008. On the separation of quartz OSL signal components using different stimulation modes. Radiation Measurements 43,742-747.

Wallinga. J., Hobo, N., Cunningham, A.C., Versendaal, A.J., Makaske, B., Middelkoop, H. 2010. Sedimentation rates on embanked floodplains determined through quartz optical dating. Quaternary Geochronology 5, 170-175.

Wintle, A.G., Murray, A.S. 2006. A review of quartz optically stimulated luminescence characteristics and their relevance in single-aliquot regeneration dating protocols. Radiation Measurements 41, 369-391

Chapter 4

Expectations of scatter in equivalent-dose distributions when using multi-grain aliquots for OSL dating

Alastair C. Cunningham, Jakob Wallinga, Philip S.J. Minderhoud
Accepted for publication in Geochronometria

Abstract

In the OSL dating of sediment, the scatter in equivalent dose (De) between grains is almost always larger than would be expected due to counting statistics alone. Some scatter may be caused by insufficient (partial) bleaching of some of the grains prior to deposition. In order to date partially bleached sediment, it is essential to estimate the amount of scatter caused by other processes (e.g. grain-to-grain variability in the natural dose rate). Measurements of such scatter are performed at the single-grain level; by contrast, most OSL dating is performed on multi-grain subsamples, for which grain-to-grain scatter is reduced through averaging g.

Here we provide a model for estimating the expected scatter (i.e. excluding that caused by partial bleaching) for multi-grain aliquots. The model requires as input the single-grain sensitivity distribution, the number of grains in the sub-samples, and the expected scatter at the single-grain level, all of which can be estimated to an adequate degree. The model compares well with measured values of scatter in De, determined using aliquots of various sizes, and can be used to help produce a minimum-age De from multi-grain subsamples that is consistent with single-grain data.

4.1 Introduction

Optically Stimulated Luminescence (OSL) dating of mineral grains requires an estimate of the radiation dose the grains have absorbed during the burial period. Commonly, the equivalent dose (De) is determined for several tens of aliquots, with each aliquot consisting of tens to thousands of grains. The De for each aliquot is estimated by comparing the 'natural' light yield from grains under optical stimulation, to the light yield observed under the same conditions following one or more artificially given radiation doses (while also correcting for changes in sensitivity). Ideally, the De of each aliquot is found to be consistent with a common value (e.g. weighted average). However, De measurements frequently show a broader distribution than would be expected from counting statistics alone (e.g. Jacobs et al., 2008; Roberts et al., 1999).

An understanding of the sources of scatter is important for accurate age determination. This is particularly the case if it is suspected that the sediment contains grains that do not yield the desired burial dose information (e.g. OSL signal not reset in all grains prior to deposition and burial, post-depositional mixing of grains of different ages). For such situations, different statistical models have been introduced: Galbraith et al. (1999) have proposed the three and four parameter Minimum Age Models (MAM3, MAM4) to estimate the palaeodose from a De distribution which contains well bleached and partially or unbleached grains. Roberts et al. (2000) have provided a Finite Mixture Model (FMM) for the case where several distinct populations are present.

The MAM3, MAM4 and FMM require the prior determination of the amount of scatter that could be expected from a single, well-bleached population of grains. Referred to as 'overdispersion' (σ), this term must incorporate every source of scatter except that from counting statistics and the scatter caused by the existence of more than one population (i.e. heterogeneous bleaching, mixing). Overdispersion is approximately the relative standard error of the underlying dose distribution (Galbraith et al., 1999).

Information on the causes of overdispersion in De distributions has been obtained from a number of studies using single-grain measurement systems (Thomsen et al., 2005; Duller et al., 2000) and/or modelling at the single grain level (Mayya et al., 2006; Nathan et al., 2003). It is likely that the majority of overdispersion comes from either micro-scale variations in natural dose rate, or from an as yet unexplained source of uncertainty in the De estimate observed for gamma-irradiated samples (Thomsen et al., 2005). Errors arising due to machine reproducibility typically make a small contribution to the overall uncertainty (e.g. 1.5% per OSL measurement for the Risø single-grain system (Thomsen et al., 2005)).

The MAM3 and FMM are designed for use with single-grain data (see e.g. Arnold and Roberts, 2009), and investigations on causes of overdispersion have also concentrated on single-grain data. By contrast, most OSL dating studies are carried out using small aliquots of quartz, with each aliquot containing tens, hundreds or thousands of grains. The use of multi-grain aliquots enables greater measurement precision and reduced measurement time; moreover, the apparatus required for single-grain measurements is not universally available. There is a need, therefore, of a means to convert information obtained from single-grain studies into a format applicable for OSL dating with multi-grain aliquots. Here we seek to address this issue, by establishing how the overdispersion parameter should be altered when the MAM3 is used with multi-grain aliquots. Furthermore, we consider an additional source of scatter relevant only to multi-grain aliquots, arising through the use of a non-homogenous laboratory beta source.

4.2 Correction for aliquot size

In single-grain dating studies of well-bleached quartz, the value of σ is commonly found to be around 20 % (Duller, 2008; Arnold and Roberts, 2009). However, when using aliquots with multiple grains, it can be expected that σ will be reduced, as a certain amount of averaging must occur. Failure to account for this effect when using the MAM3 will tend to lead to overestimation of D_e, as the MAM3 will then allow for more overdispersion than is realistic. The extent of the averaging effect depends on the number of grains on the aliquot, and their respective intensities, and is determined here using stochastic simulations.

Since the advent of single-grain luminescence-measurement technology (Bøtter-Jensen *et al.*, 2000), it has become apparent that the OSL sensitivity of quartz varies dramatically between grains (Adamiec, 2000; Duller *et al.*, 2000; Duller, 2008). Furthermore, the spread in grain sensitivity varies from sample to sample. With some highly sensitive samples, almost all quartz grains give a measurable OSL signal. More frequently however, it is only a small proportion of grains (< 5 %) which provide most of the OSL signal. This variation can be seen in Fig. 4.1, which shows the cumulative distributions of single-grain OSL intensity for four samples discussed in this paper.

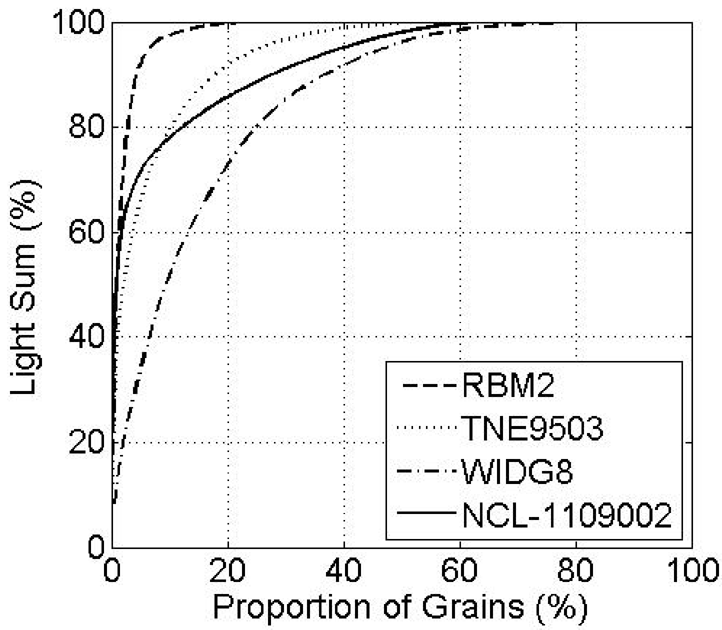

Fig. 4.1. The cumulative light sums for the four samples referred to in this paper, obtained through single-grain measurements. This figure reproduces Fig. 1 of Duller et al. (2000), with the addition of sample NCL-1109002.

We consider here a sample of n_a aliquots, with each aliquot containing n_g grains. Each grain is assigned two values: Firstly, a value representing the grain-specific D_e, which is drawn from a normal distribution with mean of zero and standard deviation of one. The normal distribution is used to simulate variation in D_e at the single grain level. The second value assigned to each grain is a sensitivity value, with each drawn randomly (with replacement) from the chosen dataset of single-grain sensitivity values. For each aliquot, we calculate the average D_e, weighted by the sensitivity values, and the square root of the sum of the sensitivity values (which becomes the weight for the aliquot).

The statistic of interest is the standard deviation of D_e across n_a aliquots. We chose n_a = 30 in this simulation, the number of aliquots typically measured for a single sample in dating applications. We use the weighted standard deviation s, taken from Galassi *et al.* (2009):

$$s = \sqrt{\frac{1}{1-v}\sum_{i=1}^{n_a} w_i (x_i - \mu)^2} \tag{1}$$

with normalized weights w and weighted average μ, and where:

$$v = \sum_{i=1}^{n_a} w_i^2 \tag{2}$$

The use of v of eq. 1 accounts for the variability in luminescence sensitivity between aliquots. If there is little difference in sensitivity between aliquots, this term has little effect; on the other hand, a luminescence signal derived from a small percentage of the aliquots will lead to a larger s.

The results of this simulation are shown in Fig. 4.2, which plots the scatter in D_e as a function of the number of grains in each aliquot, for three different sensitivity distributions. The curves can be interpreted as the correction factor that should be applied to the single-grain overdispersion term. For example, if we were to measure D_e on 30 aliquots of sample RMB2 with 22 grains in each aliquot, and we have previously determined (or estimated) inherent scatter of 20 % at the single grain level, then the n_g-corrected term is 20 % x 0.78 = 15.6 % (this assumes that the measurement reproducibility errors have already been removed). As the sensitivity distribution of sample RMB2 is dominated by only a small percentage of the grains, and the number of grains on each aliquot is small, the reduction in the dispersion term is limited. For large aliquots of 1600 grains, the corrected term would be reduced to 20 % x 0.15 = 3 %. By contrast, if we repeat the calculations with sample WIDG8 (from which most grains give a significant luminescence signal), then we obtain 20 % x 0.40 = 8.0 % and 20 % x 0.05 = 1 % for aliquots containing 22 and 1800 grains, respectively. The correction of σ creates an additional source of error, the size of which is dependent on the aliquot size and the number of aliquots used (Fig. 4.2)

It should be noted that while the averaging effect reduces scatter in De for larger aliquots, scatter caused by reproducibility error is not subject to the same relationship. The importance of reproducibility error therefore increases with the size of the aliquots, and should be accounted for separately (see section 4.5).

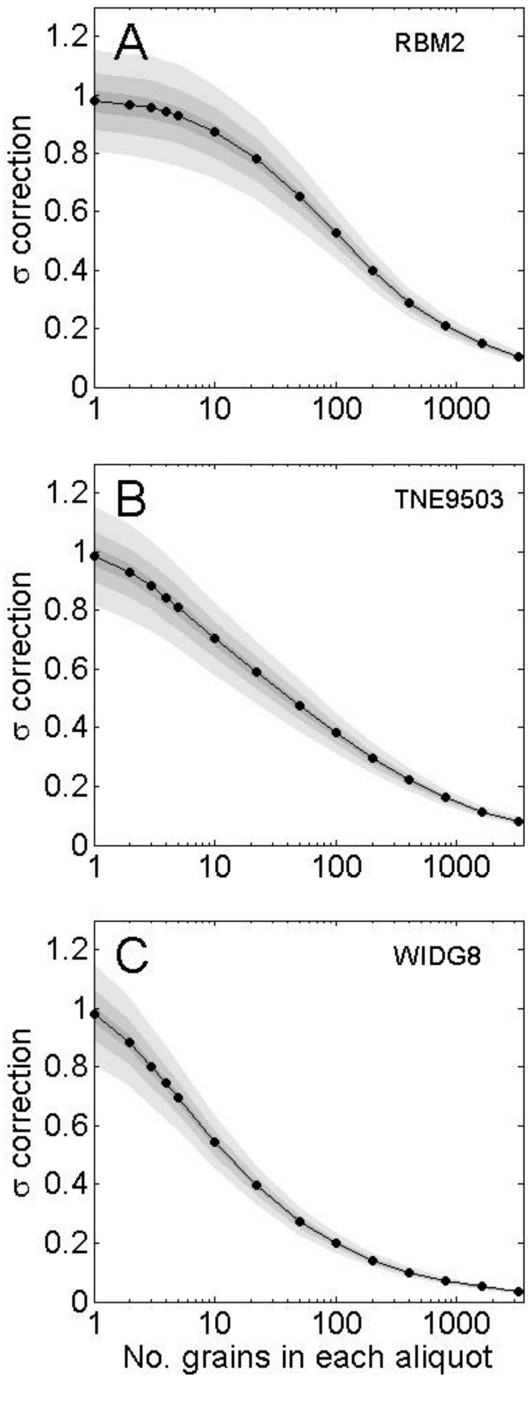

Fig. 4.2. The influence of aliquot size on overdispersion in D_e, modelled using three different single-grain sensitivity distributions (RBM2, TNE9503, WIDG8, see Fig. 4.1). The y-axis term 'σ correction' indicates the correction that must be made to the single-grain overdispersion term for use with multi-grain aliquots. The uncertainty on the correction depends on the number of aliquots n_a; standard error regions are shown for $n_a = 30$, 10, and 5. If the correction is used with the MAM3, then the uncertainty is dependent on the number of aliquots *consistent with the minimum age*, not the total number of aliquots.

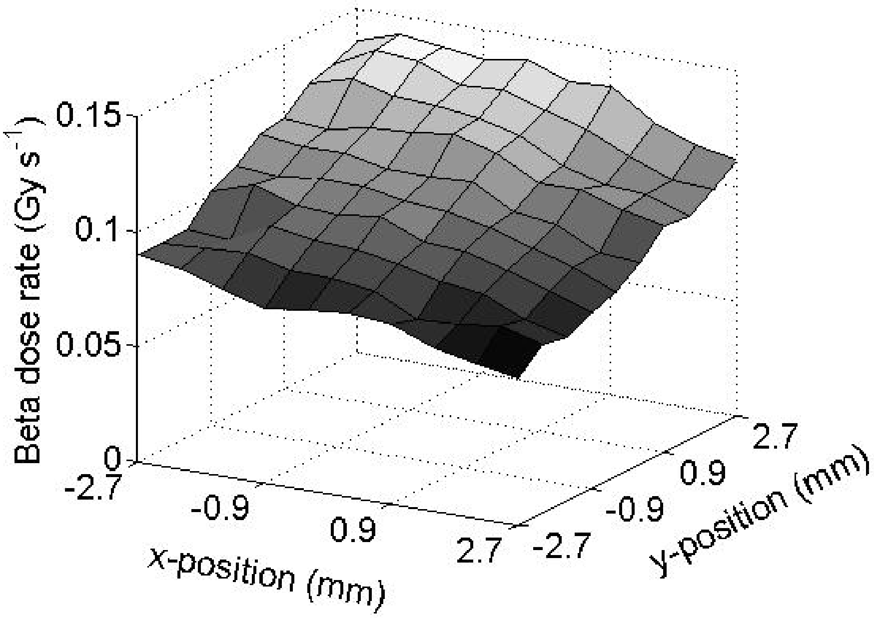

Fig. 4.3. Variation in dose rate across a single-grain disc, measured using calibration quartz on a 10 x 10 grid of single-grain holes. The minimum and maximum values are 0.064 and 0.142 (Gy s^{-1}) respectively. The data is from Ballarini et al. (2006).

4.3 Accounting for a non-homogeneous laboratory source

An additional source of scatter relevant to multi-grain aliquots may come from variation in the dose rate provided by the beta source. ^{90}Sr/^{90}Y beta sources are typically used to administer regenerative and test doses in OSL protocols. Inhomogeneity in a source may occur due to a number of reasons (see Ballarini *et al.* (2006) and references therein) and may lead to different grains receiving different regenerative doses. Under single-grain systems such source variability can be corrected for by grain-specific calibration, but this is not possible for multi-grain aliquots, as it is not known which grains in an aliquot are producing the luminescence signal. Unlike other sources of measurement error, the effects of source variability will not be accounted for by a dose recovery test because the same source is used for both administering and estimating the 'given' dose.

To estimate the increase in scatter caused by an inhomogeneous source, we performed a similar simulation to that in section 4.2, but with the addition of grain-specific dose rates. The dose rates are calculated using the data of Ballarini *et al.*

(2006), who showed an example of a non-homogeneous laboratory source. The data of Ballarini *et al.* (2006) was created by measuring the OSL of calibration quartz on a 10 by 10 grid of single-grain holes, and is reproduced in Fig. 4.3. In our simulation, the laboratory dose rate for any position is calculated using a weighted average of the nearest measured points. The number of grains in each aliquot is a simple function of grain size and mask size, assuming 80 % packing density (we use the term 'mask size' to indicate the diameter of the circular area on the disc containing the grains). Each grain is assigned two values: the laboratory dose rate determined by the position of each grain (randomly assigned within the area determined by the mask size); and a sensitivity value, drawn randomly, with replacement, from a specified dataset. We calculate the weighted-average laboratory dose rate for each aliquot. The dispersion caused by the laboratory dose-rate variability is then the standard deviation of the dose rate across n_a aliquots (equation 1), divided by the mean laboratory dose rate. In this simulation, variation in D_e is not included.

The amount of additional dispersion caused by the non-homogeneous source is shown in Fig. 4.4 for three different grain sizes, and for each of the three single-grain datasets. The importance of grain size is in determining (with mask size) the number of grains on the aliquot. As the mask size increases, there are two competing effects: firstly, an increase in the range of laboratory dose rate applied to the grains; secondly, an increase in the averaging effect across the disc due to larger number of grains. The averaging effect is dominant for smaller grain sizes, larger mask sizes, and when the single-grain sensitivity distribution is more uniform (e.g. WIDG8).

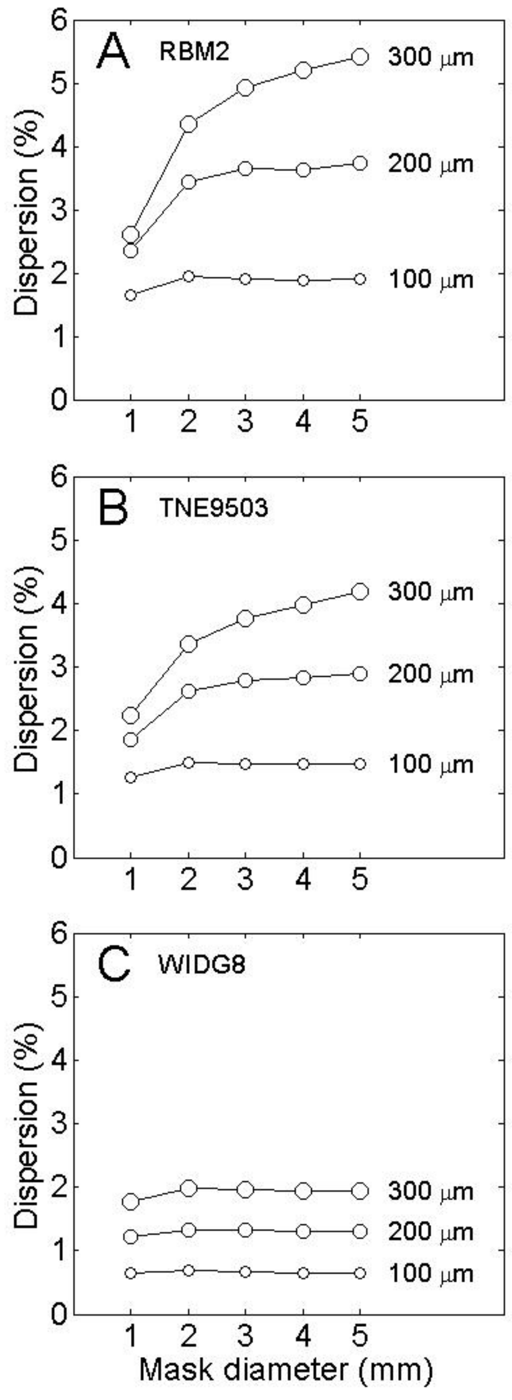

Fig. 4.4. Simulation of scatter in D_e due to a non-homogeneous beta source. Results depend on the mask size, grain size (which together determine the number of grains in the aliquot), and the single-grain sensitivity distribution (RBM2, TNE9503, WIDG8).

4.4 Validation

Sample and measurement details

The relationship between overdispersion and mask size is tested here using sample NCL-1109002, an aeolian coastal dune sample from the western Netherlands. The grain size of the sampled sediment is a relatively uniform 200-250 µm. Quartz grains of 180-200 µm were extracted by sieving and chemical treatment (HCl, H_2O_2 and HF).

Measurements were carried out on a Risø TL-DA-15 reader (Bøtter-Jensen *et al.*, 2000), using a Single Aliquot Regenerative dose (SAR) protocol described in Table 4.1 (Murray and Wintle, 2000; 2003). Optical stimulation was with 470 nm diodes with a power of ~35 mW cm^{-2} at the sample position. Irradiation was with a (homogenous) ^{90}Sr/^{90}Y beta source providing a dose rate of ~0.13 Gy s^{-1}. Infrared (IR) diodes emitted at a wavelength of 875 nm and power of ~116 mW cm^{-2}. The detection filter was a 7.5 mm Hoya U340. Single-grain measurements were made using a single-grain attachment to the reader, with stimulation by a Nd:YVO_4 diode-pumped laser (532 nm wavelength), with a 2.5 mm Hoya U340 detection filter (Ballarini *et al.*, 2005).

Multi-grain aliquot OSL signals were processed using integration channels of 0 – 0.60 s for the initial signal, and 0.60 – 2.10 s for background subtraction. These intervals were selected in order to ensure that the net signal was dominated by the 'fast' OSL component, while keeping counting errors to acceptable levels (Cunningham and Wallinga, 2010). D_e for each aliquot was estimated using a linear fit to a single regenerative dose point (see Ballarini (2006) for a discussion on this point). This was followed by a 'zero' dose point, and two repeat points (the second following IR stimulation). Aliquots were accepted if recuperation was less than 0.05 Gy or was consistent with zero within the error term, and if the two recycling ratios were between 0.9 and 1.1. For the single-grain measurements, each grain was stimulated for 0.83 s. We used the 'early background' principle for signal analysis, using the first 0.17 s for the initial signal, and the subsequent 0.42 s for background subtraction.

Treatment	Conditions
Dose	N, 3.2, 0, 3.2 Gy
Preheat	180ºC for 10 s
OSL (470 nm)	125ºC for 40 s
Test dose	3.2 Gy
Cutheat	170ºC
OSL (470 nm)	125ºC for 40 s
OSL Bleach (470 nm)	180ºC for 40 s

Table 4.1. Details of the SAR protocol used.

Overdispersion as a function of aliquot size

The dependence of overdispersion on aliquot size has been tested by measuring D_e using three different mask sizes: 2 mm (~80 grains), 3 mm (~180 grains) and 5 mm (~500 grains). The range of possible mask sizes is limited; below 2 mm there are too few grains in the aliquot to provide sufficient signal (for this sample); above 6 mm the grains on the edge of the mask area will receive a lower laboratory dose rate due to the geometry of the source (leading to larger D_e and more scatter). Results can be seen in Table 4.2 and Fig. 4.5.

As expected, the overdispersion in D_e decreases when the mask size increases. Unexpectedly, there is also a significant increase in D_e when the 5 mm mask size is used. It is possible that larger aliquots are more likely to include grains which are inappropriate for dating (e.g. feldspars, which are subject to a higher internal dose rate), but the strength of the OSL signal from other grains allows the aliquots to pass acceptance criteria. For smaller aliquots, such grains would be more likely to dominate the OSL signal, and to lead to rejection of the aliquot.

Type	Mask	No. accepted	Dose (Gy)	D_e (CAM)	σ
D_e	Single grains	31	Natural	1.150 ± 0.049	23.0 ± 3.1
D_e	2mm (~80 grains)	37	Natural	1.068 ± 0.029	13.4 ± 2.2
D_e	3mm (~180 grains)	27	Natural	1.072 ± 0.025	9.8 ± 1.9
D_e	5mm (~500 grains)	22	Natural	1.149 ± 0.021	7.6 ± 1.5
Dose Recovery (β)	3mm (~180 grains)	30	3.08	3.105 ± 0.032	3.0 ± 1.2
Dose Recovery (γ)	3mm (~180 grains)	35	?	1.155 ± 0.023	9.7 ± 1.6

Table 4.2. Measurements of D_e and σ for sample NCL-1109002, using different aliquot sizes, and results of dose recovery tests using different sources. The precise dose given with the gamma source is unknown.

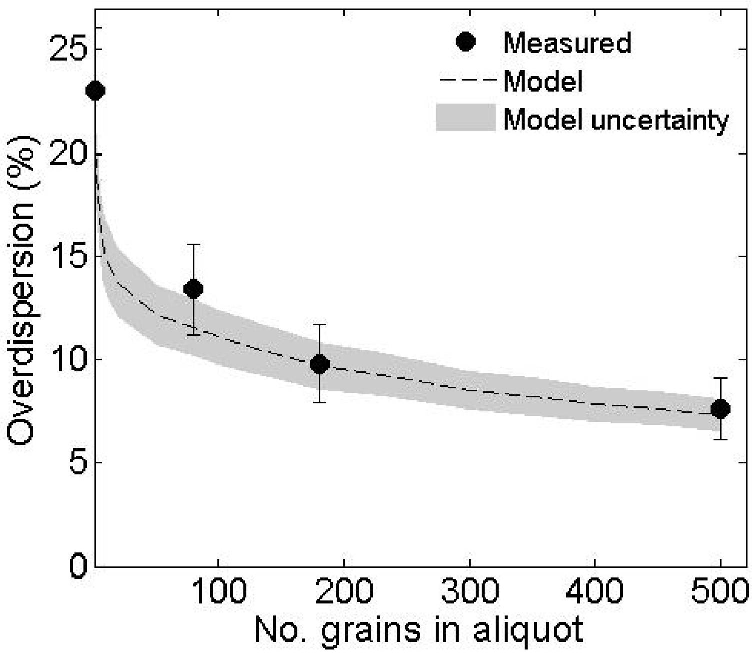

Fig. 4.5. Measured overdispersion (σ) on D_e for four different aliquot sizes of sample NCL-1109002, calculated using the Central Age Model of Galbraith et al. (1999). The model prediction is also shown, with the single-grain overdispersion (23 ± 3 %) used as the basis of the model. Model uncertainty is based solely on the error term of the single-grain overdispersion measurement.

Comparison with model

We have applied the stochastic model described in section 4.2 to the sample used here. This calculation involves several steps. Firstly, the scatter caused by non-perfect measurement reproducibility was estimated, using a dose-recovery test. This test was carried out on 3-mm aliquots, using the built-in beta source to provide the dose. The σ in the dose recovery results was found to be 3.0 ± 1.2 %. Since this figure relates to machine uncertainty, we assume that it is identical for all aliquot sizes, including single grains. While it is likely that the additional complexity of the single-grain apparatus leads to less precision in measurement reproducibility, the extra dispersion (measured as 3.3 % by Thomsen et al., 2005) is not significant when compared to the ~20 % spread in De observed at the single-grain level.

Using the stochastic model described in section 2, the expected relationship between σ and aliquot size has been modelled, and is plotted in Fig. 4.5. The model uses several pieces of information: the single-grain sensitivity distribution for the sample, which was measured using a single-grain OSL reader (Fig. 4.1); the number of grains on the disc (determined by the mask size); the amount of scatter present at the grain-to-grain level (measured with single-grain OSL); and the scatter caused by machine reproducibility error (3 %). The measured single-grain overdispersion value of 23 % is similar to previous studies: Arnold and Roberts (2009) have collated overdispersion data from published work, and found the mean overdispersion in single-grain studies of well-bleached samples to be 20 %, with a standard deviation of 9 %.

To check the source of the grain-to-grain scatter in D_e, we conducted a further dose-recovery experiment. This time, the initial 'given' dose was administered using a separate ^{60}Co gamma source, which provided a uniform dose to the grains before they were placed on the stainless-steel discs (Bos *et al.*, 2006). Using 3 mm aliquots, we found σ of 9.7 %, far higher than the standard dose recovery of 3 %, and indistinguishable from σ found on the natural sample (9.8 %). In other words, the precision with which we can recover a known dose is much poorer when that dose is given outside the measurement apparatus. A similar result was found by Thomsen *et al.* (2005), and indicates that the orientation of the grains with respect to the radiation field may be important, either through dose attenuation with depth in the grain, or some other effect.

4.5 Discussion

Aliquot size

The use of larger aliquots leads to a reduction in inter-aliquot scatter in D_e, and this process can be adequately described by the stochastic model presented above. Three pieces of information are required in order to use this model for a sample:

1. The number of grains in each aliquot.
2. The single-grain sensitivity distribution.
3. An estimate of σ at the single-grain level

In order to use this model to generate the expectation of σ, each of these items of information needs to be estimated. The number of grains in each aliquot can be estimated by counting the grains on a selection of aliquots, or by calculating the number of grains that fit into the mask area. The single-grain sensitivity distribution, and the single-grain σ, will be unmeasured for most samples. However, good approximations could be made by using prior knowledge of similar samples, or with the data presented in this paper. In the absence of prior knowledge on sample characteristics, a good starting point would be to assume that the single-grain σ is 20 %, and to pick a sensitivity distribution from Fig. 4.1 which seems most reasonable.

There is undoubtedly some uncertainty in the estimate of σ for multi-grain aliquots. It should also be noted that the probability of the estimate being correct for a given selection of aliquots depends on the number of aliquots used (if using the CAM), or the number of aliquots from the well-bleached population (if using the MAM3).

To apply the model in practice, it is also necessary to estimate the uncertainty deriving from machine reproducibility (e.g. by using the CAM overdispersion term from dose-recovery data). As this sort of uncertainty does not get averaged out with more grains, it will tend to become more important for larger aliquots.

Non-uniformity of the laboratory beta source

It is encouraging that the averaging effect of large numbers of grains largely cancels out any non-homogeneity in the laboratory beta source. This comes about for two reasons. Firstly, for the source used in our calculations, the gradient of the dose rate across the disc is relatively uniform, and the calculations assume the grains are equally likely to exist at any point within the mask area. The average dose rate is therefore largely independent of mask size, meaning that as the mask size is increased, the averaging effect caused by more grains overcomes the wider spread in laboratory dose rates between grains. Should either of these conditions not be met (e.g. a dome-shaped dose rate across the disc, or a non-uniform spread of grains across the mask area), then an increase in scatter in D_e would be observed with increasing mask size.

Example application: Estimating σ for multi-grain aliquots

We provide a brief example to demonstrate how the message of this paper can be used in practice. We use a sample of quartz grains from the banks of a stream in the Lushoto district, Tanzania (Sample code NCL-4211017). The grains are likely to have been deposited through fluvial and/or hillslope processes, and the data shows signs of insufficient bleaching. We carried out OSL measurements on small aliquots, with 2 mm mask size (~80 grains per aliquot, grainsize of 180-212 μm). The De distribution for the multi-grain aliquots is shown in Fig. 6a. To determine the burial dose using the MAM3, an appropriate value for σ must be chosen. We start with the assumption that the true single-grain overdispersion in the burial dose is 20 %, and the single-grain sensitivity distribution approximates that of sample TNE9503 (i.e. a typical quartz sample; also found to be appropriate for this sample through single-grain sensitivity measurements). The expected σ is then the sum of the following:

1. Grain-to-grain scatter, corrected for the number of grains on the disc. From Fig. 2b, the correction is ~0.40; the corrected overdispersion term is then 0.20 x 0.40 = 0.08.
2. Measurement reproducibility errors: we use 3 %, taken from the measured overdispersion of the dose-recovery data (Table 2).

Added in quadrature, the best estimate for σ is 0.085. To determine the minimum-age D_e for this sample, the σ value can be added (in quadrature) to the individual D_e error terms before using the MAM3. The outcome of this process is a minimum-age D_e of

0.306 ± 0.025 Gy (single point shown in Fig. 6c). Fig. 6c also shows the dependence of the mimimum-age D_e on the chosen value of σ; for this sample, there is relatively little change in D_e for σ between 0 and 0.15, but a significant shift in D_e for higher σ values. To validate the multi-grain aliquot approach, we also show results from single-grain D_e measurements of the same sample (Fig. 6b). Assuming a σ of 0.20 for the single grain data provides a minimum-age D_e of 0.302 ± 0.018 Gy, indistinguishable from the multi-grain aliquot estimate.

Fig. 4.6. (Overleaf) (a) Histogram of D_e for sample NCL-411017 (Tanzania), measured using aliquots of ~80 grains each. 54 aliquots passed acceptance criteria (recuperation less than 10% of regenerative dose, both recycling ratios between 0.9 and 1.1); There are 11 aliquots giving D_e greater than 2 Gy which are not shown. Using σ_b of 0.085, the MAM3 D_e is 0.306 ± 0.025, shown by vertical lines in the figure. (b) Histogram of single-grain De values for the same sample; MAM3 gives 0.302 ± 0.018 Gy (σ_b = 0.20; one imprecise negative-D_e grain was excluded). (c) The dependence of the multi-grain-aliquot MAM3 De on the specified σ_b value for this sample. The suggested σ_b value of 0.085 (single data-point) provides a minimum age in agreement with that derived from the single-grain data (horizontal lines). Measurement details are the same as those described in section 4, other the preheat and cutheat temperatures (240ºC and 220ºC, respectively, with a high-temperature bleach of 250ºC).

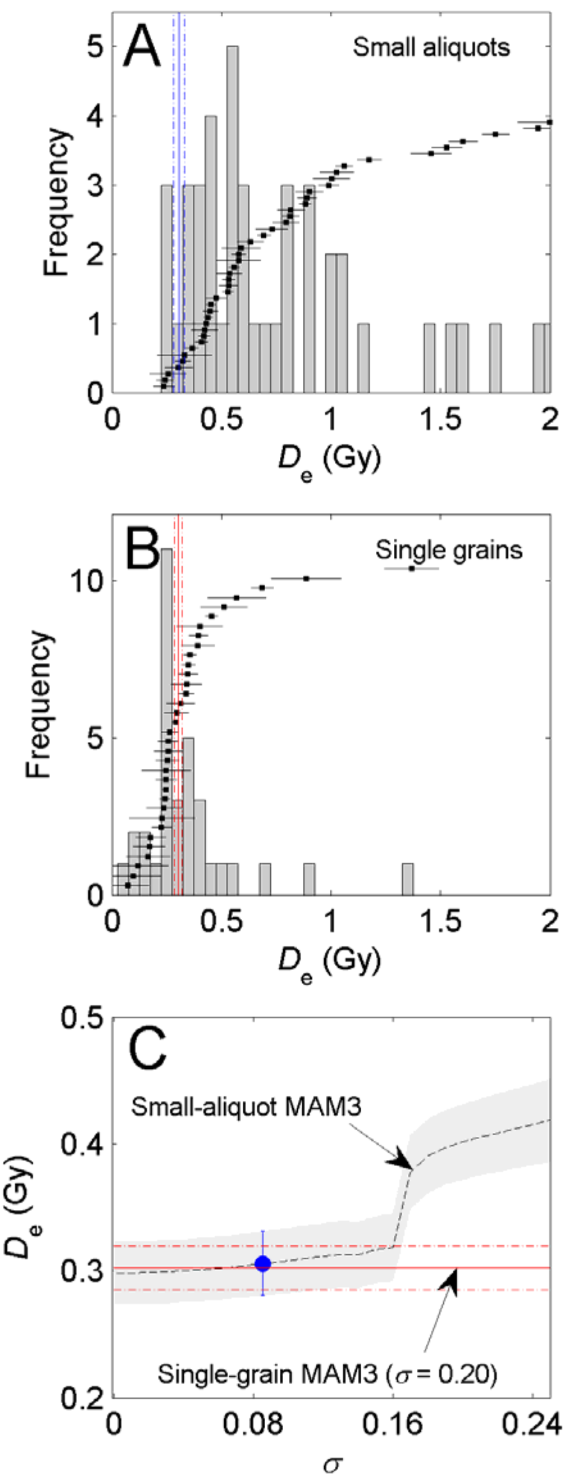
A
Small aliquots
Frequency
D_e (Gy)
B
Single grains
Frequency
D_e (Gy)
C
Small-aliquot MAM3
Single-grain MAM3 (σ = 0.20)
D_e (Gy)
σ

4.6 Conclusion

Use of the minimum age model for partially bleached (or mixed) samples requires an estimate of σ, the amount of scatter in D_e from sources other than partial bleaching (or mixing) and counting statistics. This scatter is present at the single-grain level, but with multi-grain aliquots the effect is reduced because of averaging in each aliquot. This process can be described by the stochastic model presented here, which requires the following information:

1. An estimate of overdispersion at the single-grain level.
2. The number of grains in each aliquot.
3. The single-grain sensitivity distribution.
4. The machine/measurement uncertainty

A similar model can be used to estimate the increase in scatter caused by a non-homogeneous laboratory beta-source. For the particular beta-source described in this paper, with dose rates differing by a factor two across the disc, the additional scatter was found to be largely insignificant compared with other sources of scatter for aliquots up to 5 mm diameter.

Acknowledgements

The authors are supported by NWO/STW grant DSF.7553. The scripts were written in Matlab, and are available from AC. We thank Geoff Duller for providing the information on sensitivity distributions, and Mirko Ballarini for providing the dataset on source inhomogeneity. The manuscript was improved following comments from two anonymous referees.

References

Adamiec, G. 2000. Variations in luminescence properties of single quartz grains and their consequences for equivalent dose estimation. Radiation Measurements 32, 427-432.

Arnold, L.J., Roberts, R.G. 2009. Stochastic modelling of multi-grain equivalent dose (De) distributions: Implications for OSL dating of sediment mixtures. Quaternary Geochronology 4, 204-230.

Ballarini, M. 2006. Optical dating of quartz from young deposits. PhD thesis, Delft University of Technology

Ballarini, M., Wallinga, J., Duller, G.A.T., Brower, J.C., Bos, A.J.J., van Eijk, C.W.E. 2005. Optimizing detection filters for single grain optical dating of quartz. Radiation Measurements 40, 5-12.

Ballarini, M., Wintle, A.G., Wallinga, J. 2006. Spatial variation of dose rate from beta sources using single grains. Ancient TL 24, 1-8.

Bos, A.J.J., Wallinga, J., Johns, C., Abellon, R.D., Brouwer, J.C., Schaart, D.R., Murray, A.S. 2006. Accurate calibration of a laboratory beta particle dose rate for dating purposes. Radiation Measurements 41, 1020-1025.

Bøtter-Jensen, L., Bulur, E., Duller, G.A.T., Murray, A.S. 2000. Advances in luminescence instrument systems. Radiation Measurements 32, 57-73.

Cunningham, A.C., Wallinga, J. 2010. Selection of integration time-intervals for quartz OSL decay curves. Quaternary Geochronology 5, 657-666.

Duller, G.A.T. 2008. Single-grain optical dating of Quaternary sediments: why aliquot size matters in luminescence dating. Boreas 37, 589-612.

Duller, G.A.T., Bøtter-Jensen, L., Murray, A.S. 2000. Optical dating of single sand-sized grains of quartz: sources of variability. Radiation Measurements 32, 453-457.

Galassi, M., Davies, J., Theiler, J., Gough, B., Jungman, G., Alken, P., Booth, M., Rossi, F. 2009. GNU Scientific Library Reference Manual. Network Theory Ltd.

Galbraith, R.F., Roberts, R.G., Laslett, G.M., Yoshida, H., Olley, J.M. 1999. Optical dating of single and multiple grains of quartz from jinmium rock shelter, northern Australia, part 1, Experimental design and statistical models. Archaeometry 41, 339-364.

Jacobs, Z., Wintle, A.G., Roberts, R.G., Duller, G.A.T. 2008. Equivalent dose distributions from single grains of quartz at Sibudu, South Africa: context, causes and consequences for optical dating of archaeological deposits. Journal of Archaeological Science 35, 1808-1820.

Mayya, Y.S., Morthekai, P., Murari, M.K., Singhvi, A.K. 2006. Towards quantifying beta microdosimetric effects in single-grain quartz dose distribution. Radiation Measurements 41, 1032-1039.

Murray, A.S., Wintle, A.G. 2000. Luminescence dating of quartz using an improved single-aliquot regenerative-dose protocol. Radiation Measurements 32, 57-73.

Murray, A.S., Wintle, A.G. 2003. The single aliquot regenerative dose protocol: potential for improvements in reliability. Radiation Measurements 37, 377-381.

Nathan, R.P., Thomas, P.J., Jain, M., Murray, A.S., Rhodes, E.J. 2003. Environmental dose rate heterogeneityof beta radiation and its implications for luminescence dating: Monte Carlo modeling and experimental validation. Radiation Measurements 37, 305-313.

Roberts, R.G., Galbraith, R.F., Olley, J.M., Yoshida, H., Laslett, G.M. 1999. Optical dating of single and multiple grains of quartz from Jinmium rock shelter, northern Australia: part II, results and implications. Archaeometry 41, 365-395.

Roberts, R.G., Galbraith, R.F., Yoshida, H., Laslett, G.M., Olley, J.M. 2000. Distinguishing dose populations in sediment mixtures: a test of single-grain optical dating procedures using mixturesof laboratory-dosed quartz. Radiation Measurements 32, 459-465.

Thomsen, K.J., Murray, A.S., Bøtter-Jensen, L. 2005. Sources of variability in OSL dose measurements using single grains of quartz. Radiation Measurements 39, 47-61.

Chapter 5

Extracting storm-surge data from coastal dunes for improved assessment of flood risk

Alastair C. Cunningham, Marcel A.J. Bakker, Sytze van Heteren, Bert van der Valk, Ad J.F. van der Spek, Dennis R. Schaart, Jakob Wallinga

Accepted for publication in Geology

Abstract

Future changes in climate and sea level are likely to increase the threat from storm surges in many coastal regions. Mitigation of this threat requires an understanding of storm-surge magnitude and frequency, and the relationship of these variables to climate parameters. This understanding is currently limited by the brevity of instrumental records, which rarely predate the 20th century. However, evidence of former storm surges can be recorded in coastal dunes, because the dune topography may trap high-magnitude deposits at elevated locations. Here we combine a range of techniques to extract storm-surge data from coastal-dune sediment. The sediment is tracked in the subsurface with ground-penetrating radar to assess its height and extent, and its age is determined with good precision through optically stimulated luminescence dating. The probable age of the sediment (1775/6 AD) lies within a period of increased storminess in NW Europe, and the local magnitude of the event is likely to be greater than any on instrumental record. By utilizing coastal dunes for storm-surge analysis, our approach provides a valuable new source of information for understanding storm-surge risk, which is vital for the protection of coastal regions.

5.1 Introduction

Instrumental records of sea level provide the basic return-frequency data for flood events, but reliance on these records presents two major problems for flood-risk predictions. Firstly, the records are shorter than the return frequency of extreme events, leading to imprecision in the time-magnitude estimates of major storm surges (Van den Brink et al., 2005). Secondly, the climate of the future is unlikely to remain the same as it was during the period covered by instrumental records. Future changes in climate are likely to affect storm tracks, altering the storm-surge response compared to that during the monitoring period (Lowe and Gregory, 2005).

In NW Europe, storm tracks are linked to the phase and strength of the North Atlantic Oscillation (NAO) (Ulbrich and Christoph, 1999; Pinto et al., 2009), which defines the pressure gradient between the Icelandic low and the Azores high. The relationship is not straightforward (Lozano et al., 2004), and the response of extreme events to changes in the NAO may be different to that of moderate events (Pinto et al., 2009; Ulbrich et al., 2009). This relationship would be better understood if storm-surge data existed for periods when the NAO mode was different from today, particularly for the centuries preceding the instrumental record. This period of interest corresponds to an episode of recent climate history referred to as the 'Little Ice Age' (LIA), lasting from ~1400 to ~1850 AD, when northern hemisphere temperature was up to 0.6 °C cooler than during the late 20th Century (Mann, 2002). The LIA saw an increase in wind strength in the North Atlantic and Europe (Meeker and Mayewski, 2002; Matulla et al., 2008), and a corresponding increase in sand mobility in coastal dunes fringing European seas (Clarke and Rendell, 2009).

The analysis of sediment in coastal dune environments offers great potential for increased understanding of storm-surge risk. The elevated topography of the dune environment traps sediment indicative of the magnitude of former storm surges. The ability to tap this data source would open a new avenue of research on former storm-surge magnitude, and would complement the raw frequency data available from back-barrier overwash sediment. However, the extraction of this information is challenging, and necessitates a multi-disciplinary methodology which we present in this paper. Starting from an extensive bluff-face exposure on the western coast of the Netherlands, we describe the form of the sedimentological evidence in relation to the pre-depositional environment, aided by subsurface radar tracking. The sediment is dated to the late 18th Century using optically stimulated luminescence (OSL) methods, combined with Monte Carlo simulations of radiation deposition. Finally, the interpretation of the deposit is validated against 18th century documentary sources.

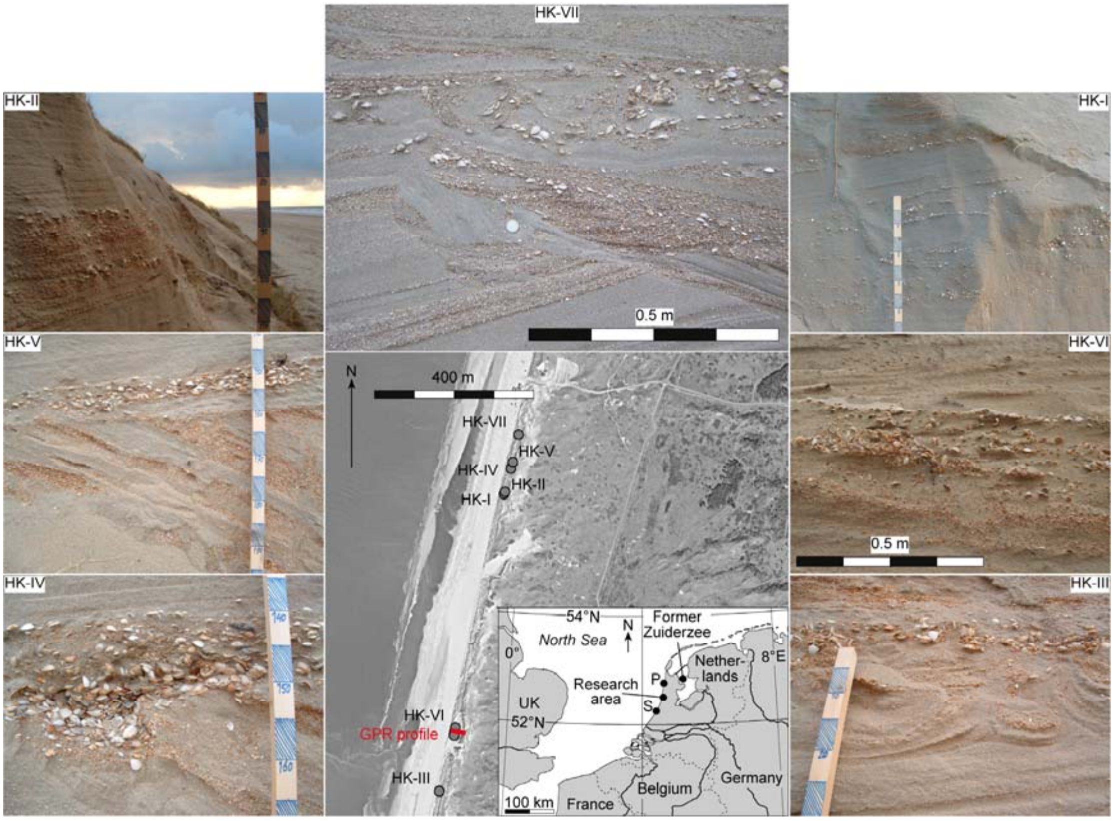

Fig. 5.1. Location of the study site, and images of seven foredune exposures (numbered HK-I to HK-VII) showing various storm-surge related sedimentary structures. The scale bar visible in five of the exposures has 5-cm sections. The seven exposures were situated along a 1 km-long stretch of scarped foredune in the western Netherlands, as shown on the aerial photograph. The GPR profile associated with HK-VI is shown as a red line; S is for Scheveningen, P is Petten. **HK-II**: 20-cm-thick unit of shells and shell hash without deformation structures. **HK-V**: Air-escape structure (to the right of the scale bar) in a unit that consists of intercalated sand and shell hash. **HK-IV**: Pocket of shells in sand. Some of the shells are articulated Cerastoderma edule. They are empty inside, indicating that they died shortly after being displaced by the storm surge. **HK-VII**: Convolute beds highlighted by the distribution of whole shells, and underlying slump structure. **HK-I**: Multiple sub-parallel horizons of single shells that are mostly oriented convex-side up. **HK-VI**: Flame structures in shell hash underlying a shell-rich unit. **HK-III**: Convolute beds highlighted by the distribution and orientation of shell hash, covered by a shell layer.

5.2 Sedimentology

For this research we described and analysed storm-surge sediment temporarily exposed within a one-kilometre-long stretch of coastal dunes near Heemskerk, the Netherlands (Fig. 5.1). This dramatic exposure was created during a significant storm surge in November 2007, which eroded the foredune back by 10-15 m at the field location. The striking feature of this exposure was a discontinuous, convolute bed of shell-bearing sand, 10-15 cm thick. The shell unit undulated in height along the exposure, commonly exceeding 4 m +NAP (NAP, the national vertical datum in the Netherlands, is roughly mean sea level), and in some places dipping below the dune foot (~2.5 m +NAP). The exposed shell unit reached it highest point of 6.5 m NAP at section HK-1, where it was observed as a series of convex-side-up shell layers separated by sand beds. Locally, the unit was observed to truncate the underlying dune sand (HK-V, HK-VII; see Fig. 1).

The mass of the shells, found with scattered pieces of brick and intact bivalves, rules out aeolian transport. Moreover, the convolute beds and other deformation structures of the shell unit are indicative of near-surface saturation by water during formation: air, trapped by a water-saturated upper zone and compressed by pressure from the water column, deforms the surrounding sediment (De Boer, 1979). As the maximum elevation of the shell unit far exceeds normal water levels (mean high water is ~0.9 m +NAP), the extensive shell layers could only have been deposited during storm-surge conditions.

The shell layers consist mainly of fossil molluscs reworked from Holocene shoreface and tidal-channel deposits. Mollusc composition differs little from that of present-day Dutch beaches, with the presence of mollusc species typical of water shallower than about 15 m –NAP (e.g. *Cerastoderma edule*, *Macoma balthica*, *Angulus fabulus*, *Angulus tenuis*), as well as species typical of deeper water (e.g. *Spisula subtruncata*, *Mactra corallina*, *Donax vittatus*, and the gastropod *Euspira pulchella*). The only double-valved specimens found in the storm-surge deposit were *Cerastoderma edule*. About 50 of these Common Cockles were clustered at section HK-IV. As there was no sand inside any of these specimens, it is likely that they were alive when they were uprooted from the seabed and washed onto shore at the time of the storm surge.

Information on the inland extent of the shell-rich unit was obtained through ground-penetrating radar (GPR). The exposed bluff face at section HK-VI provided an ideal starting point for GPR profiling, allowing immediate ground-truthing of the GPR signatures (Fig. 5.2). The shell unit is identifiable as a planar, high-amplitude reflection that shows a gentle overall dip in a landward direction. The continuous reflection extends up to 1 km inland, where it appears to be linked to former inter-dune lows. At these inland locations, wind-blown pits, boreholes and hand-dug trenches provided further verification of the GPR signature.

The distribution of the storm-surge unit reflects a contemporary frontal-dune configuration that differs from the artificially maintained sand dike marking the modern coastline. In historical times, vulnerable lows in the dune ridge were not uncommon, as testified by numerous paintings and drawings. Several dune gaps were present near Heemskerk during the 18th century (Kops, 1798). The presence of these gaps explains the nature and lateral distribution of the observed storm-surge unit. Water entered the inner dunes through gaps, scouring wide channels, overtopping low dunes and depositing extensive perched fans (cf. Morton and Sallenger, 2003) and sheets. Sand and shells were transported landward and deposited mainly behind the frontal dunes and other large obstacles, where current velocities and wave energy diminished. The fact that the exposed shell layers were overlain by thick units of aeolian sand is the result of steady coastal erosion since their deposition, and an associated landward shift of the frontal dune. Annual coastal profiles from the research area show that the dune crest and dune foot have shifted landward by 30 to 40 m since 1965. Before that time, the frontal dune was located even farther seaward, placing the initial storm-surge unit behind the ridge and therefore not or only slightly buried for part of its existence.

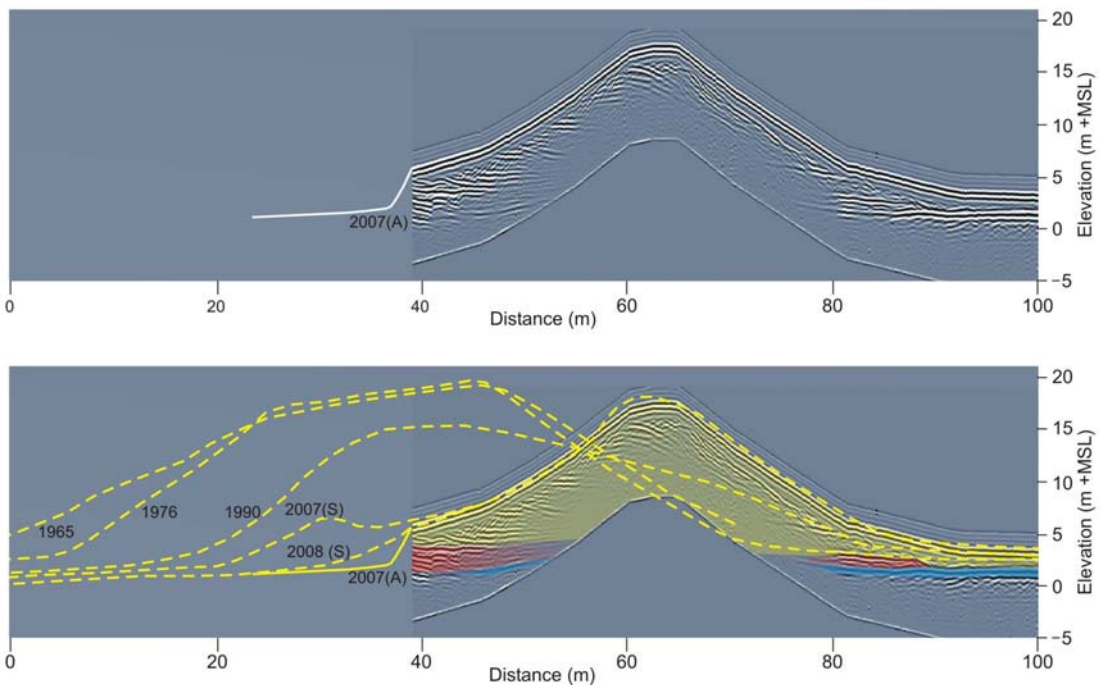

Fig. 5.2. GPR profile across the foredune at the study site, and coastal profiles from selected years. Upper panel: GPR profile (200 MHz, unshielded), starting at the exposure site HK-VI (left side of image) and tracking 60 m inland. Lower panel: Interpretation of the GPR image. The storm-surge beds (in red) are identified as planar, high-amplitude reflections, bracketed by curved facies representing aeolian strata (in yellow). The groundwater table is shown in blue. Overlain are cross-shore profiles from the governmental monitoring database ‘Jarkus’, measured annually since 1965, showing steady erosion of the dune foot and landward migration of the dune crest. Profiles marked S (dashed lines) were recorded in the spring; the profile marked A (solid line) was recorded with RTK-GPS shortly after the storm surge of November 2007.

5.3 Dating

OSL dating was conducted on three sections of the frontal dune (HK-I, HK-III and HK-VII), plus one section 600 m inland (ZN-I) that had previously been studied in a former exposure, but had not been reliably dated (Jelgersma et al., 1995). The OSL signal of quartz grains is reset by daylight exposure during transport of the grains, and builds up after burial through absorption of naturally occurring ionising radiation. By using grains of quartz embedded in the sediment, OSL provides a direct means of dating an event, often when no other dating method is suitable. However, the OSL dating of flood deposits provides two significant challenges. Firstly, the quartz grains' exposure to sunlight during the event may be insufficient to completely reset the OSL signal, leading to an overestimate of the age. However, using recent developments in signal processing (Cunningham and Wallinga, 2010), this effect was found to be insignificant for all but one sample (see Supplementary Methods, Figures and Tables). A more serious challenge lies in the heterogeneous nature of flood sediments. For several of the storm-surge samples, a high proportion of marine shells (~30% by weight) prohibits the usual approach to estimating the ambient radiation dose rate, as the shells have a significantly different radionuclide concentration to the surrounding sediment. To overcome this difficulty, we constructed a model of the deposition of beta electrons in the sediment, using a Monte Carlo transport code (Briesmeister, 2000; Schaart et al., 2002; Nathan et al., 2003), and determined the correction that should be made to the dose-rate calculations. With these techniques (detailed in the supplementary material) we found consistent ages for the storm-surge samples, validated by high-precision OSL ages on the overlying and underlying aeolian sediment.

The OSL ages (Fig. 5.3; Supplementary Table 3) obtained for the three frontal-dune sections indicate similar patterns of deposition across the three sites, categorised as follows: 1. aeolian deposition prior to the storm-surge event(s), AD 1600–1750; 2. deposition and deformation of sediment associated with the storm surge, AD 1760–1785; 3. aeolian deposition following the storm-surge event(s), AD 1775–1900. All three sections show an age gap between phases 1 and 2, most likely caused by erosion of material during the storm surge (as is apparent from the sedimentology). The inland section shows a similarly phased chronology, except that the underlying dune sand (AD 1100) was deposited during an earlier period of aeolian activity when the coastline was much farther seaward than today (Hallewas, 1981). For this site, the apparent age gap between phases 1 and 2 is more likely due to a hiatus in deposition.

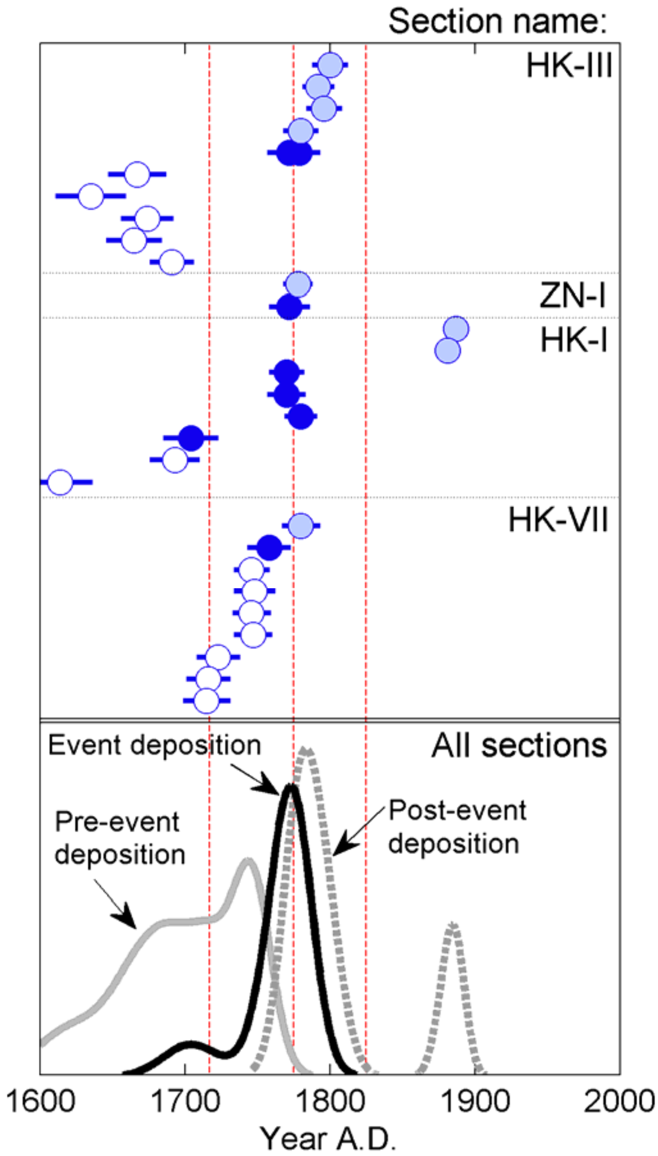

Fig. 5.3. OSL dating results. Upper panel: Each OSL age is plotted with its associated 1σ error term. Within each stratigraphical section (HK-III, ZN-I, etc.), samples are plotted in stratigraphical order. Open symbols for samples from below the storm-surge unit, solid symbols for samples from within the storm-surge unit, shaded symbols for samples from above the storm-surge unit. Lower panel: the same OSL ages plotted as summed probability densities for pre-event, event, and post-event deposition. Dashed vertical lines indicate documented storm surges in 1717, 1775/6 and 1825.

5.4 Discussion and Conclusion

The existence of a significant storm surge in the late 18th Century is confirmed by contemporary documentary sources. While reliable observations of surge height were not recorded at the time, written accounts attest to two major events taking place within the period determined by the OSL dating. These events occurred in consecutive years, 1775 and 1776 (Hering, 1776; 1778). Although there are no records concerning the field site itself, there are fragmentary records of the impact these storm surges had on more populated areas of the western Netherlands; these mostly concern the 1775 event. At the coastal town of Scheveningen, ~45 km south of the exposure site, half the town was flooded. Eyewitness accounts from Petten (20 km north of the site) recount the cutting of incipient channels into the frontal dune (Warnars and Den Hengst, 1776).

The extraction of sedimentary storm-surge records has hitherto exploited back-barrier sediment, notably in relation to hurricane overwash deposits in the western Atlantic (Donnelly et al., 2004; Boldt et al., 2010). Such records can determine storm-surge frequency during the late Holocene, and are particularly useful when they can be linked to climate parameters (Donnelly and Woodruff, 2007; Mann et al., 2009). The non-uniform topography of barrier systems makes analysis of their sedimentary record more challenging; nevertheless, an understanding of the subsurface can be gained through GPR profiling. The erosional signatures of storm-surges have previously been identified in radar profiles (Bristow et al., 2000; Buynevich et al., 2004; Switzer et al., 2006). Furthermore, Buynevich et al. (2007) were able to use buried erosional scarps in a prograding barrier as a record of storm-surge frequency, with age constraints provided by OSL dating of the overlying sediment. Our methodology offers a new dimension in flood-risk analysis. Firstly, the elevation of the deposits within the dunes can be used to infer magnitude of storm surges, information that is not recorded in back-barrier sediment or erosional features. Secondly, the dune environment enables the use of OSL to date the sediment with a high degree of precision. The importance of the dating should not be underestimated, as precise dating in the LIA time period is particularly difficult by other methods. This study further extends the use of OSL to shell-rich sediments, or indeed other sediments with heterogeneity on the millimeter scale. Given the ubiquity of coastal-dune systems, and the potential information on LIA storm surges contained within, this methodology could prove a vital tool in flood-risk prediction under a changing climate.

Acknowledgements

This paper is a contribution to IGCP project 588 “Preparing for Coastal Change”. A.C. and J.W. are supported by NWO/STW grant DSF.7553. SvH and AvdS were supported by the Delft Cluster - Safety from Flooding programme. Menno van den Bos and Paul van der Linden of PWN alerted us to the exposure at Heemskerk and provided access to the sites. Albert Oost stimulated our interest in storm-surge deposits, and helped us in the field. Roland Gehrels, Torbjörn Törnqvist, and two anonymous reviewers are thanked for their valuable comments on the manuscript.

References

Boldt, K.V., Lane, P., Woodruff, J.D., and Donnelly, J.P., 2010, Calibrating a sedimentary record of overwash from Southeastern New England using modeled historic hurricane surges: Marine Geology, v. 275, p. 127–139, doi:10.1016/j.margeo.2010.05.002.

Briesmeister, J.F., 2000, MCNP–A General Monte Carlo N-Particle Transport Code Version 4C: Report LA-13709-M, Los Alamos National Laboratory, USA.

Bristow, C.S.; Chroston P.N., and Bailey, S.D., 2000. The structure and development of foredunes on a locally prograding coast: insights from ground-penetrating radar surveys, Norfolk, UK: Sedimentology, v. 47, p. 923-944.

Buynevich, I.V., FitzGerald, D.M., and van Heteren, S., 2004, Sedimentary records of intense storms in Holocene barrier sequences, Maine, USA; Marine Geology, v. 210, p. 135–148.

Buynevich, I.V., FitzGerald, D.M., and Goble, R.J., 2007, A 1500 yr record of North Atlantic storm activity based on optically dated relict beach scarps; Geology, v. 35, p. 543–546.

Clarke, M.L., and Rendell, H.M., 2009, The impact of North Atlantic storminess on western European coasts: A review: Quaternary International, v. 195, p. 31–41, doi:10.1016/j.quaint.2008.02.007.

Cunningham, A.C., and Wallinga, J., 2010, Selection of integration time intervals for quartz OSL decay curves: Quaternary Geochronology, v. 5, p. 657–666, doi:10.1016/j.quageo.2010.08.004.

De Boer, P., 1979, Convolute lamination in modern sands of the estuary of the Oosterschelde, the Netherlands, formed as the result of entrapped air; Sedimentology, v. 26, pp. 283–294.

Donnelly, J.P., and Woodruff, J.D., 2007, Intense hurricane activity over the past 5,000 years controlled by El Niño and the West African monsoon: Nature, v. 447, p. 465–468, doi:10.1038/nature05834.

Donnelly, J.P., Butler, J., Roll, S., Wengren, M., and Webb, T., 2004, A backbarrier overwash record of intense storms from Brigantine, New Jersey: Marine Geology, v. 210, p. 107–121, doi:10.1016/j.margeo.2004.05.005.

Hallewas, D.P., 1981, Archaeological cartography between Marsdiep and IJ: Berichten van de Rijksdienst voor het Oudheidkundig Bodemonderzoek (ROB). v. 31, p. 219–272.

Hering, J.H., 1776, Bespiegeling over Neêrlandsch Waternood tusschen den 14den en 15den nov: MDCCLXXV (Reflection on the flood of November 14–15, 1775 in the Netherlands): Amsterdam, Loveringh en Allart, 2 volumes, 230 and 335 p.

Hering, J.H., 1778, Bespiegeling over Neêrlandsch Waternood tusschen den XXIsten en XXIIsten november MDCCLXXVI (Reflection on the flood of November 21–22, 1776 in the Netherlands): Amsterdam, Johannes Allart, 238 p.

Jelgersma, S., Stive, M.J.F., and Van der Valk, L., 1995, Holocene storm surge signatures in the coastal dunes of the western Netherlands: Marine Geology, v. 125, p. 95–110, doi:10.1016/0025-3227(95)00061-3.

Kops, J., 1798, Tegenwoordige staat der duinen van het voormaalig Gewest Holland zijnde het eerste deel van het Alg. Rapport der Commissie van Superintendentie over het onderzoek der duinen (Current state of the dunes of the former region Holland, being the first part of the general report of the Commission of Superintendence on dune research): Leiden, Herdingh en Du Mortier, 197 p.

Lowe, J.A., and Gregory, J.M., 2005, The effects of climate change on storm surges around the United Kingdom: Philosophical Transactions of the Royal Society A: Mathematical: Physical and Engineering Sciences, v. 363, p. 1313–1328.

Lozano, L., Devoy, R.J.N., May, W., and Andersen, U., 2004, Storminess and vulnerability along the Atlantic coastlines of Europe: analysis of storm records and of a greenhouse gases induced climate scenario: Marine Geology, v. 210, p. 205–225, doi:10.1016/j.margeo.2004.05.026.

Mann, M.E., 2002, Little Ice Age, in MacCracken, M.C., and Perry, J.S., eds., Encyclopedia of global environmental change. Volume 1, the Earth system: Physical and chemical dimensions of global environmental change: Chichester, Wiley & Sons.

Mann, M.E., Woodruff, J.D., Donnelly, J.P., and Zhang, Z., 2009, Atlantic hurricanes and climate over the past 1500 years: Nature, v. 460, p. 880–883, doi:10.1038/nature08219.

Matulla, C., Schöner, W., Alexandersson, H., von Storch, H., and Wang, X.L., 2008, European storminess: Late nineteenth century to present: Climate Dynamics, v. 31, p. 125–130, doi:10.1007/s00382-007-0333-y.

Meeker, L.D., and Mayewski, P.A., 2002, A 1400-year high-resolution record of atmospheric circulation over the North Atlantic and Asia: The Holocene, v. 12, p. 257–266, doi:10.1191/0959683602hl542ft.

Morton, R.A., and Sallenger, A.H., 2003, Morphological impacts of extreme storms on sandy beaches and barriers: Journal of Coastal Research, v. 19, p. 560–573.

Nathan, R.P., Thomas, P.J., Jain, M., Murray, A.S., and Rhodes, E.J., 2003, Environmental dose rate heterogeneity of beta radiation and its implications for luminescence dating: Monte Carlo modelling and experimental validation: Radiation Measurements, v. 37, p. 305–313, doi:10.1016/S1350-4487(03)00008-8.

Pinto, J.G., Zacharias, S., Fink, A.H., Leckebusch, G.C., and Ulbrich, U., 2009, Factors contributing to the development of extreme North Atlantic cyclones and their relationship with the NAO: Climate Dynamics, v. 32, p. 711–737, doi:10.1007/s00382-008-0396-4.

Schaart, D.R., Jansen, J.T.M., Zoetelief, J., and De Leege, P.F.A., 2002, A comparison of MCNP4C electron transport with ITS 3.0 and experiment at incident energies between 100 keV and 20 MeV: influence of voxel size, substeps and energy indexing algorithm: Physics in Medicine and Biology, v. 47, p. 1459–1484, doi:10.1088/0031-9155/47/9/303.

Switzer, A.D., Bristow, C.S., and Jones, B.G., 2006, Investigation of large-scale washover of a small barrier system on the southeast Australian coast using ground penetrating radar; Sedimentary Geology, v. 183, p. 145–156.

Ulbrich, U., and Christoph, M., 1999, A shift of the NAO and increasing storm track activity over Europe due to anthropogenic greenhouse gas forcing: Climate Dynamics, v. 15, p. 551–559, doi:10.1007/s003820050299.

Ulbrich, U., Leckebusch, G.C., and Pinto, J.G., 2009, Extra-tropical cyclones in the present and future climate: A review: Theoretical and Applied Climatology, v. 96, p. 117–131, doi:10.1007/s00704-008-0083-8.

Van den Brink, H.W., Können, G.P., and Opsteegh, J.D., 2005, Uncertainties in extreme surge level estimates from observational records. Philosophical Transactions of the Royal Society A: Mathematical: Physical and Engineering Sciences, v. 363, p. 1377–1386.

Warnars, G., and Den Hengst, P., 1776, Historisch verhaal der overstroomingen in de Nederlanden, bijzonder op den 14 en 15 van slagtmaand des jares 1775 voorgevallen (Historic account of the floods in the Netherlands, especially those that occurred on November 14–15, 1775): Amsterdam, 241 p.

Supplementary Methods

OSL Equivalent dose

Preparation and measurement procedure

Under subdued orange lighting, samples were sieved to obtain the 180-212 µm grainsize fraction, which was then treated with HCl, H_2O_2, and HF to isolate the quartz. Sub-samples were prepared for measurement by placing roughly 100-200 grains on small steel discs. OSL measurements were performed on three Risø TL/OSL-DA-15 Readers (Bøtter-Jensen et al., 2000), using optical stimulation power of ~30 mW cm^{-2} at a wavelength of 470 nm (blue light). The detection filter was a 7.5 mm Hoya U340, with transmission between 270-380 nm. An inbuilt $^{90}Sr/^{90}Y$ source provided a dose rate of either ~0.03 or ~0.13 Gy s^{-1}.

Protocol

Our protocol for estimating the Equivalent dose (D_e) is based on the Single Aliquot Regenerative dose (SAR) protocol of Murray and Wintle (2000). The samples are relatively young (mostly 100 - 400 a), returning D_e of 0.2 - 0.5 Gy. The dating of such young samples introduces several complications which are less relevant for most OSL dating studies: 1. the weakness of the OSL signal; 2. the susceptibility of the signal to unwanted thermal transfer of charge; and 3. the possibility of partial bleaching. Overcoming these issues required us to introduce certain methodological adaptations, as follows:

1. Weak signals lead to less precise measurements, and it therefore requires the processing of a large number of aliquots to arrive at a satisfactory precision in D_e. Increasing the aliquot size is undesirable, as it becomes more likely that unbleached grains, or grains otherwise unsuitable for dating, are included in the aliquot. To increase the number of aliquots processed, we constructed the dose response curve for each aliquot using a single regenerative dose point (Ballarini et al., 2007). While reducing measurement time per aliquot, this adaptation leads to an overestimate of D_e of ~1 % (assuming that the true dose-response curve conforms to a typical saturating exponential function). We consider this overestimate to be insignificant compared to other sources of error.

2. Young samples are susceptible to thermal transfer effects, because the small natural signals can be easily swamped. We attempted to minimise thermal transfer by choosing a relatively low preheat, selected using a thermal-transfer

test (Wallinga et al., 2010). The effects of high preheats can be seen in Fig. 5.4 (thermal-transfer test) and Fig. 5.5. (Preheat-plateau test). Furthermore, we used an additional OSL bleach at elevated temperature at the end of each SAR cycle, which was found by Murray and Wintle (2003) to reduce recuperation.

3. Partial bleaching occurs when the mineral grains receive too little optical exposure (from sunlight) during transport and deposition. Young samples are more susceptible to this phenomenon, because of the relatively small burial signal. Most of the samples in this paper were deposited through beach/aeolian mechanisms, and are very likely to be well-bleached. However, several samples were taken directly from storm-surge sediments, for which the bleaching conditions are more debatable. To maximize the chances of obtaining a well-bleached OSL signal, we used the 'Early Background' principal of selecting integration intervals (Cunningham and Wallinga, 2010). In this method, the OSL signal is taken from the initial portion of the OSL decay curve, with the background taken from the portion immediately following. By keeping the length of the background interval to roughly 2.5 times that of the initial signal, a high proportion of easily-bleachable 'fast'component is achieved, while maintaining a good signal-to-noise ratio. The time-intervals we used were 0 – 0.60 s for the initial signal, and 0.60 – 2.10 s for the background. Errors arising through counting statistics were calculated using the equation of Li (2007), for use with weak signals.

Three tests were included in our protocol to verify the suitability of each aliquot for dating. Firstly, the OSL response to a 'zero' dose was measured, with aliquots accepted if the dose was less than 0.05 Gy or overlapping zero within one standard error. A 'recycle' dose was given, with aliquots accepted if the recycling ratio was between 0.9 and 1.1. A second recycling ratio was measured, with the same acceptance criteria, but following an infrared bleach at room temperature. This was used to identify any remnant feldspar contamination. We used the Central Age Model (CAM) of Galbraith et al. (1999) to estimate D_e for each sample. The SAR Protocol we used varied slightly between different site locations, as detailed in Table 5.1. OSL results are detailed in Table 5.2. To test the suitability of the protocols, dose-recovery tests were carried out on all samples. The combined results for all samples are shown in Fig. 5.6, which has a central dose-recovery ratio (using the CAM) of 0.997 ± 0.005, and overdispersion (σ) of 2.2 ± 0.7 %.

Step	*HK1* [a]		*HK3*	*HK7* [a]		*ZN1*
Dose	Nat, 2.5, 0, 2.5, 2.5 Gy	Nat, 2.5, 0, 2.5, 2.5 Gy	Nat, 2.1, 0, 2.1 Gy	Nat, 2.5, 0, 2.5, 2.5 Gy	Nat, 2.5, 0, 2.5, 2.5 Gy	Nat, 2.5, 0, 2.5, 2.5 Gy
Preheat	180ºC for 10 s	180ºC for 10 s	180ºC for 10 s	180ºC for 10 s	180ºC for 10 s	180ºC for 10 s
OSL	125ºC for 40 s	125ºC for 40 s	125ºC for 40 s	125ºC for 40 s	125ºC for 40 s	125ºC for 40 s
Test dose	2.5 Gy	2.5 Gy	2.1 Gy	2.5 Gy	2.5 Gy	2.5 Gy
Cutheat	180ºC	170ºC	180ºC	180ºC	170ºC	170ºC
OSL	125ºC for 40 s	125ºC for 40 s	125ºC for 40 s	125ºC for 40 s	125ºC for 40 s	125ºC for 40 s
Bleach	220ºC for 40 s	180ºC for 40 s	200ºC for 40 s	220ºC for 40 s	180ºC for 40 s	180ºC for 40 s

[a] For sections HK1 and HK7, two different protocols were used. There was no effect when slight changes in preheat and high-temperature bleach conditions were made

Table 5.1. Details of the Optically Stimulated Luminescence measurement protocols used in this study. Minor variations in protocol occur within and across stratigraphic sections.

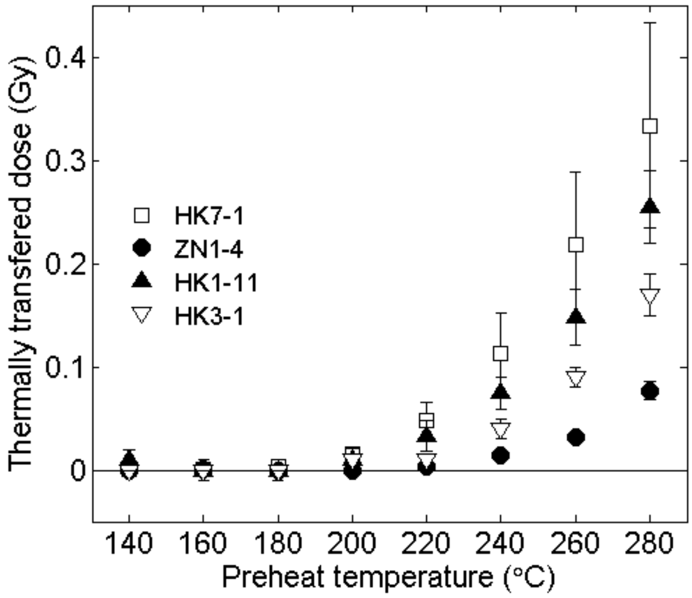

Fig. 5.4. Thermal transfer tests carried out on selected samples from all sections.

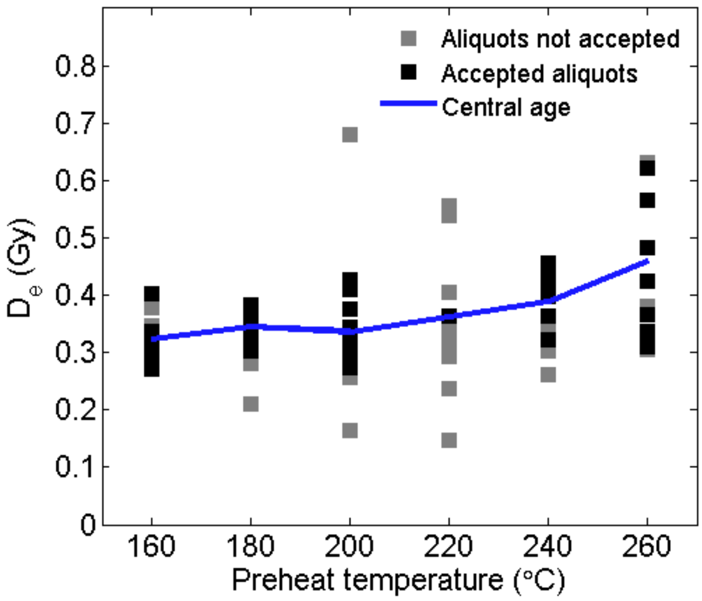

Fig. 5.5.. Results of a preheat-plateau test carried out on sample HK7-1. The 'central age' D_e was calculated using the central age model, using only the aliquots which passed the acceptance criteria.

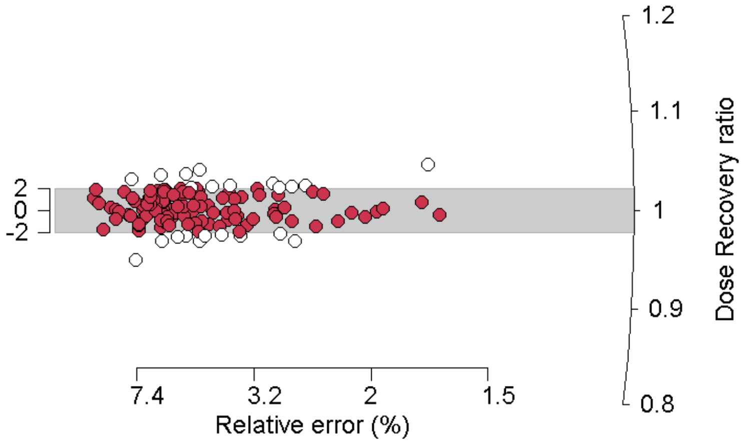

Fig. 5.6. Normalised dose recovery results from all samples. Central dose recovery ratio (using the CAM) is 0.997 ± 0.005, σ = 2.2 ± 0.7 %.

Table 5.2. (Opposite) Summary of results. Within each section, samples are listed in stratigraphical order (youngest to oldest). D_e calculated using the Central Age Model (CAM) unless stated. The mean $\dot{D}$ is given, for details see DR Methods. NAP is the ordnance datum in the Netherlands. Shading indicates samples taken directly from storm-surge units.

Section	Sample No.	*Height NAP (m)*	*De (Gy)*	*σ*	*No. aliquots*	*Dose rate (Gy ka-1)*	*Age (ka)*	*Year AD*	*footnotes*
HK1	2	8.43	0.137 ± 0.004	0.134 ± 0.028	32	1.136 ± 0.05	0.121 ± 0.007	**1887 ± 7**	
	4	7.33	0.141 ± 0.005	0.157 ± 0.032	31	1.11 ± 0.05	0.127 ± 0.008	**1881 ± 8**	
	8	*6.53*	0.296 ± 0.006	0.141 ± 0.018	65	1.242 ± 0.05	0.238 ± 0.012	**1770 ± 12**	
	11	*6.13*	0.285 ± 0.009	0.148 ± 0.025	40	1.197 ± 0.05	0.238 ± 0.013	**1770 ± 13**	a
	14	*5.93*	0.289 ± 0.006	0.114 ± 0.018	52	1.268 ± 0.05	0.228 ± 0.011	**1780 ± 11**	
	16	*5.68*	0.346 ± 0.014	0.168 ± 0.034	25	1.137 ± 0.05	0.304 ± 0.019	**1704 ± 19**	
	18	5.48	0.397 ± 0.011	0.163 ± 0.021	41	1.259 ± 0.05	0.315 ± 0.017	**1693 ± 17**	
	21	3.43	0.366 ± 0.011	0.151 ± 0.023	38	0.929 ± 0.04	0.394 ± 0.022	**1614 ± 22**	
HK3	0	5.91	0.267 ± 0.01	0.11 ± 0.035	20	1.28 ± 0.05	0.208 ± 0.012	**1800 ± 12**	
	1	5.26	0.275 ± 0.007	0.097 ± 0.023	27	1.275 ± 0.05	0.216 ± 0.011	**1792 ± 11**	
	2	5.02	0.279 ± 0.01	0.137 ± 0.029	26	1.318 ± 0.05	0.212 ± 0.012	**1796 ± 12**	
	3	4.84	0.275 ± 0.007	0.051 ± 0.032	18	1.207 ± 0.05	0.228 ± 0.012	**1780 ± 12**	
	4	*4.69*	0.233 ± 0.008	0.137 ± 0.029	36	0.989 ± 0.05	0.236 ± 0.015	**1772 ± 15**	b,c
	5	*4.69*	0.238 ± 0.008	0.106 ± 0.03	24	1.039 ± 0.05	0.229 ± 0.014	**1779 ± 14**	b,c
	7	4.49	0.427 ± 0.017	0.138 ± 0.032	17	1.254 ± 0.05	0.341 ± 0.02	**1667 ± 20**	
	8	4.25	0.411 ± 0.016	0.171 ± 0.031	25	1.101 ± 0.05	0.373 ± 0.024	**1635 ± 24**	
	9	4.00	0.403 ± 0.011	0.118 ± 0.023	35	1.204 ± 0.05	0.334 ± 0.018	**1674 ± 18**	
	10	3.68	0.399 ± 0.011	0.083 ± 0.026	16	1.163 ± 0.05	0.343 ± 0.019	**1665 ± 19**	
	11	3.13	0.408 ± 0.009	0.067 ± 0.021	21	1.289 ± 0.05	0.317 ± 0.015	**1691 ± 15**	
HK7	10	6.26	0.273 ± 0.01	0.143 ± 0.03	23	1.2 ± 0.05	0.228 ± 0.013	**1780 ± 13**	
	9	*5.91*	0.268 ± 0.008	0.164 ± 0.023	77	1.072 ± 0.05	0.25 ± 0.015	**1758 ± 15**	
	7	5.46	0.325 ± 0.005	0.079 ± 0.013	54	1.237 ± 0.05	0.262 ± 0.012	**1746 ± 12**	
	6	5.31	0.259 ± 0.008	0.13 ± 0.025	32	0.996 ± 0.04	0.26 ± 0.014	**1748 ± 14**	a,b,c
	5	5.16	0.335 ± 0.007	0.149 ± 0.017	69	1.278 ± 0.05	0.262 ± 0.013	**1746 ± 13**	
	4	4.91	0.34 ± 0.007	0.119 ± 0.018	47	1.304 ± 0.05	0.261 ± 0.013	**1747 ± 13**	
	1	5.36	0.338 ± 0.009	0.147 ± 0.02	44	1.185 ± 0.05	0.285 ± 0.015	**1723 ± 15**	
	3	4.41	0.351 ± 0.009	0.149 ± 0.021	35	1.2 ± 0.05	0.292 ± 0.015	**1716 ± 15**	
	2	3.86	0.342 ± 0.009	0.134 ± 0.022	44	1.166 ± 0.05	0.293 ± 0.016	**1715 ± 16**	
ZN1	5	2.08	0.302 ± 0.007	0.106 ± 0.021	23	1.314 ± 0.04	0.23 ± 0.01	**1778 ± 10**	d
	4	*1.95*	0.304 ± 0.013	0.100	23	1.286 ± 0.04	0.236 ± 0.014	**1772 ± 14**	e
	3	1.83	1.131 ± 0.016	0.029 ± 0.017	14	1.322 ± 0.04	0.855 ± 0.034	**1153 ± 34**	
	2	1.71	1.072 ± 0.025	0.098 ± 0.019	27	1.344 ± 0.042	0.797 ± 0.035	**1211 ± 35**	

[a]excludes 1 high outlier; [b]beta dose corrected for non-uniform matrix; [c]gamma dose corrected for non-infinite matrix; [d]excludes 2 high outliers; [e]MAM3 used for D_e estimate, using σ = 0.10

Partial Bleaching

Two storm-surge samples (HK1-16 and ZN1-4) gave anomalously old ages when processed with the central age model. One explanation for this could lie in the nature of deposition, through which the grains may not have received sufficient sunlight to fully reset the OSL signal. This 'partial bleaching' would lead to age overestimates if not accounted for. To determine whether the two samples are affected, we calculated the sample ages using two combinations of OSL decay curve integration intervals. Cunningham and Wallinga (2010) argued that for partially bleached samples, the use of 'early background' integration intervals should lead to a reduction in scatter in D_e when compared to the 'late background' intervals., due to the reduced proportion of hard-to-bleach slow component in the net OSL signal. To investigate the bleaching, we ran the CAM to determine the overdispersion on both samples, using both the late and early background integration intervals.

For sample ZN1-4, it can be seen in Table 5.3 that the use of the late background leads to an increase in both D_e and σ, as would be expected from a partially bleached sample. In addition, σ calculated using the Early Background is significantly larger than found in the surrounding samples (see Table 5.2.), implying that an additional source of scatter (most likely partial bleaching) is present. For this sample we calculated the age using the 3-parameter minimum-age model (MAM3) of Galbraith et al. (1999). The MAM3 requires a specified σ, for which we used the well-defined value of 10 % derived from well-bleached sample ZN1-2.

For sample HK1-16, it is apparent from Table 5.3 that little change in D_e or σ occurs when different integration intervals are used. Furthermore, the Early-background derived σ of 17 % is similar to those of the surrounding samples, shown in Table 5.2. We cannot rule out partial bleaching as a source of error for this sample, but we can find no evidence to support that hypothesis other than the anomalously old age estimate. For this sample, we use the CAM to derive the age, and treat it as an unexplained outlier.

	Early background		*Late background*	
	De	σ	*De*	σ
HK1-16	0.34 ± 0.01	0.17 ± 0.03	0.36 ± 0.01	0.21 ± 0.03
ZN1-4	0.36 ± 0.02	0.20 ± 0.04	0.43 ± 0.03	0.33 ± 0.05

Table 5.3. Comparison of D_e and σ for two storm-surge samples, using two different combinations of decay-curve integration intervals: Early Background uses 0-0.60 s for the initial signal, and 0.60 – 2.10 s for the background subtraction. The Late Background intervals are 0-0.30 s and 36 – 40 s.

The dose rate to quartz grains

Measurements for determining the dose rate to quartz grains were made on the light-exposed end-sections of the sample tubes. Samples were homogenized by grinding, and the radionuclide concentration was determined through high-precision gamma-spectrometry. The dose rate ($\dot{D}$) to the grains was estimated according to standard conversion factors for grain size (Mejdahl, 1979), water and organic content (assumed to be 5 ± 2 %) (Aitken, 1998), and including an internal alpha contribution of 0.01 Gy ka^{-1} (Vandenberghe et al., 2008). With the exception of the shell-rich samples described below, dose rate calculations assume an infinite and uniform sediment matrix.

The cosmic dose

The contribution of cosmic radiation to $\dot{D}$ depends largely on the depth of the sample. For our samples this was made complicated by the build-up and movement of the overlying dunes, which may have altered the sample depth over time. Moreover, the depth of the sample just prior to sample collection was also uncertain because of erosion of the dune cliffs during the storm surge of 2007. We used two sources of information to help make an adequate approximation of the cosmic dose rate. Firstly, the approximate OSL ages of samples overlying the storm-surge sediment (this is only slightly circular, since the cosmic-dose contribution to the total dose rate is usually less than 10 %). Secondly, we make use of 'Jarkus' cross-shore profiles of the area. These profiles have been carried out roughly every 10 years since 1965, at 500 m intervals along coastline of the Netherlands. One profile was measured just prior to the storm surge of 2007 (Fig. 5.2).

HK1 and HK3 – for these sections the nearest Jarkus profiles indicate approximately 12 m of sediment above the storm surge unit, stable over the period 1965 - 2008. For the cosmic dose calculations, we assumed a gradual dune build-up to 12 m until 1965, and a constant depth of 12 m for 1965 - 2009.

HK7 – Jarkus profiles for this section indicate ~12 m of overlying sediment in 1965, reduced to 4 m in 2007. For our calculations, we assumed a gradual dune build-up to 12m until 1965, and a constant depth of 8.5 m from 1965-2009.

ZN1 – This inland site is situated in a dune low, with the storm surge unit < 1 m below the surface. The sample depth is unlikely to have changed since deposition, and the overlying sample indicates an age ~1800 AD. We therefore assumed an instant burial to its present depth.

Uncertainty in the sample depth inevitably leads to error in the age calculations. However, since the Jarkus profiles give evidence for dune stability over the last 50 years, and given the small contribution of cosmic dose to the total dose (~10 %), the actual error resulting from cosmic-dose uncertainty is unlikely to be significant.

The gamma dose

Estimates of the gamma contribution to the dose rate for each sample are calculated from the measured radionuclide concentrations, using the infinite matrix assumption. However, for shell-rich or hash-rich samples HK3-4, HK3-5 and HK7-6, this assumption is not valid because the sedimentary units they come from are relatively thin (10-15 cm), and have a lower radionuclide concentration than the bracketing sediment. For these samples, we applied an upward correction of the gamma dose rate, using the gamma gradient estimates of Aitken (1985) in combination with the measured radionuclide concentrations of the bracketing sediment.

The beta dose

For most samples, we use the 'infinite matrix' assumption when converting the measured radionuclide concentration into $\dot{D}$, and we further assume that the activity distribution is uniform throughout the sample. However, should there be discrete, non-radioactive material present, of a size comparable to (or greater than) the mean range of the typical beta particles (~1 mm), then the assumption of a uniform matrix becomes invalid. This has occurred for two samples taken directly from the storm-surge sediment (HK3-4, HK3-5), where significant amounts of marine shell are present, and one sample with significant proportion a fine shell fragments, or 'hash' (HK7-6). Gamma spectrometry measurements indicated that a sample of pure shell would provide a beta dose rate to quartz grains of 0.025 Gy ka^{-1}, compared to roughly 0.70 Gy ka^{-1} typical of sandy samples. In addition, the density of the shell (~2.70 g cm^{-3}) is significantly higher than the density of the sandy matrix in which the quartz grains are embedded (~1.82 g cm^{-3}, assuming porosity of 35 %). Measurements of radionuclide concentration are carried out on the bulk sediment (including the shells), which presents two complications. Firstly, the shells create a low dose-rate zone in the sediment within which no quartz grains exist; the quartz grains are found in the surrounding sand, which has more typical radionuclide concentrations. Secondly, the high density of the shells means they are better absorbers of radiation than sand grains of the same bulk volume; the beta dose must therefore be lower than a pure sand sample.

The net influence of the shell material on the beta dose rate is determined by the size, shape, and density of the shell material, and by the energy of the beta electrons. To estimate the average beta dose to quartz grains in the shell-rich environments, we used a Monte Carlo transport code, MCNP4C (Briesmeister, 2000). This code enables the generation of beta electrons of specified energy, and tracks them through a pre-defined geometry. Previous studies have shown that MCNP4C allows for accurate beta particle dose calculations in heterogeneous media (Schaart et al., 2002a; Schaart et al., 2002b; Maigne et al., 2011).

Two geometries were constructed: Model A, to simulate the shell-rich storm-surge deposit from which samples HK3-4 and HK3-5 were taken; Model B to simulate the hash-rich, pre storm-surge sample HK7-6. The two geometries varied only in the size and shape of the shell material, and the weight fraction of shell material. Visualisations of the two geometries are shown in Fig. 5.7.

Geometries are based on a simple grid structure, in which shells and hash are rectangular cuboids of a sizes corresponding to the average (measured) shell size or hash size. Each shell fragment occupies one ‘cell’ of the geometry, and is composed of $CaCO_3$ with density 2.70 g cm^{-3}. Shell cells were added to the geometry at random locations, using one of two orientations, until the (mass corrected) volume of shell material reached the desired fraction. All other space in the geometry is defined as a single cell, and represents the sand-matrix in which quartz grains are contained. The sand matrix material is a combination of SiO_2 (i.e. quartz, density = 2.66 g cm^{-3}) with a packing density of 65 % (typical for coarse sand deposits, Weerts, 1996); and H_2O, density = 1.00 g cm^{-3}, with mass equalling 5 % of the mass of the quartz. When combined, the density of the sand matrix is 1.82 g cm^{-3}. Air is ignored in the models; the low density of air (~0.0013 g cm^{-3}) compared with solid materials means that the interaction of beta electrons with air is not significant in our models.

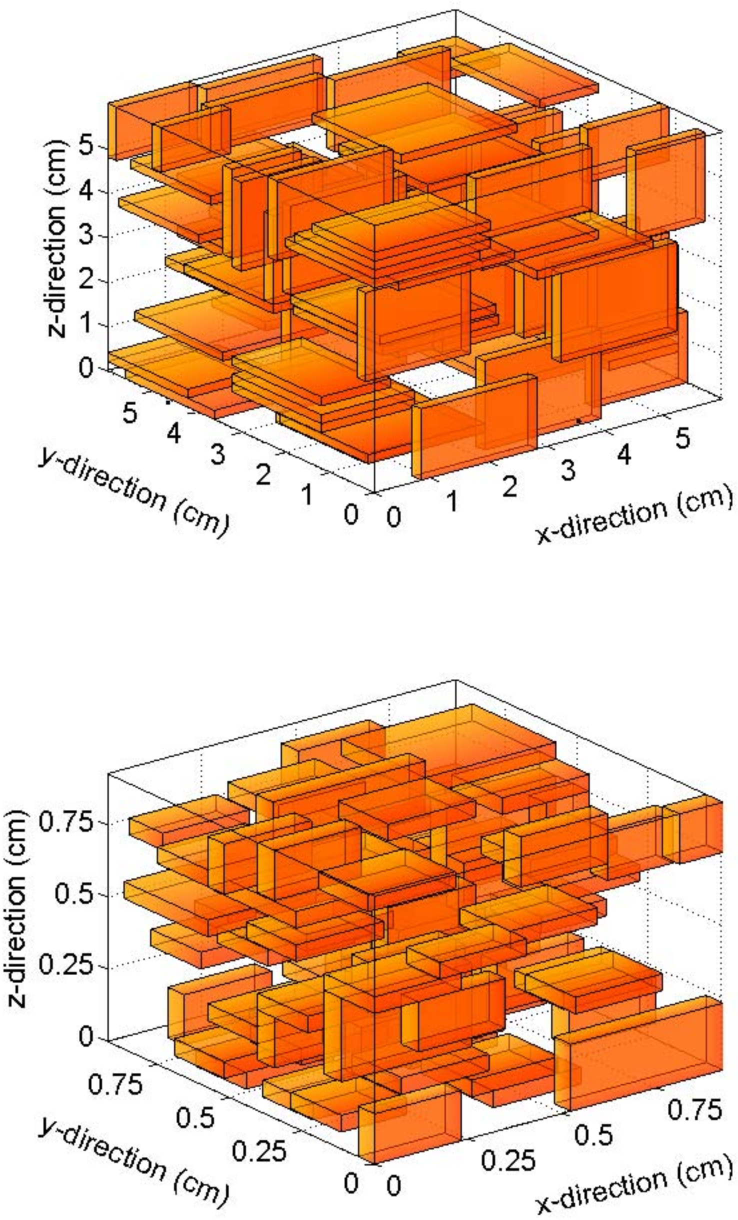

Fig. 5.7. Visual representations of the geometries used for Monte Carlo simulations of beta-radiation transport. Filled rectangular cuboids represent individual pieces of shell material. (a) The geometry designed for the shell-rich samples HK3-4 and HK3-5. (b) The similar representation of hash-rich sample HK7-6.

The energy of each beta electron is randomly sampled from a customised spectrum for each material (sand matrix or shell; Fig. 5.8). These were created using the measured radionuclide concentrations (Table 5.4) in combination with the isotope-specific beta spectra, downloaded from www.doseinfo-radar.com. Charged particle equilibrium was maintained by specifying 'white' surfaces at the boundaries of the geometry, which reflect charged particles back into the model in random directions. The large sand matrix cell acts as the dosimeter, for which the average energy deposited per history is recorded using the *F8 energy deposition tally (Briesmeister, 2000). All simulations were performed in coupled photon-electron mode, using the el03 and mcnplib2 electron and photon interaction data libraries and selecting the ITS electron energy indexing algorithm (Schaart et al., 2002a). The upper photon and electron energy limits were set to 3.0 MeV. The photon and electron cut-off energies were set to 1 keV and 10 keV, respectively. Other simulation parameters were left at the default setting. No variance reduction techniques were applied.

To apply the model output to the measured beta dose rate, we define a correction factor:

$$r = \frac{E_{sand}}{E_{total}} \cdot \frac{m_{sand}}{m_{total}}$$

where E_{sand} is the energy deposited in the sand matrix as recorded in the *F8 tally, E_{Total} is to total energy released, m_{sand} is the mass of the sand-matrix material, and m_{total} is mass of all the material. The ratio r reflects the dose absorbed by the sand matrix relative to the energy emitted per unit mass of bulk sediment. The true dose rate applicable to the quartz grains is found by correcting the measured bulk beta dose rate by the factor r.

	Radionuclide concentration (Bq kg^{-1})		
	^{40}K	^{238}U	^{232}Th
Sand fraction (HK3-3)	320 ± 5	6.58 ± 0.15	6.24 ± 0.33
Shells only	3.0 ± 1.6	1.0 ± 0.1	0.27 ± 0.03

Table 5.4. Measured radionuclide concentrations determined through high-resolution gamma spectrometry, used as input in Monte Carlo modelling of energy deposition. Sample HK3-3 is the dune sample immediately above the shell layer in section HK3; A separate measurement was made on a sample of pure shells from the HK3 shell layer.

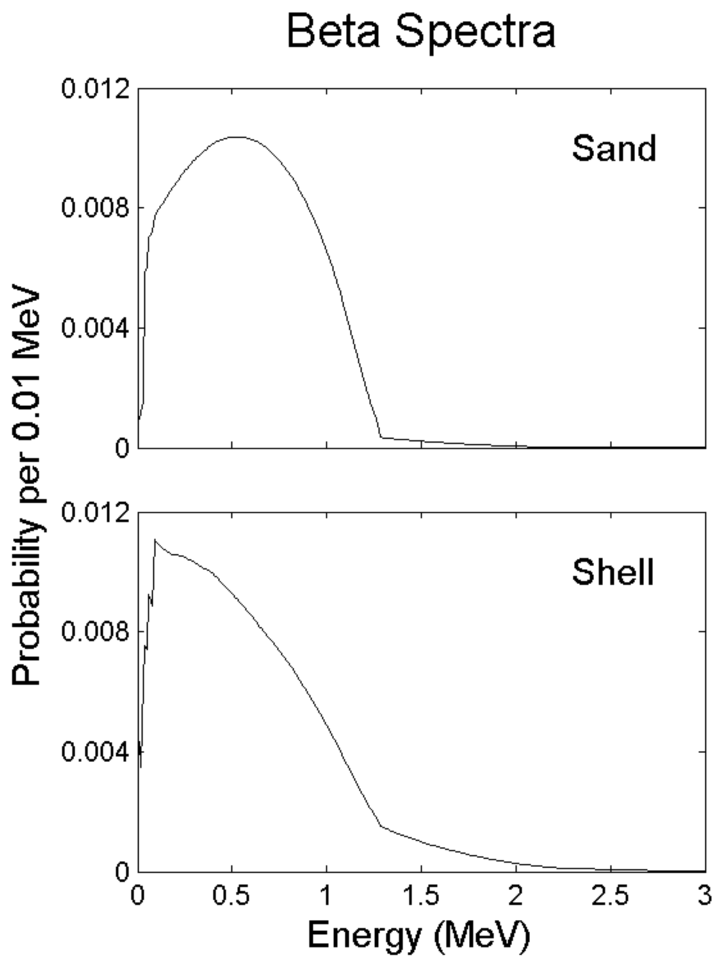

Fig. 5.8. The beta energy spectra used to sample electrons in the Monte Carlo model. Spectra were created using the measured radionuclide concentrations (Table 5.4) and isotope data from www.doseinfo-radar.com.

Model Results

The computational time required for the models is short, because each model has only one, large dosimeter. For Model A (shells), $r = 1.31$, with a relative statistical error of 0.35 % (1σ) after 154,000 particle histories; for Model B (hash), $r = 1.17$, with a relative statistical error of 0.45 % (1σ) after 99,000 particle histories. To estimate the overall uncertainty associated with r (i.e., including possible systematic errors), we conducted a series of sensitivity tests in which r is modelled, for both geometries, while three key parameters are varied. The outcomes of the sensitivity tests are shown in Fig. 5.9, and are discussed in the following paragraphs.

The parameter with the largest influence on *r* is the shell content (Fig. 5.9 (a) and (b)). The more shell material in the sample, the greater the correction factor. When the proportion of shell material is low, the response of the correction factor is roughly linear; when the proportion of shell mass is increased beyond ~20 %, the chance increases that more than one shell is located close enough to a given sand grain to absorb part of the beta energy emitted by that grain, leading to a steeper curve. The shell content of our samples was measured directly (28 % for HK3-4 and HK3-5, 30 % for HK7-6). An estimated uncertainty of 3 % on the shell content leads to an uncertainty in *r* of roughly 0.03.

The influence of packing density of the sand-matrix material can be seen in Fig. 5.9 (c) and (d). Unlike the shell mass, the packing density of the sand-matrix material was not measured. For our models we use a packing density 65 %, which was determined by Weerts (1996) to be typical for coarse sand. While there is clearly uncertainty over this value (estimated here as 5 %) it is also clear from Fig. 5.9 (c-d) that an error in the packing density will not significantly affect the value of *r*.

Lastly, the sensitivity of *r* to a change in the volume of individual shells (or shell fragments) is displayed in Fig. 5.9 (e-f). As with the sensitivity to packing density, a small error in individual shell volume has little effect on *r*. It is interesting to note, however, that even with a very small volume for each shell (e.g. a grain of 1 mm diameter), there is a considerable effect on *r*. As such this is not surprising given that the range of the beta particles is also in the order of millimetres. However, the implication is that even small non-emitting objects may affect the pattern of energy deposition, with the magnitude of the effect controlled by the proportion of that material in the sediment. This result could have implications for wider OSL dating, and is worthy of further investigation.

In summary, the known uncertainties in the beta-dose models are very small, and are barely significant when added to other sources of error in the age estimates. The correction values we use are 1.31 ± 0.05 for Model A (Shells, samples HK3-4 and HK3-5), and 1.17 ± 0.05 for Model B (Hash, HK7-6).

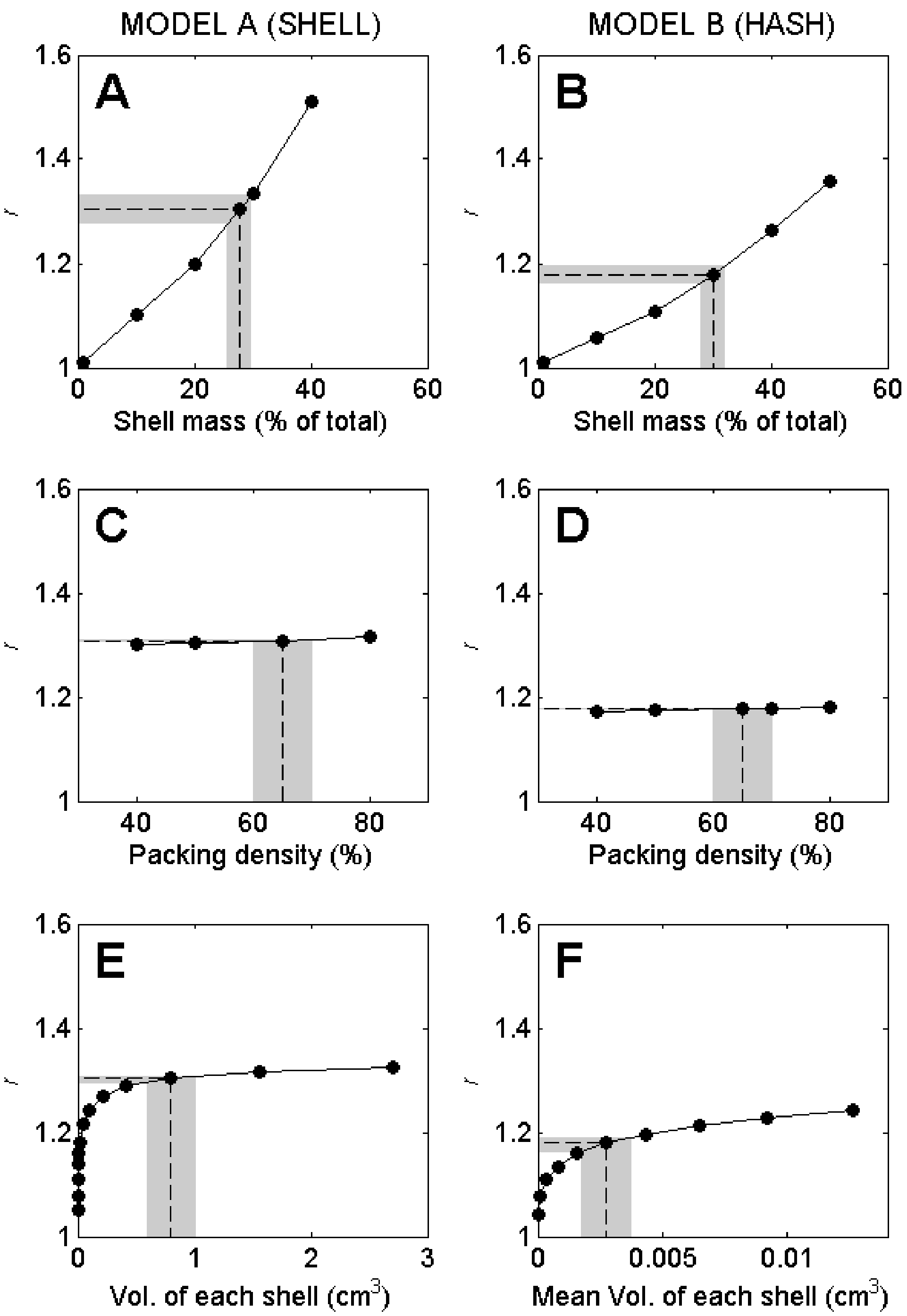

Fig. 5.9. Sensitivity analysis of the Monte Carlo simulation of beta-radiation transport. In each panel, the outcome (*r*) of the shell model (left side) or hash model (right side) is plotted as a function of one key parameter. Also shown are the central values used in the models (dotted lines), and the estimated 1σ uncertainty regions (shaded areas)

References

Aitken, M.J. 1985. *Thermoluminescene Dating*, Academic Press, London.

Aitken, M.J. 1998. *Introduction to Optical Dating: The Dating of Quaternary Sediments by the Use of Photon-stimulated Luminescence,* Oxford University Press, Oxford.

Ballarini, M., Wallinga, J., Wintle, A.G., and Bos, A.J.J. 2007. A modified SAR protocol ofr optical dating of individual grains from young quartz samples. Radiation Measurements 42, 360-369.

Boldt, K.V., Lane, P., Woodruff, J.D., Donnelly, J.P. 2010. Calibrating a sedimentary record of overwash from Southeastern New England using modeled historic hurricane surges. Marine Geology 275, 127-139.

Bøtter-Jensen, L., Bulur, E., Duller, G.A.T. and Murray, A.S. 2000. Advances in luminescence instrument systems. Radiation Measurements 32, 57-73.

Briesmeister, J.F. 2000. MCNP – A General Monte Carlo N-Particle Transport Code Version 4C: Report LA-13709-M, Los Alamos National Laboratory, USA.

Clarke, M.L., Rendell, H.M. 2009. The impact of North Atlantic storminess on western European coasts: A review. Quaternary International 195, 31–41.

Cunningham, A.C., Wallinga, J. 2010. Selection of integration time intervals for quartz OSL decay curves. Quaternary Geochronology 5, 657-666.

Donnelly J.P., Butler, J., Roll, S., Wengren, M., Webb, T. 2004. A backbarrier overwash record of intense storms from Brigantine, New Jersey. Marine Geology 210, 107-121.

Donnelly, J.P., Woodruff, J.D. 2007. Intense hurricane activity over the past 5,000 years controlled by El Niño and the West African monsoon. Nature 447, 465-468.

Galbraith, R.F., Roberts, R.G., Laslett, G.M., Yoshida, H., Olley, J.M. 1999. Optical dating of single and multiple grains of quartz from Jinmium rock shelter, northern Australia, part 1, Experimental design and statistical models. Archaeometry 41, 339-364.

Hallewas, D.P. 1981. Archaeological cartography between Marsdiep and IJ. Berichten R.O.B. 31, 219-272.

Hering, J.H. 1776. Bespiegeling over Neêrlandsch Waternood tusschen den 14den en 15den nov: MDCCXXVI (Reflection on the flood of November 14-15, 1775 in the Netherlands). Loveringh en Allart, Amsterdam, 2 volumes.

Hering, J.H. 1778. Bespiegeling over Neêrlandsch Waternood tusschen den XXIsten en XXIIsten november MDCCXXVI (Reflection on the flood of November 21-22, 1776 in the Netherlands). Johannes Allart, Amsterdam.

Jelgersma, S., Stive, M.J.F., Van der Valk, L. 1995. Holocene storm surge signatures in the coastal dunes of the western Netherlands. Marine Geology 125, 95-110.

Kops, J. 1798. Tegenwoordige staat der duinen van het voormaalig Gewest Holland zijnde het eerste deel van het Alg. Rapport der Commissie van Superintendentie over het onderzoek der duinen (Current state of the dunes of the former region Holland, being the first part of the general report of the Commission of Superintendence on dune research). Herdingh en du Mortier, Leiden.

Li, B. 2007. A note on estimating the error when subtracting background counts from weak OSL signals. Ancient TL 25, 9-14.

Lowe, J.A., Gregory, J.M. 2005. The effects of climate change on storm surges around the United Kingdom. Philosophical Transactions of the Royal Society A: Mathematical, Physical and Engineering Sciences 363, 1313-1328.

Lozano, L., Devoy, R. J. N., May, W., Andersen, U. 2004. Storminess and vulnerability along the Atlantic coastlines of Europe: analysis of storm records and of a greenhouse gases induced climate scenario. Marine Geology 210, 205-225.

Maigne, L., Perrot, Y., Schaart, D.R., Donnarieix, D., Breton, V. 2011. Comparison of GATE/GEANT4 with EGSnrc and MCNP for electron dose calculations at energies between 15 keV and 20 MeV. Physics in Medicine and Biology 56, 811-827.

Mann, M.E., 2002, Little Ice Age, *in* MacCracken, M.C., Perry, J.S. eds, Encyclopedia of global environmental change. Volume 1, the Earth system: physical and chemical dimensions of global environmental change. Wiley & Sons, Chichester.

Mann, M.E., Woodruff, J.D., Donnelly, J.P., Zhang, Z. 2009. Atlantic hurricanes and climate over the past 1500 years. Nature 460, 880-883.

Matulla, C., Schöner, W., Alexandersson, H., von Storch, H., Wang, X.L. 2008. European storminess: late nineteenth century to present. Climate Dynamics 31, 125-130.

Meeker, L.D., Mayewski, P.A. 2002. A 1400-year high-resolution record of atmospheric circulation over the North Atlantic and Asia. Holocene 12, 257-266.

Mejdahl, V. 1979. Thermoluminescence dating: beta-dose attenuation in quartz grains. Archaeometry 21, 31-72.

Morton, R.A., Sallenger, A.H. 2003. Morphological impacts of extreme storms on sandy beaches and barriers. Journal of Coastal Research 19, 560-573.

Murray, A.S., Wintle, A.G. 2000. Luminescence dating of quartz using an improved single-aliquot regenerative-dose protocol. Radiation Measurements 32, 57-73.

Murray, A.S., Wintle, A.G. 2003. The single aliquot regenerative dose protocol: potential for improvements in reliability. Radiation Measurements 37, 377-381.

Nathan, R.P., Thomas, P.J., Jain, M., Murray, A.S., Rhodes, E.J. 2003. Environmental dose rate heterogeneity of beta radiation and its implications for luminescence dating: Monte Carlo modelling and experimental validation. Radiation Measurements 37, 305-313.

Pinto, J.G., Zacharias, S., Fink, A.H., Leckebusch, G.C., Ulbrich, U. 2009. Factors contributing to the development of extreme North Atlantic cyclones and their relationship with the NAO. Climate Dynamics 32, 711-737.

Schaart, D.R., Jansen, J.T.M., Zoetelief, J., de Leege, P.F.A. 2002a. A comparison of MCNP4C electron transport with ITS 3.0 and experiment at incident energies between 100 keV and 20 MeV: influence of voxel size, substeps and energy indexing algorithm. Physics in Medicine and Biology 47, 1459-1484.

Schaart, D.R., Bos A.J.J., Winkelman, A.J.M., Clarijs, M.C. 2002b. The radial depth-dose distribution of a $^{188}W/^{188}Re$ line source measured with novel, ultra-thin TLDs in a PMMA phantom: Comparison with Monte Carlo simulations. Physics in Medicine and Biology 47, 3605-3627.

Ulbrich, U., Christoph, M. 1999. A shift of the NAO and increasing storm track activity over Europe due to anthropogenic greenhouse gas forcing. Climate Dynamics 15, 551-559.

Ulbrich, U., Leckebusch G. C., Pinto J. G. 2009. Extra-tropical cyclones in the present and future climate: a review. Theoretical and Applied Climatology 96, 117-131.

Van Den Brink, H.W., Können, G.P., Opsteegh, J.D. 2005. Uncertainties in extreme surge level estimates from observational records. Philosophical Transactions of the Royal Society A: Mathematical, Physical and Engineering Sciences 363, 1377-1386.

Vandenberghe, D., De Corte, F., Buylaert, J.-P., Kučerac, J., Van den haute, P. 2008. On the internal radioactivity in quartz. Radiation Measurements 43, 771-775.

Wallinga, J., Hobo, N., Cunningham, A.C., Versendaal, A.J., Makaske, B., Middelkoop, H. 2010. Sedimentation rates on embanked floodplains determined through quartz optical dating. Quaternary Geochronology 5, 170-175.

Warnars, G., Den Hengst, P. 1776. Historisch verhaal der overstroomingen in de Nederlanden, bijzonder op den 14 en 15 van slagtmaand des jares 1775 voorgevallen (Historic account of the floods in the Netherlands, especially those that occurred on November 14-15, 1775). Amsterdam, 1776.

Weerts, H.J.T. 1996. Complex confining layers: Architecture and hydraulic properties of the Holocene and Late Weichselian deposits in the fluvial Rhine-Meuse delta, The Netherlands. PhD thesis, University of Utrecht.

Chapter 6

Realizing the potential of fluvial archives using robust OSL chronologies

Alastair C. Cunningham, Jakob Wallinga

Submitted to Quaternary Geochronology

Abstract

Optically Stimulated Luminescence (OSL) dating has enormous potential for interpreting fluvial sediments, because the mineral grains used for OSL dating are abundant in fluvial deposits. However, the limited light exposure of mineral grains during fluvial transport and deposition often leads to scatter and inaccuracy in OSL dating results. We argue that scatter between OSL ages is due to inadequate assessment of the uncertainty associated with an OSL age. We propose a new approach, in which OSL ages are presented as probability distribution functions, created by bootstrap re-sampling of the equivalent-dose dataset. This approach has the considerable advantage that it permits Bayesian methods to be used to help interpret partially bleached OSL data. The combination of bootstrap uncertainty distributions with Bayesian processing can provide robust OSL chronologies for fluvial sediment, and allows OSL ages from partially bleached samples to be combined with other age information.

6.1 Introduction

Sedimentary deposits of river-transported material provide an important record of environmental history. Fluvial sediments are widely studied to understand modern fluvial sedimentation rates (e.g. Owens et al., 1999; Hobo et al., 2010), determine fluvial response to climatic, tectonic and sea-level forcing (e.g. Busschers et al., 2008), and to reconstruct flood risks (e.g. Benito et al., 2008). However, the use of fluvial archives is severely hindered by the lack of consistent dating. Accurate and precise dating is clearly essential for correlating fluvial sedimentation with external forcing. Because fluvial sediments are non-continuous and lack the annual layering necessary for high-precision methods, dating control must be obtained through radiometric methods. Radiocarbon dating offers the most precision, but is of limited use for direct dating of fluvial activity due to the frequent absence of organic carbon, and because the carbon is often re-worked from older deposits. In contrast, Optically Stimulated Luminescence (OSL) dating is nearly always possible, because the raw material for OSL dating - sand-sized mineral grains - is abundant in fluvial sediment. OSL dating also has the advantage of a wide age-range of applicability (~10 a to >100 ka). With these advantages, OSL dating could provide continuity in a multi-dating-method chronology, and become the standard method for dating fluvial sediments (Wallinga, 2002; Rittenour, 2008).

OSL dating requires determination of the radiation dose absorbed by the mineral grains since burial (the burial dose, obtained from the measured equivalent-dose (D_e) distribution), and the yearly radiation dose (the dose rate). It is the determination of the burial dose that presents difficulties in dating fluvial sediments. The problem lies with the most fundamental requirement for obtaining an age with OSL techniques – that the mineral grains were exposed to enough sunlight during the last episode of transport and deposition for the OSL signal to be reset. A few tens of seconds of bright sunlight is enough for resetting, but the equivalent light exposure is not always received by grains transported within the water column. The effect is usually known as ‘partial bleaching’ (or ‘heterogeneous bleaching’), and the consequences for age determination depend on the severity of the effect. Partial bleaching tends to be most problematic where deposition is more recent (e.g. within the last 2000 a, Jain et al., 2004), or where transport distances are short (Stokes et al., 2001).

It is notable that where OSL has proven successful in interpreting fluvial systems (e.g. Rittenour et al., 2005; Rodnight et al., 2005; Busschers et al., 2007), the degree of partial bleaching in the data is minimal. The appearance of partial bleaching in a dataset necessitates some statistical processing, although the selection and application of ‘age models’ is a frequent source of discussion (Bailey and Arnold, 2006; Rodnight et al., 2007; Arnold and Roberts, 2009; Thrasher et al., 2009). Difficulties arise due to the sensitivity of the burial dose to the lowest D_e value, which may or may not be an outlier, and in assessing the amount of spread in the data that can be assigned to the burial-dose population. As there is no commonly agreed procedure for coping with these issues, there is a degree of inconsistency in age-model application. More devastatingly, the error terms assigned to the burial ages reflect (at best) the uncertainty in fitting the model to the data, and take no account of uncertainty in the decision process itself. As a consequence, OSL ages for fluvial sediments often appear scattered or inaccurate, with error terms that are less than meaningful.

The aim of this paper is to provide a robust protocol for the analysis of OSL data from fluvial (or glaciofluvial) sediment. We show that by embedding partially bleached OSL data in a Bayesian framework, the coherence of an OSL chronology can be increased. The use of Bayesian methods requires a realistic assessment of uncertainties associated with the OSL age, for which we develop a new method based on bootstrap re-sampling of the multi-aliquot D_e distribution. The method is able to incorporate uncertainties in the D_e distribution and age-model parameters, and through the combination with Bayesian statistics leads to an objective means of identifying outliers.

6.2 Methods

6.2.1 Sample details

We use a sequence of OSL samples taken from a single core through the embanked floodplain of the River Waal, The Netherlands. The samples we use were deposited over the last 1000 years, and show a relatively high degree of partial bleaching. For the majority of this time period, there is no alternative dating method available for these sediments. OSL measurement details are described in Wallinga et al. (2010); additional site information and alternative dating methods are presented by Hobo et al. (2010). For the current paper we include three additional samples of the underlying channel deposits taken from the same core; all OSL decay curves were re-analysed using the ‘early background’ strategy described in Cunningham and Wallinga (2010).

6.2.2 Bayesian chronological framework

Bayesian methods have long been recognised as a powerful aid in the analysis of age information (Buck et al., 1991, Bronk Ramsey, 1995). A Bayesian chronological framework has two particular uses: it provides a formal method of combining multiple age estimates into a meaningful chronology (including an objective means of identifying outliers), and it utilises stratigraphic relationships between the samples to increase dating precision. Bayesian methods have gained widespread use with radiocarbon-based chronologies (e.g. Blockley et al., 2007, Jacobi and Higham, 2009, Bronk Ramsey et al., 2010), where the analysis helps discriminate between multiple peaks in age probability distributions.

The power in Bayesian techniques comes through the incorporation of 'prior' information, i.e. information known before measurement of any sample. For sedimentary sections, this comes from the stratigraphic relationship between the sample locations, which may simply constrain the order in which the samples were deposited, or may contain more detailed assumptions about the depositional process (Bronk Ramsey, 2008). The chronological model is developed through the combination of the prior model with the age information (the 'likelihood'), input in the form of a probability distribution function (PDF).

Given the ability of Bayesian analysis to identify outliers and increase precision, it is clearly of interest in processing OSL ages derived from heterogeneously bleached samples. The freely available OxCal program (Bronk Ramsey, 1995) is widely used for Bayesian analysis of radiocarbon dated sequences, and can also be used to include age information from other methods (e.g. OSL ages from well-bleached samples; Rhodes et al., 2003). However, the wholesale inclusion in OxCal of a sequence of fluvial OSL samples has not been attempted, and this could be a reflection of inaccuracy or spurious precision in ages assigned to fluvial samples.

OxCal requires age information in PDF form. For a well-bleached OSL sample with the age defined with a 1σ error term, this is easily achieved using the internal functions of OxCal (see Rhodes et al. (2003) for details). For partially bleached samples, the creation of a PDF is not so straightforward: the OSL age may be dependent on the age model used and the assumptions that go with that model, and the use of a normally distributed error term may not be valid. What is required, therefore, is a means of estimating the PDF for the age of a sample, while incorporating all the likely sources of error. In the sections that follow, we describe a statistical process by which this can be done.

6.2.3 Bootstrap re-sampling

The first step in the production of a PDF[1] is the use of a model to obtain the burial dose from a D_e dataset of heterogeneously bleached aliquots. Aliquots may

[1] The PDFs discussed in this paper are not the same as those often seen in the OSL-dating literature, see Galbraith (2010) for a discussion.

consist of a single mineral grain, but usually contain many more, so the age model needs to be applicable to multi-grain aliquots. A vital requirement for such a model is that it must be able to account for the scatter that exists in a dataset, but which is derived from processes *other* than partial bleaching. This scatter may come about through imperfections in the measurement process, or through variation in the natural radiation dose rate received by different grains. A suitable model was proposed by Galbraith et al. (1999), who introduced the overdispersion parameter σ_b into their 3- and 4-component minimum age models (MAM-3 and MAM-4 respectively). Of these, the MAM-3 is simpler to apply in practice, and is based on a parametric model of partially bleached distributions which is more suitable for use with multi-grain aliquots.

For the creation of a PDF of the minimum ages, one approach would be to take the MAM-3 burial-dose estimate, and use the confidence intervals derived through the 1-parameter log-likelihood function to define a normal distribution for the burial dose. However, there are uncertainties in the age determination which are not accounted for in this method, which means that the error term produced may not be a good reflection of the true uncertainty. This is because there are two inputs that determine the MAM-3 outcome (minimum age): the D_e dataset which is used, and the value for σ_b which is chosen. Slight changes in either the data or σ_b will alter the minimum age, and there is a considerable degree of uncertainty in both these inputs. Each D_e is associated with an error term based on counting statistics, and these can vary dramatically between aliquots. There is also considerable uncertainty in the selection of σ_b, which can vary due to heterogeneity of the natural dose rate, and is affected by the OSL sensitivity distribution of the grains and the number of grains in each aliquot (Cunningham and Wallinga, submitted).

To solve the issue of uncertainty estimation, we use an approach based on bootstrap re-sampling of the D_e dataset. Boostrapping (Efron, 1979) is a means of estimating the variance of a statistic (in this case the minimum age), by repeatedly constructing a new sample dataset and re-calculating the statistic. Each new D_e dataset is created by random sampling (with replacement) of the original empirical data, with the number of samples equal to the size of the original dataset. In this version of the bootstrap methodology, we also include stochastic variation in the two inputs: firstly, each re-sampled D_e value is randomized according to a normal distribution described by its error term; secondly, the value of σ_b is randomized for each call to the MAM-3. A normal distribution is also used for the randomization of σ_b. For this study, σ_b was estimated at 0.11 ± 0.04; this value combines the effects of an assumed single-grain overdispersion value of 20 % (e.g. Duller, 2008), a highly-skewed sensitivity distribution, and the averaging that occurs within aliquots of 100-200 grains (Cunningham and Wallinga, submitted).

The MAM-3 is run for every re-sampled dataset, each time producing a unique minimum age. With a large number of iterations (e.g. 2000), the distribution of minimum ages is converted into a PDF after suitable binning. We used a bin width w determined by w = range/sqrt($0.8n_{it}$), where n_{it} is the number of iterations. A final step in the process is to incorporate additional sources of uncertainty that are systematic between aliquots, but random between samples. For example, an error in the dose-rate measurement, or water content correction, will affect all aliquots within a single sample in the same way. Following Rhodes et al. (2003), we refer to this sort of error as unshared systematic (USS) error. The USS is incorporated by randomizing each iterative outcome of the minimum age according to a normal distribution, with standard deviation of 5 % of the outcome.

Because the MAM-3 is called thousands of times within the script, we added some additional processing to the model to ensure the output is meaningful (i.e. not scuppered by programming limitations). Before running the MAM-3, any extreme high outliers in the D_e distribution are removed, obviating the need for the age-model to account for them. The MAM-3 is then called with a variety of starting values, with the maximum likelihood outcome giving the minimum age, provided that the minimum age is greater than the lowest individual-aliquot D_e value.

6.3 Results

We have applied the bootstrap uncertainty methodology to the sequence of young floodplain sediments described above. For the samples discussed, we used the unlogged version of the minimum-age model (MAM-3_{ul}) within the bootstrapping script, which is necessary when using very young samples (Arnold et al., 2009). The resulting age distributions are rather informative, and are shown in stratigraphical order in Fig. 6.1, along with the standard MAM-3_{ul} minimum age. For all samples, the bootstrap distribution is considerably wider than the 1σ error region of the original MAM-3_{ul} model. For sample NCL-1107141, the bootstrap distribution is rather skewed, with the peak of the curve offset from the original MAM-3_{ul} minimum age. Furthermore, sample NCL-1107144 shows a double-peaked distribution, which is due to the presence of one relatively precise aliquot at the young end of the D_e dataset which has a controlling effect on the minimum age. In some iterations of the bootstrap re-sampling this aliquot is not present, and a second peak in the distribution is created.

With the help of Bayesian analysis, the bootstrap age distributions can be used to create a coherent chronology for the floodplain sediment. The PDFs were saved as text files in the OxCal directory, with the units as years AD, and the file suffix *prior*. OxCal provides a number of depositional models and constraints to help define the chronology. We used the *P_Sequence* mode of deposition, as it is most consistent with non-continuous floodplain deposition; we assumed an average of 4 depositional events per metre. We also included a *Tau_Boundary* at the top of the sequence, which formulates a prior model for an exponentially decreasing floodplain sedimentation rate over time. The full list of commands is:

```
Plot()
 {
  P_Sequence("Site1107",4)
  {
   Boundary("b_old");
   Prior(p1107147){ z=9.42; };
   Prior(p1107146){ z=3.55; };
   Prior(p1107144){ z=1.64; };
   Prior(p1107143){ z=1.26; };
   Prior(p1107142){ z=0.77; };
   Prior(p1107141){ z=0.31; };
   Prior(p1107140){ z=0.13; };
   Tau_Boundary("b_young");
  };
 };
```

After running the model, OxCal produces a new series new PDFs, referred to as *Posteriors*. These have been plotted in Fig. 6.2 according to depth, along with the prior PDFs. OxCal also determines an ‘agreement index’ for each sample (Table 6.1), and for the overall model. The agreement index gives an objective score of the overlap between the modelled posteriors and the prior likelihoods. It is suggested that a lower threshold of 60 % should be applied to the samples, i.e. data should be rejected if the agreement index for the sample is below 60 %. This is clearly relevant for the sequence discussed here, because two samples have a low agreement index, leading to a low score for the overall model (47 %). However, as the threshold is arbitrary, it is worth considering the reasons behind the low scores for the two samples. First, sample NCL1107144 has a double-peaked prior likelihood distribution, caused by a low D_e value for one aliquot (Fig. 6.1). Since the Bayesian model rejects the entirety of the younger peak, it would be fair to assume that the low D_e value is a genuine outlier. As the posterior does not overlap with the younger (and larger) peak, the agreement index is low (29 %). However, we can have no hesitation in accepting the posterior distribution, because it agrees very well with the alternative (older) peak in the prior PDF.

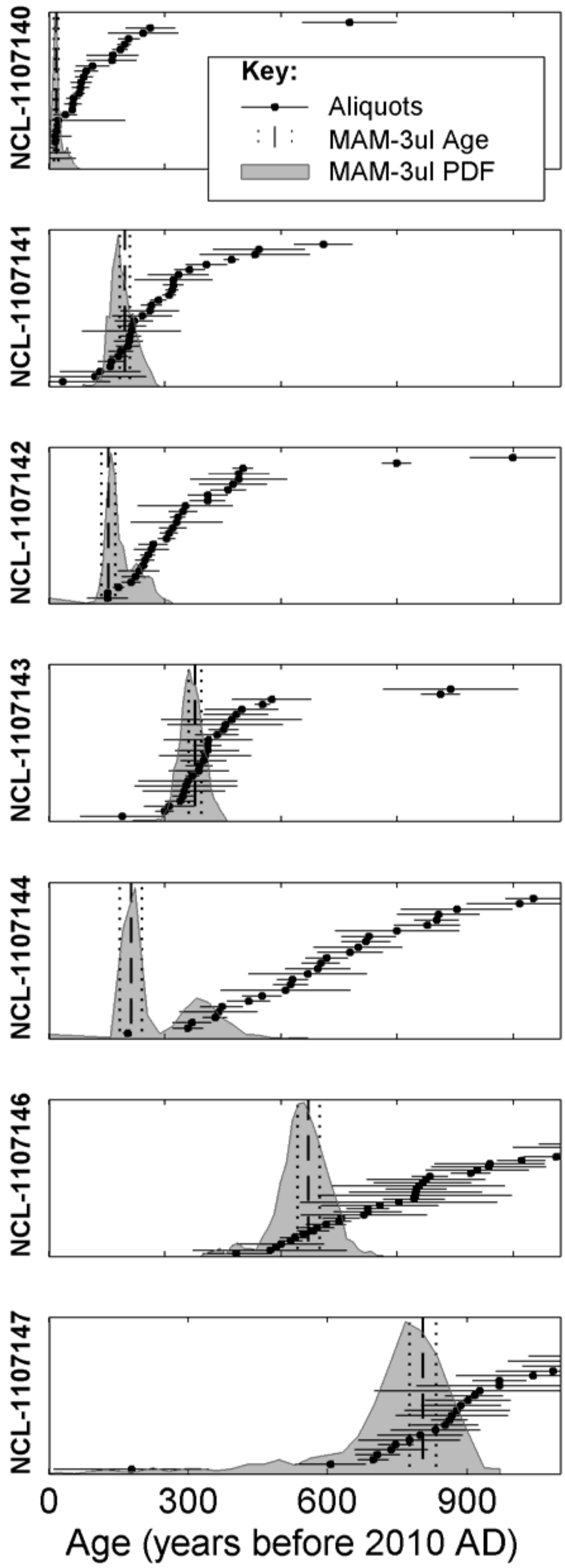
Key:
Aliquots
MAM-3ul Age
MAM-3ul PDF
NCL-1107140
NCL-1107141
NCL-1107142
NCL-1107143
NCL-1107144
NCL-1107146
NCL-1107147
0
300
600
900
Age (years before 2010 AD)

Fig. 6.1. (Opposite) Probability distribution functions (PDFs) of the MAM-3_{ul} minimum age, created using the bootstrap procedure described in section 6.2.3. The samples come from a single core through an embanked floodplain of the River Waal, the Netherlands (Wallinga et al., 2010, Hobo et al., 2010), and are plotted in depth order. The PDFs have been converted from a D_e scale to an age scale, using the sample-specific dose rates, and can be used to define the prior likelihoods in OxCal.

For sample NCL110142, the low agreement score (44 %) may be due to uncertainty in the deposition model, particularly in the mean number of deposition events per metre, specified in the *P_Sequence* function. The value we use is somewhat arbitrary, and may not be appropriate for the whole sequence. In summary, the agreement index is intended as a tool to help identify outliers, but not as a replacement for expert judgment (Bronk Ramsey, 2009).

6.4 Discussion

The potential benefit of using Bayesian methods for fluvial sediments is large, but rests on a number of basic assumptions. The first of these is that the prior likelihood distribution is a good reflection of the uncertainty associated with the OSL measurements. If the prior likelihood distribution is too narrow, then the lack of coherence between the samples will make it difficult to fit a depositional model; too broad and the model will tend towards a slower and more uniform rate of deposition.
The bootstrap routine presented above provides a robust estimation of the minimum-age uncertainty. By testing the sensitivity of the minimum age to (plausible) variation in the input data, the width of the probability distribution is made dependent on the quality of the original data. For example, sample NCL1107143, for which 23 aliquots (80 %) are consistent with the original MAM-3_{ul} minimum age, the relative standard deviation (r.s.d.) of the bootstrap distribution is 6 %. In contrast, for sample NCL1107142, which has 8 aliquots (30 %) consistent with the minimum age, the r.s.d. of the bootstrap distribution is 23 %. In a given sequence of fluvial samples, it is probable that some samples will appear better bleached than others. With the Bayesian procedure described above, it should be possible to ‘anchor’ the chronology on the most well-bleached samples.

The application of Bayesian statistics requires careful consideration of the sources of error. In the model discussed so far, systematic errors that are shared between the samples are not included, and must be added to the final (post-OxCal) age estimates. If independent age information is included in the deposition model, then the shared systematic errors should be added before the Bayesian modelling.

However, the likely size of shared systematic errors (< 5 %) may be insignificant compared to the width of the bootstrap uncertainty distributions, which range from roughly 6 % to 85 % for the samples used here.

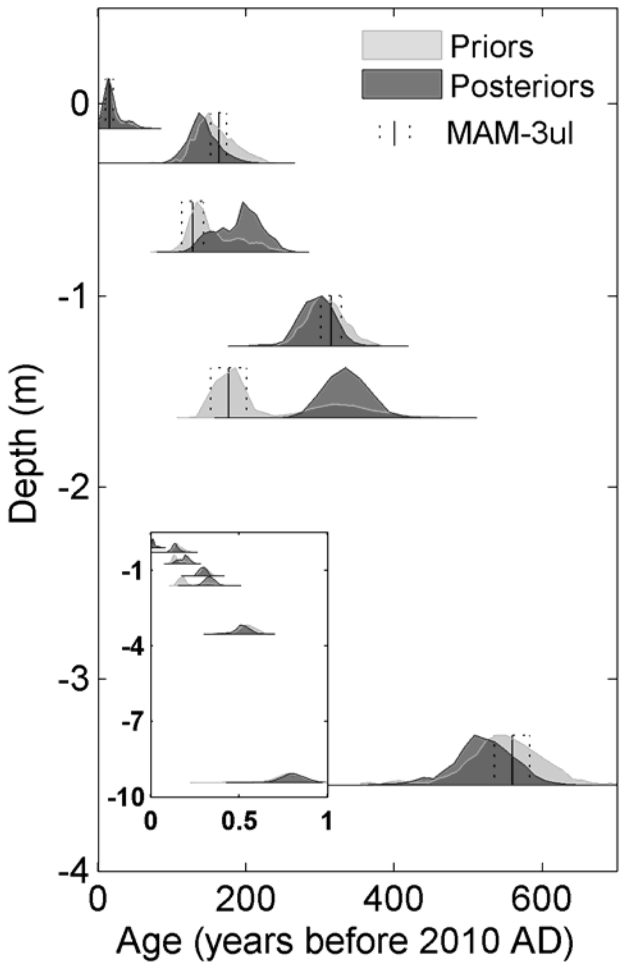

Fig. 6.2. Age-depth profile for the floodplain sequence. The ‘priors’ are the likelihood distributions of Fig. 6.1, created with the bootstrap-MAM-3ul procedure. The ‘posteriors’ show the age distributions after Bayesian processing in OxCal. The deposition model was based on a *P_Sequence*, with an average of 4 depositional events per metre, and an exponentially decreasing rate of deposition over time.

	Prior range (68.2%)	Posterior range (68.2%)	Agreement (%)
NCL1107140	1984 - 2007	1983 - 2006	89.4
NCL1107141	1833 - 1883	1849 - 1890	102.8
NCL1107142	1851 - 1895	1783 - 1859	44.9
NCL1107143	1680 - 1731	1690 - 1739	99
NCL1107144	1658 - 1867	1643 - 1710	29.2
NCL1107146	1415 - 1516	1444 - 1527	103.7
NCL1107147	1137 - 1335	1134 - 1277	112.7

Table 6.1. Confidence ranges (1σ) for the OSL ages, before the Bayesian modelling (Prior range) and after (Posterior range). Also shown is the agreement index, which measures the overlap between prior likelihood and posterior likelihood distributions. The agreement index of the overall model is 47 %.

6.5 Implications

The combination of bootstrap uncertainty distributions with Bayesian chronological modelling has the potential to greatly increase the accuracy and precision in dating fluvial deposits. However, for this potential to be realised there are two important requirements of the sampling strategy:

1. *High-resolution sampling*. The use of Bayesian statistics is only beneficial when the uncertainty distributions of different samples overlap. It is therefore essential that sampling resolution is high.
2. *High-quality stratigraphic information*. The more prior information that can be incorporated into the Bayesian modelling, the greater the precision of the chronological model.

The importance of these points can be seen by considering the chronological model of in Fig. 6.2. In the lower part of the core sequence, the posterior distributions are almost identical to the prior distributions, because the poor sampling resolution has lead to prior likelihood distributions that do not overlap. Furthermore, from consideration of the prior likelihood distributions alone, it appears possible that samples NCL-1107141 and NCL-1107142 were deposited in a single event. If there were solid stratigraphical evidence that this is the case, as might be obtained from x-ray core-scanning techniques, then that constraint could be incorporated into the chronological model by specifying a ‘phase’ of deposition. In the absence of this information, no such constraints can be legitimately included, so the posterior distributions are relatively broad (Fig. 6.2).

6.6 Conclusions

This paper bridges a gap between two powerful statistical techniques. The first is the minimum-age model (Galbraith et al., 1999), which is able to explain the distribution in D_e observed in partially bleached OSL samples. The second is the chronological tool OxCal (Bronk Ramsey, 1995), which provides a Bayesian framework for combining age and stratigraphic information. The bridge between the two methods is built with some straightforward computational statistics, and empowers OSL dating for use in the study and interpretation of fluvial sediments. Furthermore, this approach provides a framework for attaching future improvements in OSL methods. For example, an improved age-model, or a better assessment of dose-rate variation between grains, could easily be incorporated into the bootstrap approach. Finally, to get maximum benefit from a Bayesian analysis of OSL sequences, focus should be put on high-resolution sampling and the collection of detailed stratigraphic information.

Acknowledgements

Scripts for the bootstrap re-sampling of the MAM-3 and MAM-3_{ul} have been written in Matlab, and can be obtained from www.ncl.tudelft.nl or directly from the authors. The age models were translated from the S-Plus versions of Arnold et al. (2009). We thank Noortje Hobo for the samples, and for discussion on dating methods. The authors are supported by NWO/STW grant DSF.7553.

References

Arnold, L.J., Roberts, R.G. 2009. Stochastic modelling of multi-grain equivalent dose (De) distributions: Implications for OSL dating of sediment mixtures. Quaternary Geochronology 4, 204-230.

Arnold, L.J., Roberts, R.G., Galbraith, R.F., DeLong, S.B. 2009. A revised burial dose estimation procedure for optical dating of young and modern-age sediments. Quaternary Geochronology 4, 306-325.

Bailey, R.M., Arnold, L.J. 2006. Statistical modelling of single grain quartz De distributions and an assessment of procedures for estimating burial dose. Quaternary Science Reviews 25, 2475-2502.

Benito, G., Thorndycraft, V.R., Rico., M., Sanchez-Moya, Y., Sopena, A. 2008. Palaeoflood and floodplain records from Spain: Evidence for long-term climate variability and environmental changes. Geomorphology 101, 68-77.

Blockley, S.P.E., Blaauw, M., Bronk Ramsey, C., van der Plicht, J. 2007. Building and testing age models for radiocarbon dates in Lateglacial and Early Holocene sediments. Quaternary Science Reviews 26, 1915-1926.

Bronk Ramsey, C. 1995. Radiocarbon calibration and analysis of stratigraphy: the OxCal program. Radiocarbon 37, 425-430.

Bronk Ramsey, C. 2008. Deposition models for chronological records. Quaternary Science Reviews 27, 42-60.

Bronk Ramsey, C., Dee, M.W., Rowland, J.M., Higham, T.F.G., Harris, S.A., Brock, F., Quiles, A., Wild, E.M., Marcus, E.S., Shortland, A.J. 2010. Radiocarbon-based chronology for dynastic Egypt. Science, 328, 1554-1557.

Buck, C., Kenworthy, J., Litton, C., Smith, A. 1991. Combining archaeological and radiocarbon information – a Bayesian approach to calibration. Antiquity 65, 808-821.

Busschers F.S., Kasse, C.,van Balen, R.T., Vandenberghe, J., Cohen, K.M., Weerts, H.J.T., Wallinga, J., Johns, C., Cleveringa, P., Bunnik, F.P.M. 2007. Late Pleistocene evolution of the Rhine-Meuse system in the Southern North Sea basin: imprints of climate change, sea-level oscillation and glacio-isostacy. Quaternary Science Reviews 26, 3216-3248.

Busschers, F.S., Van Balen, R.T., Cohen, K.M., Kasse, C., Weerts, H.J.T., Wallinga, J., Bunnik, F.P.M. 2008. Response of the Rhine-Meuse fluvial system to Saalian ice-sheet dynamics. Boreas 37, 377-398.

Cunningham, A.C., Wallinga, J. 2010. Selection of integration time intervals for quartz OSL decay curves. Quaternary Geochronology 5, 657-666.

Cunningham, A.C., Wallinga, J. Expectations of scatter in equivalent-dose distributions when using multi-grain aliquots for OSL dating. Submitted to Geochronometria.

Duller, G.A.T. 2008. Single-grain optical dating of Quaternary sediments: why aliquot size matters in luminescence dating. Boreas 37, 589-612.

Efron, B. 1979. Bootstrap methods: another look at the Jackknife. The Annuls of Statistics 7, 1-26.

Galbraith, R.F. 2010. On plotting OSL equivalent doses. Ancient TL 28, 1-9.

Galbraith, R.F., Roberts, R.G., Laslett, G.M., Yoshida, H., Olley J.M. 1999. Optical dating of single and multiple grains of quartz from jinmium rock shelter, northern Australia, part 1, Experimental design and statistical models. Archaeometry 41, 339-364.

Hobo, N., Makaske, B., Middelkoop, H., Wallinga, J. 2010. Reconstruction of floodplain sedimentation rates: a combination of methods to optimize estimates. Earth Surface Processes and Landforms 35, 1499-1515.

Jacobi, R.M., Higham, T.F.G. 2009. The early Lateglacial re-colonization of Britain: new radiocarbon evidence from Gough's Cave, southwest England. Quaternary Science Reviews 28, 1895-1913.

Jain, M., Murray, A. S., Bøtter-Jensen, L. 2004. Optically stimulated luminescence dating: How significant is incomplete light exposure in fluvial environments? Quaternaire 15, 143-157.

Owens, P.N., Walling, D.E., Leeks, G.J.L. 1999. Use of floodplain sediment cores to investigate recent historical changes in overbank sedimentation rates and sediment sources in the catchment of the River Ouse, Yorkshire, UK. Catena 36, 21–47.

Rhodes, E.J., Bronk Ramsey, C., Outram, Z., Batt, C., Willis, L., Dockrill, S., Bond, J. 2003. Bayesian Methods applied to the interpretation of multiple OSL dates: high precision sediment ages from Old Scatness Broch excavations, Shetland Isles. Quaternary Science Reviews 22, 1231-1244.

Rittenour, T.M. 2008. Luminescence dating of fluvial deposits: applications to geomorphic, palaeoseismic and archaeological research. Boreas 37, 613-635.

Rittenour, T. M., Goble, R. J. & Blum, M.D. 2005. Development of an OSL chronology for late Pleistocene channel belts in the lower Mississippi valley. Quaternary Science Reviews 24, 2539-2554.

Rodnight, H., Duller, G.A.T., Tooth, S., Wintle, A.G. 2005. Optical dating of a scroll-bar sequence on the Klip River, South Africa, to derive the lateral migration rate of a meander bend. The Holocene 15, 802-811.

Rodnight, H., Duller, G.A.T., Wintle, A.G., Tooth, S. 2006. Assessing the reproducibility and accuracy of optical dating of fluvial deposits. Quaternary Geochronology 1, 109-120.

Thrasher, I.M., Mauz, B., Chiverrell, R.C., Lang, A., Thomas, G.S.P. 2009, Testing an approach to OSL dating of Late Devensian glaciofluvial sediments of the British Isles. Journal of Quaternary Science 24, 785-801.

Wallinga, J. 2002. Optically stimulated luminescence dating if fluvial deposits: a review. Boreas 31, 303-322.

Wallinga, J., Hobo, N., Cunningham, A.C., Versendaal, A.J., Makaske, B., Middelkoop, H. 2010. Sedimentation rates on embanked floodplains determined through quartz optical dating. Quaternary Geochronology 5, 170-175.

Chapter 7

Experimental simulation of beta-dose heterogeneity in sediment, using artificial radionuclides

Alastair C. Cunningham, Daniel J. DeVries, Dennis R. Schaart
To be submitted

Abstract

Understanding the spread in equivalent-dose (D_e) measurements is an important aspect of OSL dating. Ideally, prior to age estimation, an assessment should be made of the likely spread in D_e that is caused by dose-rate heterogeneity in the sediment. Such a procedure would greatly increase the validity of OSL ages, particularly for sediments susceptible to partial bleaching, and for sediments with coarse or poorly sorted grain-size distributions. In this paper we take a step towards a general model of dose-rate heterogeneity, by simulating the ^{40}K-derived beta dose to quartz. It is likely that the ^{40}K beta dose is the major source of dose-rate heterogeneity in sandy sediments. Here we present an experimental simulation of the ^{40}K beta dose, and compare the results with a Monte Carlo simulation of the same experiment. The experiment uses artificially produced ^{24}Na to simulate the ^{40}K beta dose to quartz, thereby allowing a large dose to be administered in a short space of time. Single grain measurements are performed on the quartz grains, and the resulting D_e distribution is accurately reproduced through Monte Carlo simulations. The combination of Monte Carlo simulations with experimental validation is found to be a powerful means of investigating beta-dose heterogeneity.

7.1 Introduction

For any single sample, OSL measurements are made on a number of subsamples (aliquots), which may contain a single grain or multiple grains. The equivalent dose (D_e) is determined for each aliquot, providing a distribution of D_e values from which the burial dose is estimated. The D_e values are rarely, if ever, consistent with a common burial dose; there is usually more scatter in the data than can be expected from counting statistics alone.

Understanding the source of scatter in D_e is vital for OSL dating. A misinterpretation of the source of scatter can lead to an inaccurate age estimate, because the estimate of the burial dose is dependent of how the scatter is interpreted. For example, where scatter is attributed to insufficient bleaching, an age model will be chosen that assigns a burial dose consistent with the younger part of the D_e distribution; should the interpretation be wrong, then the burial-dose (and hence the age) is likely to be an underestimate.

For determining the burial dose for partially bleached samples, it is necessary to estimate the amount of variation that could be expected in the data in the absence of partial bleaching. One way to do this is to examine the D_e distributions found with indisputably well-bleached samples, for which a value of 20 % is typical at the single grain level (Duller, 2008). However, there is a considerable amount of variation between different samples (Arnold and Roberts, 2009), which suggests that physical differences between samples (e.g. grain size, mineralogy) may influence spread in the data. In fact, a mechanism for such an effect has long been known, and is variously described as microdosimetric variation, or beta-dose heterogeneity. The effect is caused by the non-uniform distribution of beta-emitting radionuclides in the sediment, combined with the short range of beta electrons. The consequence is that the beta-dose rate may be different for each grain of quartz. As beta radiation typically accounts for around half of the total dose to quartz, heterogeneity in the beta dose is likely to be a significant source of scatter in D_e.

There is a solid explanation for why the concentration of beta-emitting radionuclides in sandy sediment may be non-uniform. Typically around 90 % of the beta dose to quartz comes from the decay of ^{40}K, which occurs at high concentrations in K-feldpsars. Grains of K-feldspar could act as ‘hotspots’ of activity, leading to positively skewed D_e distributions (Mayya et al., 2006). It is likely that the extent of the effect is dependent on physical parameters of the sediment, particularly the grain-size distribution and concentration of K-feldspar grains. Ideally, an assessment of the likely influence of hotspots would be made for each OSL sample. Such an approach would be based on a general model of dose-rate heterogeneity, something which does not yet exist. A possible source of such a model would be through a series of Monte Carlo simulations of energy deposition, in combination with experimental validation.

Beta-dose heterogeneity is not a topic which is easy to investigate. Monte Carlo calculations can be complex, while experiments simulating the natural dose rate may take many months to perform. Progress has therefore been relatively slow. Nathan et al. (2003) investigated the influence of macrobodies within artificial sediment, and showed the benefit of Monte Carlo techniques when combined with experimental methods. Monte Carlo methods have also proven useful in determining the mean dose rate, regardless of scatter between grains (Grine et al., 2007; Cunningham et al., submitted). Nathan et al. (2003) and Kalchgruber et al. (2003) also performed experimental measurements of dose rate heterogeneity between grains, using grains of Al_2O_3:C to record the dose in natural or artificial sediment over a period of time.

This paper takes a novel approach to the analysis of dose-rate variation in sediment. Starting from the assumption that the principle source of scatter is the K-feldspar 'hotspot' hypothesis of Mayya et al. (2006), we design an experiment to determine the likely effect of these hotspots under extreme conditions. Our approach combines experimental and numerical simulations, and is relatively efficient in terms of experimental duration. As such, the set-up we describe could provide a practical framework for investigating dose-rate heterogeneity in sediment.

Our Approach

We construct a 'sand box' experiment, in which grains of quartz are mixed with beta-emitting hotspot grains. Rather than using feldspar for the hotspot material, we use grains of sodium hydroxide (NaOH). Before mixing the materials, the NaOH is bombarded with neutrons in a nuclear reactor to produce ^{24}Na. ^{24}Na has a half life of 15 hours, decaying to ^{24}Mg by the emission of a beta electron, and two gamma photons. The beta-spectrum of ^{24}Na is almost identical to ^{40}K (Fig. 7.1), while the gammas are relatively high energy (1.37 and 2.75 MeV). The advantage of this set-up is that a large, heterogeneous beta dose can be given to the quartz grains in a short space of time (2 weeks), after which the material is safe to handle. The beta emission from ^{24}Na in the NaOH grains mimics the ^{40}K beta emission from feldspar grains in sandy sediment. Provided the overall mass is small, the probability of gamma interaction is low. The dose deposited to quartz grains in the experimental set-up is determined using single-grain OSL measurements.

To complement the experimental simulation, we construct a numerical model of the same experiment using a Monte Carlo transport code. The code we use is MCNP 4C (Briesmeister, 2000) which has been shown to work well when applied to problems of dose determination in sediment (Nathan et al., 2003; Cunnigham et al., submitted).

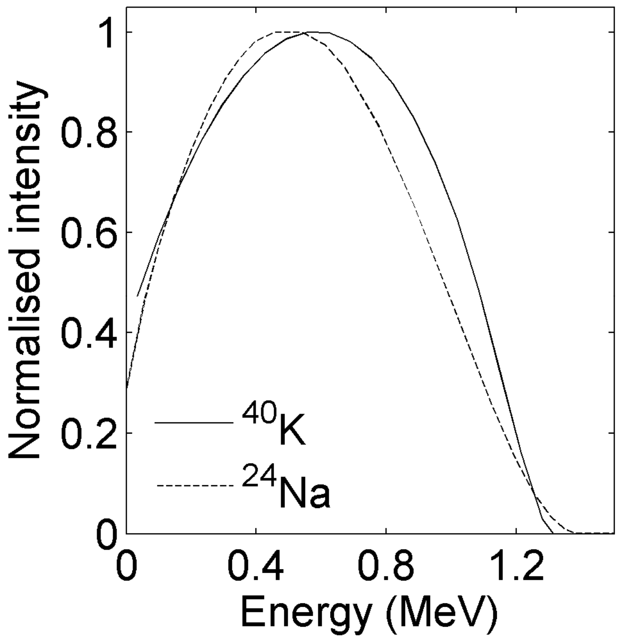

Fig. 7.1. Beta-energy spectra of ^{40}K and ^{24}Na. The ^{24}Na spectrum extends to 4 MeV at very low probability, and is not shown in the figure. The data comes from ENDSF.

7.2 Experimental Simulation

7.2.1 Equipment and protocols

The sand box mixture contained two materials, quartz (5.51g) and NaOH (0.33 g, giving 8 % by volume). The quartz grains were taken from a sand dune on the coast of the Netherlands (section HK3 of Cunningham et al. submitted). Grains of 180-212 μm diameter were isolated by sieving, and chemical treatment with HCl, H_2O_2 and HF. The quartz was bleached for several hours in a solar simulator; the residual OSL signal from the quartz was equivalent to 0.016 ± 0.004 Gy. NaOH grains (mesh 20-40, 97 % purity) were purchased from Perkin Elmer.

Irradiation Procedure

A polyethylene sample tube containing NaOH grains was irradiated with neutrons. The activated NaOH was given a cooling period of 26 hours, to allow the short-lived activation products to decay. Following this, the sample tube was placed into a lead container, and the quartz grains then added to the NaOH. The sealed container was vigorously shaken by hand, and placed in storage. After two weeks (22 half-lives of ^{24}Na), the mixture was opened, and the (water-soluble) NaOH washed out. A scale drawing of the experimental apparatus is shown in Fig. 7.2.

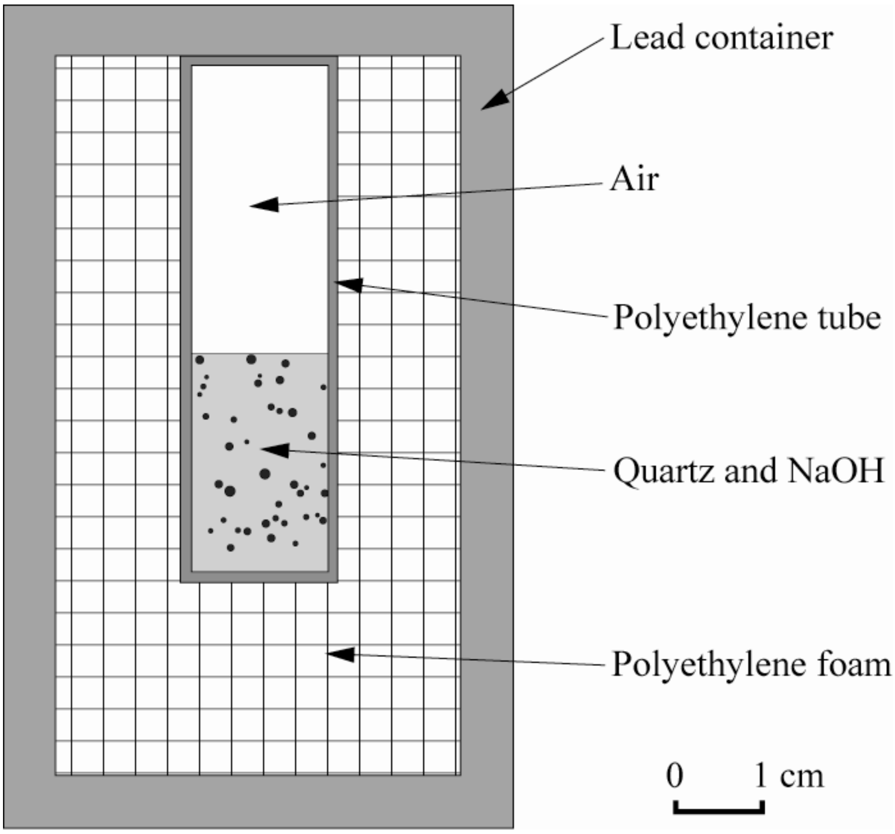

Fig. 7.2. Cross-section of the geometry used for Monte Carlo simulations, based on the experimental set-up. The circles represent the randomly positioned NaOH spheres, and are to scale with the rest of the image. The quartz dosimeters are much smaller and fewer in number; none are visible in this cross-section. The containers are cylindrical.

OSL measurements

Single-grain OSL measurements were performed using a Risø TL/OSL-DA-15 reader with single-grain attachment (Bøtter-Jensen et al., 2000). Individual grains were stimulated with an Nd:YVO4 diode-pumped laser (λ = 532 nm), delivering 50 W cm^{-2}. The detection filter was a 2.5 mm Hoya U340, shown by Ballarini et al. (2005) to optimize signal collection for young samples. OSL measurements followed a SAR protocol (Murray and Wintle, 2000), modified for single-grains from young samples following Ballarini et al. (2007), and similar to the multi-grain protocol used to date the same quartz (Cunningham et al., submitted). The details are given in Table 7.1. OSL signals were measured for 0.83 s each, recorded in 50 channels of 0.017 s. We used the early background approach for signal analysis (Cunningham and Wallinga, 2010), with the first 0.23 s used for the initial signal, and the subsequent 0.60 s used for background. We added further modifications to reduce the measurement time. Firstly, only a single regenerative dose was used, with the dose-response curve assumed to be a saturating exponential with D_0 = 80 (where D_0 is the dose indicative of saturation). We also checked the sensitivity of each grain after the first test dose (formula of Li (2007)), and only continued to measure grains with RSD on the test-dose OSL of less than 6.5 %. We measured the response of each sensitive grain to a zero dose (recuperation test) and repeated dose (recycling ratio test); grains were accepted if recuperation was less than 0.10 Gy, and the recycling ratio was between 0.90 and 1.10. Irradiation was administered with the inbuilt $^{90}Sr/^{90}Y$ beta source, providing ~0.12 Gy s^{-1}, with the dose rate to each single-grain position calibrated separately.

Treatment	Conditions
Dose	Nat, 3,0,3 Gy
Preheat	180ºC, 10 s
SG OSL	125ºC, 1 s
OSL bleach	125ºC, 40 s, Blue diodes
Dose	3 Gy
Cutheat	170ºC
SG OSL	125ºC, 1 s
OSL bleach	125ºC, 40 s, Blue diodes
OSL bleach	180ºC, 40 s, Blue diodes

Table 7.1. The SAR protocol used for determination of $D_{e,}$ for single grains of quartz.

7.2.2 Experimental results

The D_e was determined for 50 individual grains of quartz, which had been irradiated in the sand-box described above. There is a large amount of scatter in D_e, which ranges from 0.53 Gy to 22.15 Gy (Fig. 7.3). Part of this scatter is likely to be due to non-perfect measurement reproducibility using the single-grain reader, which is typically found to create scatter around the mean of 3 % (Thomsen et al., 2005; Truscott et al., 2000). It has also been observed that when an apparently uniform gamma dose is given to a batch of quartz, the amount of scatter in the OSL data is more than could be expected from counting statistics alone (Kalchgruber et al., 2003; Thomsen et al., 2005; 2007). The cause of this scatter is a bit of an enigma, but it does need to be accounted for when estimating scatter from other sources. We therefore carried out single-grain OSL measurements on the bleached quartz, after irradiating a batch with gamma rays from a ^{60}Co source. The apparatus used for the irradiation is crucial in providing a uniform gamma-dose; we used the apparatus described in Bos et al. (2006), minus the Fricke solution. The precise dose administered is not known (the calculation is complicated by the time taken to load the sample into position). Thirty-three grains were accepted, giving a central age of 5.23 ± 0.024 Gy, and overdispersion of 0.12 ± 0.018 (Fig. 7.4)

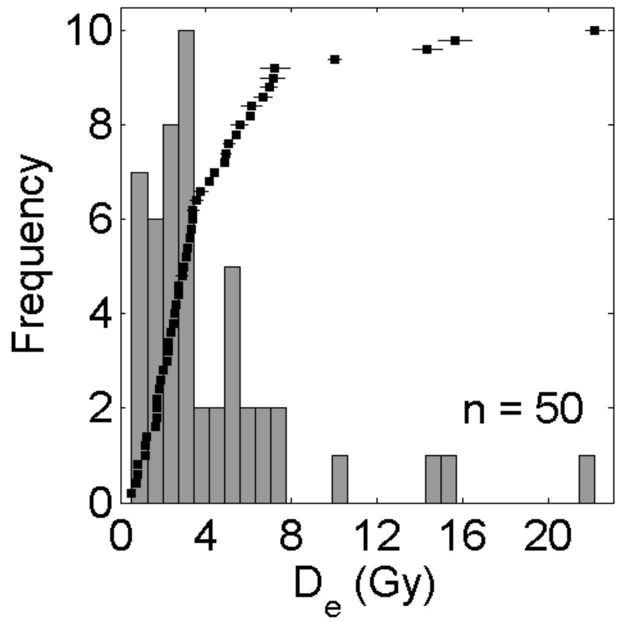

Fig 7.3. Single-grain D_e distribution of the sand-box quartz. Overdispersion is 0.765 ± 0.077.

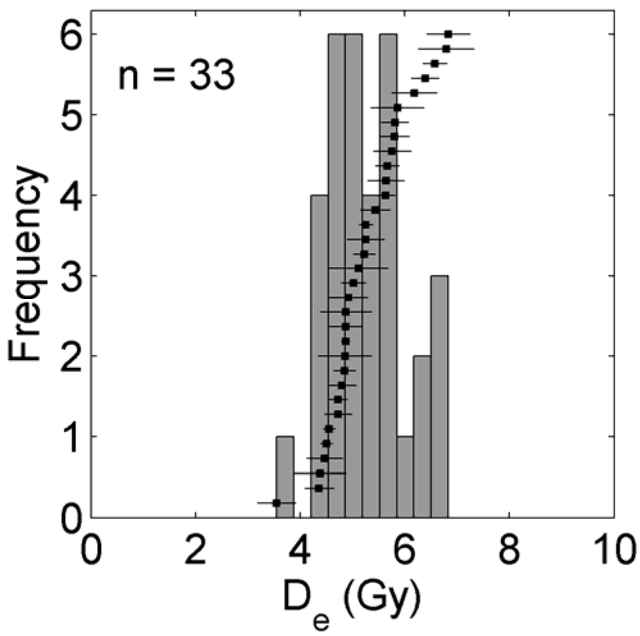

Fig. 7.4. Single-grain D_e measured after administering a uniform gamma dose from an external ^{60}Co source. Overdispersion is 0.121 ± 0.018.

7.3 Monte Carlo Simulations

7.3.1 Geometry

Monte Carlo simulations were designed to replicate the experimental simulations as closely as possible. The geometry of the containers is cylindrical, which slightly simplifies the code. A cross section of the geometry can be seen in Fig. 7.2. The placement of the grains was carried out as follows:

1. Source grains were randomly selected from the measured distribution of NaOH grainsize (Fig. 7.5). This distribution was carefully measured by taking photographs of NaOH grains with a digital camera attached to a microscope (Fig. 7.6), and comparing their diameters to a ruler photographed at the same scale. Random selection continued until the combined mass of the grains reached 0.33 g.
2. The source grains were randomly placed inside the container, with the condition that no grains overlapped. The height of the permissible region was determined by the mass off the combined quartz and NaOH, assuming a packing density of 53 %. This packing density was found to be appropriate to the experimental simulation, after weighing the same quartz in a container with known volume. Ninety-nine spherical quartz grains of 196 μm diameter were added, using the same placement conditions.

The material of interest contains ~650 NaOH source grains, with 99 quartz dosimeters. The remaining volume is defined as quartz, with density of 1.41 g cm^{-3}, i.e. the average density when pore space is included. This represents a significant simplifying assumption, and has a number of advantages. The alternative would be to assume all grains are spherical, and use an algorithm to pack the spheres into the correct density. However, this approach would present a number of issues. Firstly, the packing of spheres to a realistic density is not a trivial problem, and there is no guarantee that it would provide a significant improvement in model performance. Secondly, there are a number of limits within the Monte Carlo software controlling the number of objects which can be included. These limits would be exceeded if every grain were to be included individually. From first principles, we could expect that the irregular packing of the grains would create an additional source of scatter in absorbed dose. However, it is likely to be a second or third-order effect (behind grainsize and source concentration), and may not make a noticeable difference to the dose distribution.

7.3.2 Sources and tallies

Each geometry was used in two separate runs, one with beta electrons, one with gammas. The beta spectrum (Fig. 7.1) and discrete gamma energies of ^{24}Na were obtained from the ENSDF database via nucleardata.nuclear.lu.se. For the beta runs, 30 million histories were made, with the spectrum biased towards the high end to ensure a sufficient number of high-energy particles were initiated. Due to the low probability of gamma interaction with the region of interest, more histories were initiated (120 million). For the gamma runs, we also set the importance of the lead container to 5 %; this function terminates the majority of particles which enter the lead container, and increases the weight of the remainder by a corresponding amount. This is necessary because the gamma photons are more likely to interact with the larger mass of the lead than with the quartz, but the interaction with the lead is not of interest besides the small percentage of Compton scattered photons re-entering the quartz. Simulations were performed in coupled photon-electron mode, using the el03 and mcnplib2 electron and photon interaction data libraries and selecting the ITS electron energy indexing algorithm (Schaart et al., 2002). The upper photon and electron energy limits were set to 4.3 MeV. The photon and electron cut-off energies were set to 1 keV and 10 keV, respectively. Other simulation parameters were left at the default setting. The energy deposited in each of the 99 dosimeter grains was recorded using the *F8 tally.

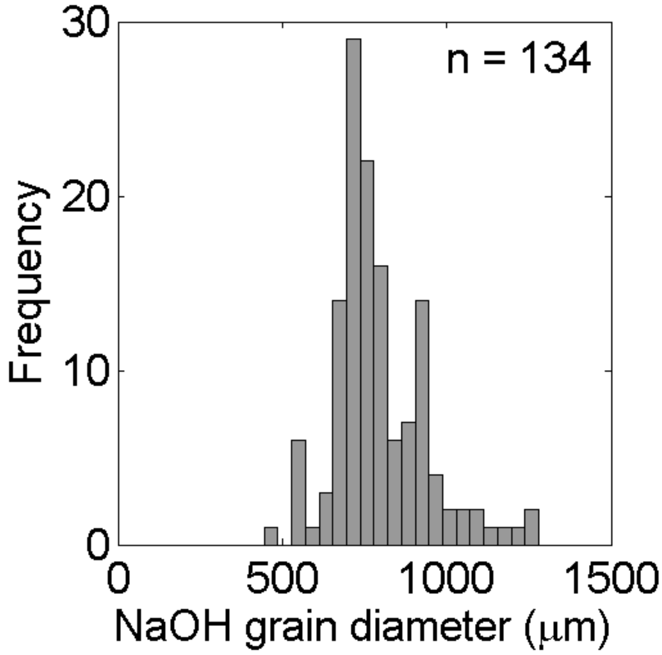

Fig. 7.5. Histogram of NaOH grain diameters. Bin width is arbitrary.

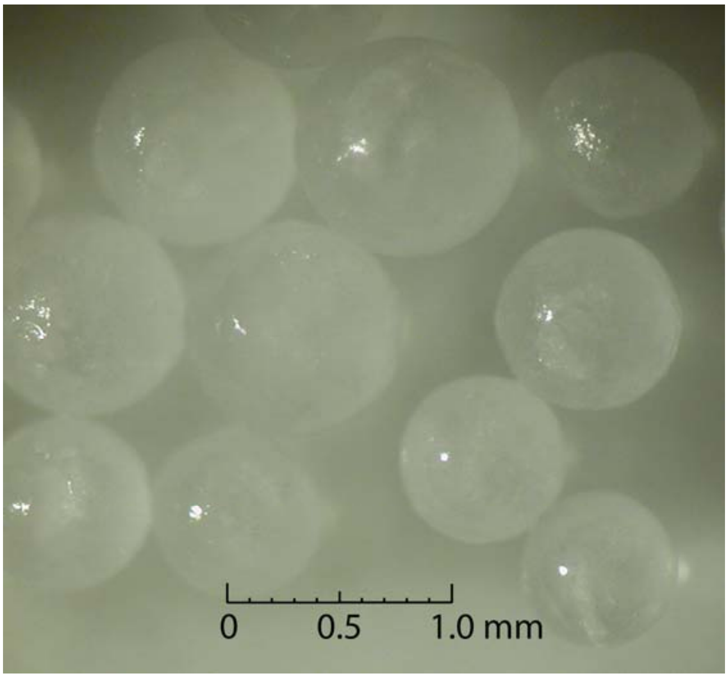

Fig. 7.6. Photograph of NaOH granules used in this study. The grainsize distribution of the NaOH was estimated using this image (and others).

7.3.3 Model results

An analysis of the Monte Carlo results is presented in Figs 7.7 and 7.8. In Fig. 7.7, the energy recorded in each dosimeter grain is plotted as a function of grain location. Considering the beta-derived energy only, it can be seen that the majority of the scatter between grains is unrelated to radial distance (Fig. 7.7(a)) or height (Fig. 7.7(c)). However, on the edge of the sand volume (radial distance > 0.65 cm) there is a cluster of low points, caused by disequilibrium in the flux of charged particles. The same effect can be seen for grains located close to the base or top of the sand volume (Fig. 7.7(c)). A similar issue also affects the energy recorded under the gamma-only conditions, although a much greater number of dosimeters are affected. It is also curious that despite the considerable range of the ^{24}Na gammas in sediment, there remains a certain amount of scatter in the energy deposited in the dosimeter grains.

Fig. 7.8 shows the output of the Monte Carlo simulations plotted as a series of histograms. The combined results of the beta and gamma runs can be seen in Fig. 7.8(c). Fig 7.8(d) plots the same data, but excluding grains that are located close to the edge of the sand volume. This provides a better indication of the distribution that could be expected under charged-particle equilibrium (although the wall effects still apply to the gamma component).

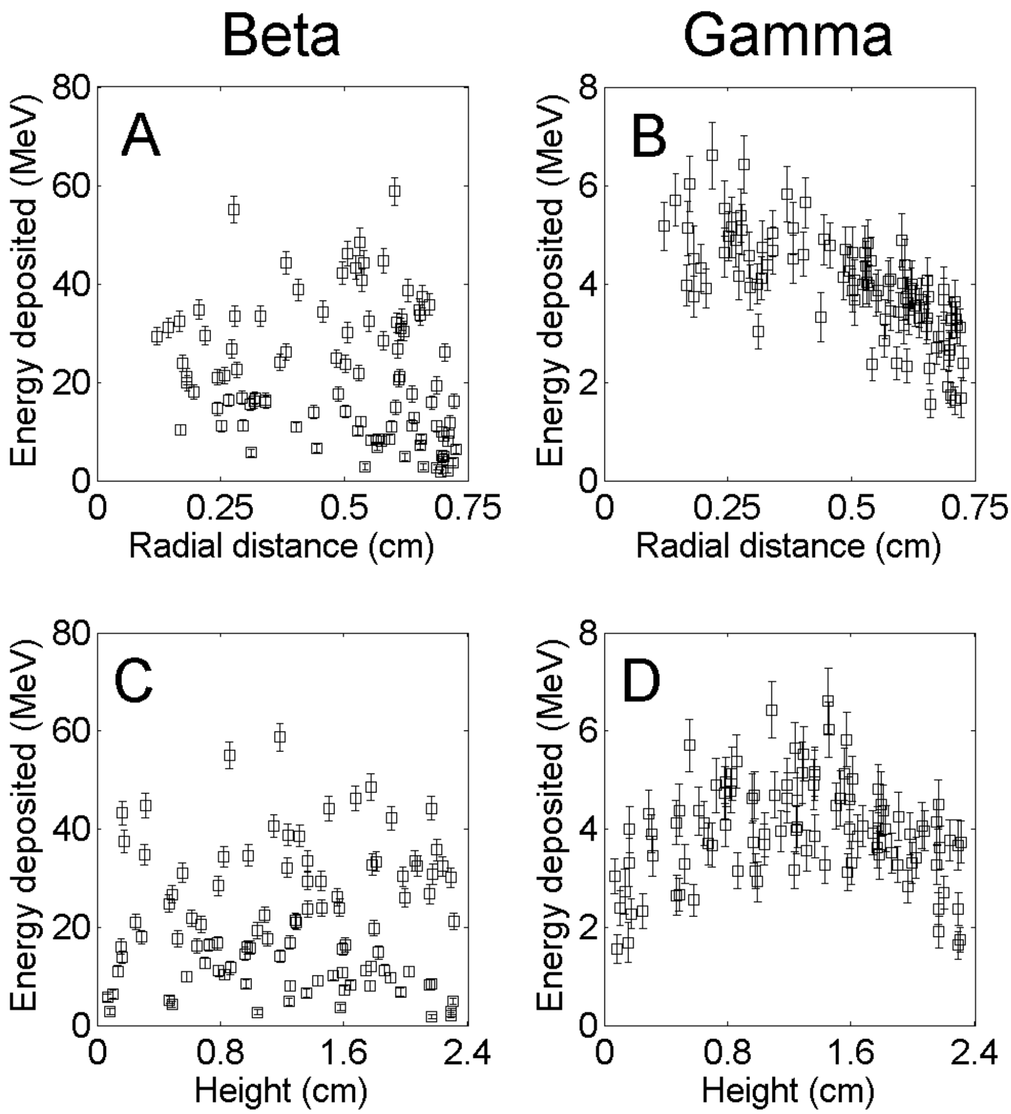

Fig. 7.7. Monte Carlo simulations of the energy deposited to individual grains of quartz in the experiment described in section 7.2.1, plotted as a function of grain location. On the left-hand side, the energy deposited due to the ^{24}Na beta emission from the NaOH grains: (a) according to the distance of each grain from the central axis of the cylindrical container, (b) according to the height position of each grain. On the right-hand side, (c) and (d) plot the same information for the gamma emission from ^{24}Na. In all cases, the y-axis show the energy deposited after 30 million disintegrations (with each disintegration yielding one beta electron and two gamma rays).

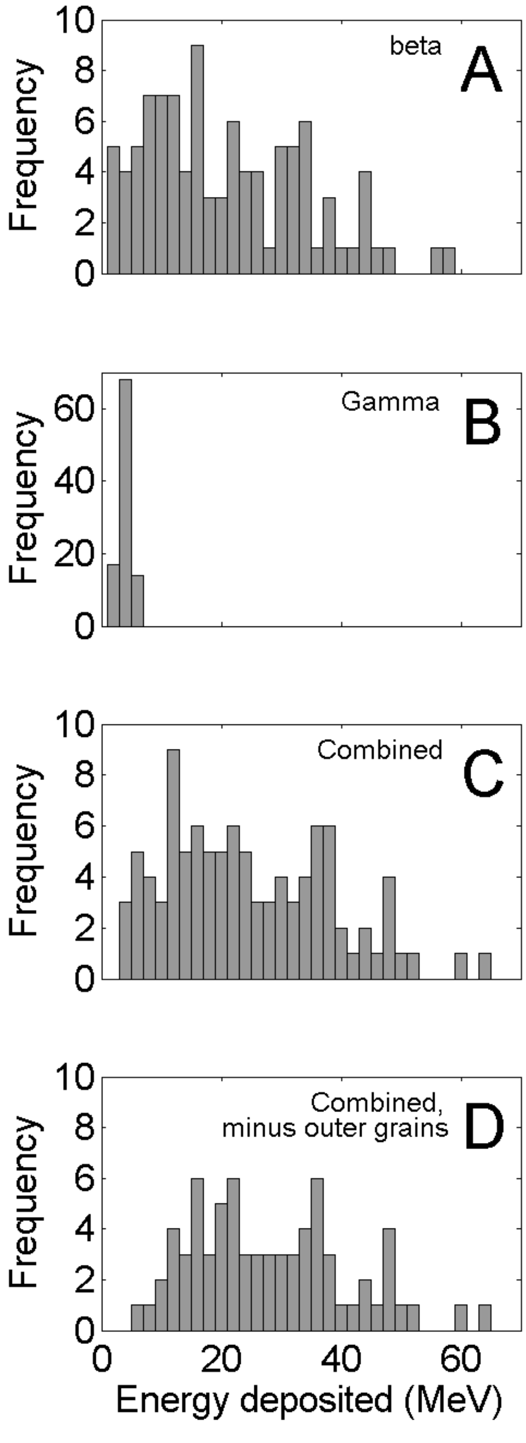

Fig. 7.8. Histograms showing the output of Monte Carlo simulations of the experimental set-up. The x-scale indicates the energy deposited in the dosimeter cells after 30 million disintegrations (producing 1 electron and 2 photons); bin width is 2 MeV in all cases. (a) Beta dose only; (b) Gamma dose only; (c) Sum of beta and gamma contributions; (d) same as (c), but only for grains lying at least 1 mm away from all edges of the sand/NaOH region. Graphs (a) to (c) contain 99 datapoints, graph (d) has 71.

	Experiment	*Overdispersion*
Measured	Sand box	0.77 ± 0.08
	Gamma dose	0.12 ± 0.02
Modelled	Beta only	0.76 ± 0.05
	Gamma only	0.25 ± 0.02
	Beta and gamma	0.60 ± 0.05

Table 7.2. Summary or results for both experimental and numerical simulations. Overdispersion calculated using the central-age model (Galbraith et al., 1999).

7.4 Discussion

7.4.1 Comparison of experimental and numerical simulations

For comparison of the experimental and numerically derived distributions, it is useful to identify a statistic which describes the scatter in the data, and which can be applied to all datasets. This could be done by fitting a suitable model to the data. The positively skewed distributions of the modelled and measured data lend themselves to fitting with a log-normal function. However, such a procedure should not be performed on the histograms directly, because each datapoint comes with an error term that must also be considered. The best approach is to use a maximum likelihood estimator (MLE) to identify the most likely values of the parameters of the log-normal function. In fact, just such a procedure is used frequently in the OSL dating literature, and is known as the Central Age Model (CAM) of Galbraith et al. (1999). The application of the CAM to a dataset of D_e (with error terms) determines the 'central age' and 'overdispersion (σ)', which together describe the form of the underlying log-normal distribution. For our purposes, the central age is not relevant, but σ may give a good indication of the relative spread in the data.

The overdispersion values for the measured and modelled distributions are given in Table 7.2. Both the measured and modelled distributions show a high degree of scatter, with slight differences between them (77 % for the measurements, 60 % for the combined model). The highly skewed distribution found in the sand-box measurements is also observed in the Monte Carlo simulations: an encouraging result given the complexity of the modelling. There remains a difference in overdispersion between the two simulation techniques, and there are a number of reasons why this might have occurred; these are discussed below in approximate order of likelihood:

1. *Random uncertainty in the placement of the source grains*. It is impossible to reconstruct the exact placement of the source grains in the experimental set-up,

and since the experiment is relatively small, the random positioning of the source grains may be particularly important.

2. *The number of single-grain measurements made.* Because such a small percentage of quartz grains give a significant OSL signal, the time taken to obtain the D_e data for 50 grains was significant (about 2 weeks). The relative uncertainty on the measured overdispersion (10 %) could be reduced with more measurements.
3. *Sensitivity of the model to the parameters.* It is possible that the modelled overdispersion is sensitive to some of the input parameters. Preliminary exploration of the model sensitivity indicated that the overdispersion particularly sensitive to the grain-size distribution of the source grains (hence the attention given in section 7.2.3).
4. *Inappropriate description of the distributions.* While comparing the relative width of the fitted log-normal function may be useful, it is not a perfect tool for comparison. Differences in overdispersion may not necessarily reflect actual differences in the distribution. The log-normal function is not a perfect fit, particularly given the wall effect (which leads to excessively low values). Furthermore, the nature of the error terms in the modelled and measured distributions are not the same – the error terms in the modelled data are dependent on the amount of energy deposited; for the measurement errors this is not the case.
5. *Mixing of materials.* Given the different grainsizes of the two materials, there is always the possibility that the grains were not mixed sufficiently, or that some of the (hydroscopic) NaOH grains became stuck together. It is likely that the experimental mixture was more heterogeneous than in the truly random numerical simulation. An experiment using more uniform grain size would reduce the likelihood of poor mixing

There are clearly a number of outstanding issues, and many of the points listed above could be clarified with further measurements and modelling. Furthermore, by substituting some of the quartz for highly sensitive Al_2O_3:C grains, future measurements would benefit from a dramatically reduced OSL measurement time.

7.4.2 Understanding the gamma dose

It was implied in the introduction that while the beta dose to quartz may be heterogeneous, the range of gamma rays in sediment (tens of centimetres) would lead to a uniform gamma dose. Surprisingly, the Monte Carlo simulations show that this is not the case for the experiment described here. The overdispersion in the energy deposited to the dosimeters is 0.25 for the gamma-only simulation. A considerable amount of this scatter is caused by the proximity of some the grains to the edges of the sand volume; However, a recalculation of σ using only grains in the central region (between 0.7 and 1.7 cm in height, and a radial location less than 0.4 cm) still shows overdispersion of 0.08 ± 0.03. The existence of this remaining scatter demonstrates that there are two separate effects involved: firstly, the attenuation of dose due to the mass between the source particle and dosimeter; secondly, the dependence of the dose rate on the proximity of the source (i.e. the inverse square law). The gamma dose may hardly be affected by the first of these, but is affected by the second in the same way as the beta dose.

While ^{40}K is responsible for most of the beta dose in natural sediments, it also contributes a significant proportion of the gamma dose. Although dose heterogeneity in this experiment represents and extreme case, it is possible that the gamma dose in natural sediment is not exactly uniform. Furthermore, as the 7 % overdispersion in the gamma-derived energy must also apply to the beta-derived energy, it implies that virtually all of the 76 % overdispersion in the beta dose is due to attenuation through matter. Therefore, overdispersion should not be sensitive to the packing density of the sediment.

7.5 Conclusion

The way that ionising radiation deposits dose in natural sediments is of great interest for OSL dating. This chapter has opened a new avenue of research by which to solve outstanding issues in the field. The key conclusions are:

- Artificially produced ^{24}Na can be used to mimic dose delivered by ^{40}K hotspots in natural sediment. Spherical grains of NaOH are easy to obtain.
- Numerical simulations, using a Monte Carlo transport code, can reproduce the observed spread in the experimental data, and help to understand the causes of that spread.
- The combination of Monte Carlo simulations with experimental simulation could provide a framework for increased understanding of dose-rate heterogeneity in sediment. Ultimately, a general model to predict dose-rate heterogeneity would prove invaluable for OSL dating; the procedure outline here could help to achieve this goal.

References

Arnold, L.J., Roberts, R.G. 2009. Stochastic modelling of multi-grain equivalent dose (De) distributions: Implications for OSL dating of sediment mixtures. Quaternary Geochronology 4, 204-230.

Ballarini, M., Wallinga, J., Duller, G.A.T., Brower, J.C., Bos, A.J.J., van Eijk, C.W.E. 2005. Optimizing detection filters for single grain optical dating of quartz. Radiation Measurements 40, 5-12.

Ballarini, M., Wallinga, J., Wintle, A.G., Bos, A.J.J. 2007. A modified SAR protocol for optical dating of individual grains from young quartz samples. Radiation Measurements 42, 360-369.

Bøtter-Jensen, L., Bulur, E., Duller, G.A.T., Murray, A.S. 2000. Advances in luminescence instrument systems. Radiation Measurements 32, 57-73.

Briesmeister, J.F. 2000. MCNP – A General Monte Carlo N-Particle Transport Code Version 4C. Report LA-13709-M (Los Alamos National Laboratory).

Cunningham, A.C., and Wallinga, J. 2010. Selection of integration time intervals for quartz OSL decay curves. Quaternary Geochronology 5, 657-666.

Cunningham, A.C., Bakker, M., van Heteren, S., van der Valk, B., van der Spek, A.J.F., Schaart, D.R., Wallinga, J. Extracting storm-surge data from coastal dunes for improved assessment of flood risk. Submitted to Geology.

Duller, G.A.T., 2008. Single-grain optical dating of Quaternary sediments: why aliquot size matters in luminescence dating. Boreas 37, 589-612.

Galbraith, R.F., Roberts, R.G., Laslett, G.M., Yoshida, H., Olley, J.M. 1999. Optical dating of single and multiple grains of quartz from jinmium rock shelter, northern Australia, part 1, Experimental design and statistical models. Archaeometry 41, 339-364.

Grine, F.E., Bailey, R.M., Harvati, K., Nathan, R.P., Morris, A.G., Henderson, G.M., Ribot, I, Pike, A.W.G. 2007. Late Pleistocene human skull from Hofmeyr, South Africa, and modern human origins. Science 315, 226-229.

Kalchgruber, R., Fuchs, M., Murray, A.S., Wagner, G.A. 2003. Evaluating dose-rate distributions in natural sediments using α-Al_2O_3:C grains. Radiation Measurements 37, 293-297.

Li, B. 2007. A note on estimating the error when subtracting background counts from weak OSL signals. Ancient TL 25, 9-14.

Mayya, Y.S., Morthekai, P., Murari, M.K., Singhvi, A.K. 2006. Towards quantifying beta microdosimetric effects in single-grain quartz dose distribution. Radiation Measurements 41, 1032-1039.

Murray, A.S., Wintle, A.G. 2000. Luminescence dating of quartz using an improved single-aliquot regenerative-dose protocol. Radiation Measurements 32, 57-73.

Nathan, R.P., Thomas, P.J., Jain, M., Murray, A.S., Rhodes, E.J. 2003. Environmental dose rate heterogeneity of beta radiation and its implications for luminescence dating: Monte Carlo modelling and experimental validation. Radiation Measurements 37, 305-313.

Schaart, D.R., Jansen, J.T.M., Zoetelief, J., de Leege, P.F.A. 2002 A comparison of MCNP4C electron transport with ITS 3.0 and experiment at incident energies between 100 keV and 20 MeV: influence of voxel size, substeps and energy indexing algorithm. Physics in Medicine and Biology 47, 1459-1484.

Thomsen, K.J., Murray, A.S., Bøtter-Jensen, L. 2005. Sources of variability in OSL dose measurements using single grains of quartz. Radiation Measurements 39, 47-61.

Thomsen, K.J., Murray, A.S., Bøtter-Jensen, L., Kinahan, J. 2007. Determination of burial dose in incompletely bleached fluvial samples using single grains of quartz. Radiation Measurements 42, 370-379.

Truscott, A.J., Duller, G.A.T., Bøtter-Jensen, L., Murray, A.S., Wintle, A.G. 2000. Reproducibility of optically stimulated luminescence measurements from single grains of Al2O3:C and annealed quartz. Radiation Measurements 32, 447-451.

Synthesis

Storm-surge sediment

The analysis of storm-surge sediment has the potential to provide new information on storm-surge risk, and give an understanding of how storm-surges affect the coastal zone. While reliable measurements of storm surges have been collected over the last hundred years or so, the data that can be obtained from the geological archive has two particular benefits. Firstly, storm-surge deposits can be created from high-magnitude events over a period of hundreds or thousands of years. The low frequency of these events means they are unlikely to occur during the relatively short time-span of instrumental measurements. Secondly, high-magnitude events of the past may have occurred under subtly different climatic conditions. Studying palaeo storm surges allows a better appreciation of how storm surges respond to climate parameters, vital information given the changes in climate patterns and sea level that are likely in the near future.

In this thesis a unique analysis of storm-surge sediment is carried out (Chapter 5). The sediment of interest is located within the dunes of the North Holland coast, and became exposed in 2007 following a period of storm erosion. The fact that the sediment is located within the dunes creates two advantages for analysis:

1. *The elevation of the deposits is indicative of the magnitude of the event*. The storm-surge sediment was identified by a 10-20 cm thick layer of marine shells, which truncated the underlying dune deposits (see Fig 1.1, 5.0). The shell unit was found to undulate in height along several hundred metres of frontal dune, with a maximum height of 6.5 m NAP. The dominance of marine shells in the sediment, and the occasional pieces of brick, means that the sediment could not have been deposited by the wind. The height of the shell layer therefore indicates the minimum height that water has reached at the shell locations.
2. *The bracketing dune sand allows OSL dating to be used for age control*. Accurate dating of sediment from the last 1000 years is rarely straightforward. However, when applied to aeolian sand dunes, Optically Stimulated Luminescence (OSL) dating is a well proven method for obtaining an accurate age during this time period. This means that by taking OSL samples from above and below the storm-surge sediment, the age of the deposit can be reliably bracketed. The OSL dating results in chapter 5 bracket the storm-

surge sediment to between ~1760 and ~1795 AD; documentary sources show that major storm surges struck the area in 1775 and 1776 AD.

Chapter 5 also contains two further advances, through which analysis of similar deposits can be undertaken without the need for a large bluff-face exposure. Ground-penetrating radar was used to track the storm-surge sediment, after the radar signature of the shell-rich layer was verified with the visible exposures. OSL dating was also carried out on the storm-surge sediment directly, for which a Monte Carlo based model of radiation transport in the shell-rich sediment was created. These two points are vital for future research: a single core through a sand dune would not benefit from bluff-face sedimentology, while there may be a large gap between the ages of the bracketing material.

Implications for OSL dating

A significant part of this thesis is devoted the development of methods of analysis in OSL dating, designed to permit the direct dating of storm-surge sediment. However, the problems that had to be overcome are not unique to storm-surge sediment. The developments described in this thesis apply equally well to OSL dating in other types of depositional environment. In particular, samples from young fluvial deposits may require the use of several new methods of analysis to obtain an accurate age estimate. These new methods are summarised below.

Signal collection

For fluvial samples, the primary concern is whether the sunlight exposure during the last cycle of transport and deposition was enough to reset the OSL signal: if not, the OSL measurement is likely to overestimate the equivalent dose (D_e), and therefore the depositional age. One way to reduce this effect is to use only the part of the OSL signal which is most likely to be well bleached. This is achievable because the OSL signal from quartz contains several different components, which bleach at different rates. The components can be separated by curve fitting of the OSL decay curve; chapter 2 describes a technique for curve fitting when the signals are very weak.

For OSL dating applications, curve fitting is not usually a practical solution. In chapter 3, the curve-fitting method is used to identify a simple technique which can be used to maximise the amount of 'fast' component in the net OSL signal. Instead of the standard method of signal collection, in which the background is taken from the end of the stimulation period, it is proposed that the background signal should immediately follow the initial signal, and be ~2.5 times the length of that initial signal.

By keeping this ratio, the proportion of easily bleached 'fast' component in the net signal will be high, while the signal-to-noise ratio will be reasonably good.

Understanding scatter in D_e

Differential bleaching in nature can lead to a broad D_e distribution, but it is not the only source of scatter between different grains. It is likely that in most sediments, spatial variation in the concentration of radionuclides leads to a non-uniform radiation dose rate between different grains. Much of the beta dose in sandy sediments comes from the decay of ^{40}K, which is largely located within grains of K-feldspar. The beta dose that a quartz grain receives is therefore dependent on the number of feldspar grains in the vicinity.

The influence of ^{40}K 'hotspots' has been discussed for years, but quantification of the scatter they induce has not been an easy topic to investigate. Chapter 7 of this thesis introduces a new type of experiment, designed to simulate and thus quantify the effect of ^{40}K in sandy sediment. A 'sand box' experiment is conducted, in which a beta dose is delivered to quartz through the decay of ^{24}Na, located in grains of NaOH mixed into the sediment. The ^{24}Na is artificially produced through neutron bombardment in a nuclear reactor, and due to its short half-life of 15 h, it can deliver a substantial beta dose to the quartz and decay to background levels within a couple of weeks. Single-grain measurements of quartz show that the sand-box simulation is a viable tool to deliver a non-uniform beta dose. Monte Carlo simulations of the same experiment produce similar results. The combination of these two simulation techniques is a powerful way to investigate beta-dose heterogeneity.

While it is necessary to understand beta-dose heterogeneity at the single-grain level, it is notable that most OSL dating is carried out on multi-grain aliquots. Chapter 4 shows how information on grain-to-grain scatter can be converted for use with multi-grain aliquot dating applications. A stochastic model for this is presented, which takes in to account the sensitivity distribution of the single-grain population and the number of grains on the aliquots.

Age estimation

The final part of OSL age determination is to estimate the true 'burial' dose from a D_e distribution. If partial bleaching has caused additional scatter in the data, a statistical model must be used to account for that scatter, in addition to the scatter expected to occur through other effects. The selection of such a model has been a continuing source of debate in the field of OSL dating. In chapter 6 of this thesis, a new approach to age determination has been proposed, which overcomes the problem of age-model selection and outlier identification. The new approach uses a bootstrap re-sampling method to determine the uncertainty associated with an OSL age, producing a probability distribution function of the age. The benefit of this approach is twofold: it can provide a multi-peaked probability distribution in the presence of outlier D_e values; and it allows Bayesian analysis to be carried out on a suite of samples for improved chronological precision.

Further research questions to be addressed

This thesis has presented a suite of analysis methods for OSL dating of partially bleached samples. Taken together, these methods greatly increase the applicability of OSL dating. OSL dating has long been proven successful for dating well-bleached aeolian samples. Fluvially deposited sediments are often dated with OSL, but reliable ages are rarely published unless the samples happen to have been well-bleached. OSL is therefore underutilised for fluvial samples, even though there is frequently no other method capable of directly dating fluvial sediment. The suite of analysis methods described above could help to change this situation, by allowing OSL to be used with confidence for fluvial samples, even when partial bleaching causes an excessive amount of scatter in the data.

There is now an urgent need for OSL researchers to develop a full understanding of the dose rate, and dose-rate variability between grains. The dose rate represents half of the age equation, yet receives very little research attention. There are perhaps two reasons for this: until recently, the potential error in the dose-rate calculations has been dwarfed by error in the equivalent-dose calculations; but more fundamentally, questions on dose-rate variability have been too difficult to answer. There are two burning questions, both of which have been tackled in this thesis to some extent:

1. *How variable is the dose rate between grains?* It is vital to get a grip on dose-rate variability to enable interpretation of D_e distributions. Chapter 7 has provided a basis for investigating this question, which will require a series of Monte Carlo models combined with experimental validation. However, for this understanding to be useful to OSL users, any insights need to be combined into a simple model, or developed into a usable program.
2. *What if the standard dose-rate assumptions are broken?* There are two key assumptions in dose rate calculations, known as the ‘infinite-matrix’ and ‘uniform-matrix’ assumptions. Virtually all OSL sampling is carried out with these assumptions in mind, i.e. with homogeneous sandy or silty sediment from large sedimentary units. Dating of more complex sediment

may invalidate these assumptions, in which case a suitable dose-rate model must be created. An example of this can be found in chapter 5 for the dating of shell-rich storm-surge sediment: the shells and sand were separated, their radionuclide concentrations determined, and the fractions combined again in a numerical model to estimate the dose rate to quartz.

Progress on both of these points is likely to involve a significant amount of numerical modelling with Monte Carlo transport codes. Perhaps the most important step for the near future is therefore to simplify the use of Monte Carlo techniques, so that they can become a practical tool for OSL dating specialists.

Samenvatting

Stormvloedsediment

Het analyseren van stormvloedsediment kan nieuwe kennis verschaffen betreffende het risico op stormvloeden, en kan bovendien inzicht geven in hoe stormvloeden de kustzone beïnvloeden. Gedurende de afgelopen 100 jaar hebben mensen betrouwbare gegevens over stormvloeden gedocumenteerd. De gegevens die opgeslagen liggen in het geologisch archief bieden echter twee grote voordelen ten opzichte van historische documentatie. Ten eerste worden stormvloedsedimenten gevormd tijdens gebeurtenissen (events) met een grote magnitude; deze komen met een lage frequentie voor in een tijdsbestek van honderden tot duizenden jaren en het is onwaarschijnlijk dat ze terug te vinden zijn in het korte tijdsbestek van de instrumentele metingen. In het ruime tijdsbestek van het geologische archief kunnen de sporen van deze events echter wel worden opgeslagen en teruggevonden. Ten tweede kunnen omvangrijke stormvloeden uit het verleden plaats hebben gevonden onder verschillende klimaatsomstandigheden. Het bestuderen van paleostormvloeden kan in combinatie met geologische klimaatgegevens inzicht geven in hoe stormvloeden reageren op klimaatparameters; deze informatie is onmisbaar gezien de veranderingen in klimaat en zeespiegelniveau die hoogstwaarschijnlijk in de nabije toekomst op stapel staan.

In deze thesis is een unieke analyse op stormvloedsedimenten uitgevoerd (zie Hoofdstuk 5). Het studiegebied ligt in de duinen langs de kust van Noord-Holland, waar een unieke ontsluiting met stormvloedsedimenten werd blootgelegd tijdens een grote storm in 2007, die een deel van de voorste duinenrij erodeerde. De stormvloedsedimenten liggen ingebed tussen eolische duinafzettingen en dat creëert twee voordelen voor analyse:

1. *De hoogte waarop het sediment zich bevindt geeft een indicatie over de magnitude van het event.* Het stormvloedsediment werd geïdentificeerd aan de hand van een 10-20 cm dikke laag met marine schelpen, die de onderliggende laag duinsediment had afgesneden (zie fig. 1.1, 5.0). Deze enigszins golvende schelpenlaag kon worden vervolgd over een afstand van aan aantal honderden meters in de voorste duinenrij, waarbij een maximum hoogte van de laag gemeten werd op 6.5 m boven NAP. De grootschalige aanwezigheid van schelpen in het sediment en het voorkomen van hier en daar een stuk baksteen geeft aan dat dit sediment niet kan zijn afgezet door de wind. De hoogte waarop de schelpenlaag is gevonden geeft daarom aan wat de minimum waterhoogte is geweest ten tijde van afzetting van het sediment.

2. *Duinafzettingen zijn goed te dateren met OSL en kunnen als leeftijdscontrole worden gebruikt.* Het nauwkeurig dateren van sedimenten uit de afgelopen 1000 jaar is zelden rechtlijnig. Eolisch duinsediment is echter uitermate geschikt materiaal voor leeftijdsbepaling door middel van optische gestimuleerde luminescentie (OSL): een uitgebreid geteste methode waarvan is bewezen dat deze accuraat de leeftijd kan bepalen van eolisch sediment uit de afgelopen 1000 jaar. Dit betekent dat de leeftijd van de stormvloeddepositie afgebakend kan worden door OSL monsters te nemen uit het duinsediment boven en onder de afzetting. De OSL dateringen die zijn uitgevoerd op het duinsediment plaatsen de stormvloed tussen ~1760 en ~1795 AD; dit komt overeen met historische documentatie, waarin wordt aangegeven dat twee hevige stormvloeden het gebied troffen in 1775 en 1776 AD.

Naast de uitgebreide analyse en datering van de stormvloedafzetting in Noord Holland, bevat Hoofdstuk 5 twee ontwikkelingen waarmee in de toekomst de analyse van stormvloeddeposities uitgevoerd kan worden zonder dat daar per se een klifachtige ontsluiting voor nodig is: het gebruik van grondpenetrerende radar en het dateren van de stormvloedsedimenten zelf.

Door middel van grondpenetrerende radar (GPR) werd de sedimentologie rond het stormvloedsediment in beeld gebracht. Door het radarsignaal van de schelpenlaag te verifiëren aan de hand van zichtbare ontsluitingen, kon het stormvloedsediment worden gelokaliseerd. In het geval dat er geen ontsluiting beschikbaar zou zijn, zou een sedimentkern gestoken kunnen worden. Een enkele kern biedt echter niet het voordeel van de duidelijke sedimentologie die te zien is bij een klifachtige ontsluiting. GPR kan in die situatie meer informatie over de sedimentologie rondom de kern verschaffen.

Verder werd OSL datering uitgevoerd op de stormvloedsedimenten zelf; voor dit doel werd een op Monte Carlo simulaties gebaseerd model van het stralingstransport in het schelpenrijke sediment gecreëerd. Door het mogelijk te maken het stormvloedsediment zelf te dateren is men in de toekomst minder afhankelijk van omringend materiaal: er zouden immers grote verschillen kunnen zijn tussen de leeftijden van het boven- en onderliggende materiaal.

Gevolgen voor OSL datering

Een groot deel van deze thesis is gewijd aan het ontwikkelen van nieuwe methoden voor de analyse van OSL dateringen, die specifiek ontworpen werden voor het direct dateren van stormvloedafzettingen. De problemen die hierbij moesten worden opgelost, komen echter niet alleen voor in stormvloedsediment; de beschreven ontwikkelingen zijn net zo goed toepasbaar in andere afzettingsmilieus. Vooral bij het dateren van jonge fluviatiele sedimenten kunnen soortgelijke problemen voorkomen als bij het dateren van stormvloedsediment. Een aantal van de in dit werk beschreven methodes zouden in dat geval gebruikt kunnen worden om toch een accurate leeftijd te verkrijgen. Deze nieuwe methodes worden hieronder samengevat.

Signaalcollectie

Voor fluviatiele monsters is het grootste punt van aandacht de mate van expositie aan daglicht gedurende de laatste transportcyclus; als het sediment niet aan genoeg licht is blootgesteld om het OSL signaal volledig op nul te zetten, dan is het waarschijnlijk dat de equivalente dosis (D_e) wordt overschat tijdens de meting. Een manier om dit effect te reduceren is het gebruiken van het deel van het OSL signaal dat de grootste kans heeft om te zijn gebleekt. Het OSL signaal in kwarts bestaat uit verschillende componenten die elk een verschillende gevoeligheid voor licht hebben. De zogenaamde ‘snelle component’ is het meest gevoelig voor licht en bleekt het snelst; deze component is het meest geschikt om te gebruiken voor datering. De componenten kunnen geïdentificeerd worden door de OSL vervalcurve te fitten met een aantal exponenten. In Hoofdstuk 2 wordt beschreven hoe men zelfs curves van erg zwakke signalen kan fitten.

Het fitten van OSL curves is echter een langdurige klus en daarmee niet altijd een praktische oplossing voor datering. In Hoofdstuk 3 wordt beschreven hoe een nieuwe simpele techniek werd ontwikkeld, gebaseerd op het fitten van OSL vervalcomponenten, die de gebruiker van OSL dateringen in staat stelt het aandeel van de snelle OSL component te maximaliseren voor leeftijdsbepaling. In de standaard methode voor signaalcollectie wordt het laatste deel van de OSL vervalcurve als achtergrondsignaal van het initiële signaal afgetrokken. In de nieuwe techniek volgt het achtergrondsignaal direct op het initiële signaal. Bovendien is het aanbevolen om het achtergrondsignaal 2.5 maal zo lang te nemen als het eerste deel van het OSL signaal. Als deze ratio wordt aangehouden is het aandeel van de snelle component hoog, terwijl de helderheid van het overgebleven signaal nog vrij goed is.

Het begrijpen van verstrooiing in D_e

Differentiële bleking in de natuur kan leiden tot een brede distributie van D_e waardes, maar dit is niet de enige bron van verstrooiing tussen verschillende korrels binnen één monster. In veel sedimenten zal de ruimtelijke variatie van radionuclideconcentraties leiden tot een niet-uniform dosistempo voor de verschillende korrels. Een groot deel van de totale bètadosis in sedimenten is afkomstig van het verval van ^{40}K, dat over het algemeen geconcentreerd is in korrels Kaliumveldspaat. De bètadosis die een kwartskorrel ontvangt zal daarom afhankelijk zijn van de hoeveelheid veldspaatkorrels in de omgeving.

De invloed van zogenaamde ^{40}K 'hotspots' is al jaren onderwerp van discussie, maar het kwantificeren van de verstrooiing die ze veroorzaken is tot nu toe erg ingewikkeld gebleken. In Hoofdstuk 7 van deze thesis wordt een nieuw type experiment geïntroduceerd, dat ontworpen is om het effect van ^{40}K in sediment te simuleren en daarmee te kwantificeren.

Het gaat om een zogenaamd zanddoos experiment: In een gesloten omgeving werden kwarts korrels gemengd met door neutronen geactiveerde NaOH korrels om zo de natuurlijk voorkomende 'hotspots' na te bootsen. Door de NaOH korrels te bombarderen met neutronen in een nucleaire reactor werd het instabiele ^{24}Na geproduceerd dat een bètadosis afgeeft. Door de korte halfwaardetijd van 15 uur kan de ^{24}Na in korte tijd een behoorlijke bètadosis afgeven, en vervalt het stralingsniveau in een aantal weken tot achtergrondwaardes. Metingen op solitaire kwartskorrels uit de zanddoos laten zien dat dit experiment een goede manier is om een niet-uniforme bètadosis te geven. Monte Carlo simulaties van hetzelfde experiment geven soortgelijke resultaten. De combinatie van de twee technieken is een krachtige manier om bètadosis heterogeniteit te onderzoeken.

Het is nodig om de bètadosis heterogeniteit in solitaire korrels te begrijpen, maar de meeste OSL dateringen worden uitgevoerd op submonsters (aliquots) met meerdere korrels. Hoofdstuk 4 laat zien hoe de informatie uit de verstrooiing tussen solitaire korrels omgezet kan worden voor het gebruik in aliquots met meerder korrels. Hiervoor wordt een stochastisch model geïntroduceerd, waarin rekening wordt gehouden met de distributie van gevoeligheid in de populatie solitaire korrels en de hoeveelheid korrels op een aliquot.

Leeftijdsschatting

Het laatste deel van het OSL leeftijdsbepaling bestaat uit het schatten van de ware dosis ten tijde van depositie uit de D_e distributie. Als gedeeltelijke bleking extra verstrooiing heeft veroorzaakt in het monster, moet een statistisch model worden gebruikt om die verstrooiing te beschrijven, naast de verstrooiing die kan worden verwacht ten gevolge van andere effecten. De selectie van een soortgelijk model blijft tot op heden een bron van discussie binnen de wereld van luminescentiedatering. In Hoofdstuk 6 van dit proefschrift is een nieuwe aanpak van leeftijdsbepaling voorgesteld die een oplossing vormt voor de problemen van het kiezen van het juiste statistische leeftijdsmodel en het identificeren van uitbijters. Deze nieuwe aanpak maakt gebruik van een serie steekproeftrekkingen met teruglegging om de onzekerheid van de OSL ouderdom te bepalen en een waarschijnlijkheidsverdeling van de leeftijd te produceren. Er is op twee manieren voordeel te behalen met deze aanpak. Ten eerste kan er, in het geval dat er uitbijters in de D_e waardes zijn, een waarschijnlijkheidsverdeling met meerdere pieken worden gevormd. Ten tweede is het mogelijk om een Bayesiaanse analyse uit te voeren op een reeks monsters; hiermee kan de chronologische precisie worden verbeterd.

Suggesties voor toekomstig onderzoek

In dit proefschrift is een reeks van analyse methodes gepresenteerd die het OSL dateren van gedeeltelijk gebleekte monsters mogelijk maken. Gezamenlijk vergroten deze methodes de toepasbaarheid van OSL datering.

Sinds lange tijd wordt OSL datering beschouwd als een succesvolle manier om de leeftijd van goed gebleekte eolische monsters te bepalen. Fluviatiele monsters worden ook vaak gedateerd met OSL, maar slechts zelden worden daadwerkelijk betrouwbare leeftijdsbepalingen gepubliceerd, tenzij er een goed gebleekt monster voorhanden was. OSL wordt dan ook te weinig gebruikt om fluviatiel sediment te dateren, zelfs al is er over het algemeen geen alternatieve dateringsmethode beschikbaar die het sediment direct kan dateren. De reeks analyse methodes die in dit proefschrift worden beschreven, kunnen deze situatie veranderen; met behulp van de juiste analyses zou OSL als betrouwbare dateringsmethode kunnen worden gebruikt op fluviatiele monsters, zelfs als slechte bleking een grote hoeveelheid verstrooiing in de data veroorzaakt.

Op dit moment is er een grote vraag binnen de wereld van luminescentiedatering naar meer kennis en begrip van het natuurlijke dosistempo en de variatie in dosistempo tussen verschillende korrels. Het dosistempo behelst de helft van de leeftijdsvergelijking in OSL datering, maar is desalniettemin zwaar onderbelicht. Er zouden twee redenen hiervoor kunnen worden aangegeven: allereerst werden fouten in de berekening van het dosistempo tot voor kort meestal overschaduwd door onzekerheden in de D_e bepaling. De tweede, fundamentelere reden is dat de vragen rond variabiliteit in het dosistempo te moeilijk waren om te beantwoorden. Twee prangende vragen zijn in deze thesis aan bod gekomen:

1. *Hoe variabel is het dosistempo tussen verschillende korrels?* Het is uitermate belangrijk om begrip te vormen van dosistempo variabiliteit, opdat D_e distributies juist geïnterpreteerd kunnen worden. In Hoofdstuk 7 is de basis gelegd voor het beantwoorden van deze vraag. Hiervoor zijn simulaties nodig met een serie Monte Carlo modellen, in combinatie met een experimentele validatie van de simulaties. Om deze kennis echter toepasbaar te maken voor gebruikers van OSL datering, moeten de inzichten vergaard in deze

experimenten worden gecombineerd tot een simpel model, dan wel een bruikbaar programma.

2. *Wat als de standaard aannames voor het dosistempo niet opgaan?* Er worden twee grote aannames gedaan bij de bepaling van het dosistempo die bekend staan als de ‘oneindige matrix’ en ‘uniforme matrix’ aannames. Bijna iedere OSL monsterneming wordt uitgevoerd met deze aannames in het achterhoofd; er wordt zoveel mogelijk bemonsterd uit grote homogene units met zandig of siltig sediment. Het dateren van meet complexe sedimentaire units kan deze aannames echter ongeldig maken en in dit geval is een nieuw model voor het dosistempo nodig. Een voorbeeld hiervan kan in Hoofdstuk 5 worden gevonden voor het dateren van schelpenrijk stormvloedsediment: de schelpen en het zand werden gescheiden, hun radionuclide concentratie bepaald. Vervolgens werden de fracties weer gecombineerd in een numeriek model om het dosistempo in kwarts te bepalen.

Om vooruitgang te boeken op beide voornoemde punten zal het waarschijnlijk nodig zijn een aanzienlijk aantal numerieke modelleringen uit te voeren met Monte Carlo transport codes. Het is daarom misschien voor de toekomst de belangrijkste stap om Monte Carlo technieken zodanig te simplificeren, dat ze een praktisch instrument worden voor specialisten op het gebied van OSL datering.

Curriculum Vitae

Alastair Charles Cunningham was born in London in 1982. He grew up in Acton, west London, where he was educated at Twyford Church of England High School. From 2001 until 2004, Alastair studied BSc Geography at the University of Plymouth, obtaining a 2:1. His bachelor dissertation investigated the use of salt-mash foraminifera for reconstructing sea level in western France.

In 2005-6 Alastair studied at Royal Holloway and University College London, where he obtained an MSc in Quaternary Science from the University of London. Alastair was introduced to Luminescence dating at Royal Holloway, and for his Masters dissertation applied OSL to a series of sea-level linked sand dunes in South Australia. In April 2007 he began working on his PhD research at Delft University of Technology; this thesis is the result of that work.

Acknowledgments

The thesis presented here is the result of several years of research, and naturally could not have been done without support form many other people. To properly recognise everyone would be impossible, and I apologise to anyone I miss.

First of all, I would like to thank my daily supervisor, Jakob Wallinga. I am very lucky to work with someone who is prepared to give so much time to his students. Jakob can usually see the silver lining (often prefaced with the words "reading between the lines…"), and maintains a marvellously inappropriate sense of humour. Furthermore, his willingness to let me pursue interesting lines of research, even when the payoff is not immediately obvious, showed a great deal of faith. My promotor, Pieter Dorenbos, has also helped me to focus on my research, and ensured that my thesis was finished on time.

The first two years of this project involved many fieldtrips to the coastline of Holland, usually led by Marcel Bakker, Sytze van Heteren or Bert van der Valk. Our collaborative paper has required a great deal of work from all, and has ultimately been worthwhile. I am very grateful for their patience and commitment.

I owe a debt of gratitude to several other people who have formally or informally contributed to this research. There are many knowledgeable people in the department, and I am always impressed by their willingness to engage in discussion, and to spend time explaining things to the lesser-minded amongst us. In particular, the advice of Adrie Bos, Dennis Schaart, Marc Korevar, Meno Blaauw and Dan deVries has greatly helped in my understanding of physics, and opened up fruitful avenues of research.

I would like to thank my colleagues and friends who create a pleasant atmosphere in the department. Romee has been a constant source of amusement over the last four years, and also translated the summary of this thesis. Alice, Candice, Christina, Patrick, Femke, and assorted guests have made it a pleasure to be part of the NCL, and have been ready to provide an OSL-themed joke when I least expect.

I have fond memories of rambling lunchtime discussions at the coffee table with present and former colleagues, and the numerous drinking sessions after work: Jose, Gus, Stefan, Herman, Sam, Edith, Jan, Lorette, Andreas, Marnix, Ivan, Michiel, Pieter, Ola, Patricia, Micha, Melvin, Francesco, and assorted RID barflies, to name just a few. The discussions are often thought-provoking, sometimes rude and always fun. Keep up the good work.

Finally, I thank Joost, Robin, Michiel, Roderick and Femke for putting up with me. I have had a lot of fun during my time in Delft; the boys and girls at Scoop hockey club are responsible for much of that. The gentlemen at Concordia have kept my cricket dream alive. I will be sorry to leave both.

Alastair C. Cunningham
Delft, August 2011